“DEVELOPMENT AND CHARACTERIZATION OF NITRIC OXIDE-RELEASING PLATFORMS FOR BIOMEDICAL DEVICE AND TISSUE ENGINEERING APPLICATIONS"

by

JITENDRA PANT

(Under the Direction of Hitesh Handa)

ABSTRACT

Every year more than 80,000 different types of medical devices enter the US market. Although the use of such medical devices including stents, catheters, dialysis bags, sutures, wound dressings, and extra corporeal circuits (ECC) is inevitable in hospital care, medical challenges such as biocompatibility, infection, and thrombosis limit their application. Hence there is a dire need to develop advance biopolymers that can be used in the fabrication of medical device and tissue engineering applications.

In 1992, the free radical nitric oxide received approbation as ‘molecule of the year’ by the journal Science and was the subject of a Nobel Prize. Nitric oxide (NO) is a water-soluble, ubiquitous gas, which influences various biological functions including infection, angiogenesis, inflammation, vasodilation, thrombosis, smooth muscle cell proliferation and migration, wound healing, cardiovascular diseases, nervous system diseases, mammalian cell growth, and tumor formation. Nitric oxide is synthesized endogenously from L-arginine by the enzyme nitric oxide synthase (NOS).

The potential role of endogenously released NO in controlling physiological processes has also led to the development of NO-releasing/generating materials that can provide an exogenous

supply of NO to be utilized in biomedical applications. In general, the current NOreleasing (NOrel) strategies can be achieved by two mechanisms: (i) NO generating materials (NOgen) that alter the endogenous NO production from physiological NO donors such as S-nitrosothiols (RSNOs) using catalytic metal ions, heat, light, moisture or temperature as stimulants; and (ii) NOrel exogenous NO donor molecules that actively release NO or its redox analogues. The NOgen materials take advantage of several endogenous high and low molecular weight RSNOs, including S-nitroso-albumin (high molecular weight), S-nitroso-cysteine, and S-nitrosoglutathione (both low molecular weight). My dissertation entitled, *"Development and Characterization of Nitric Oxide-Releasing Platforms for Biomedical Device and Tissue Engineering Applications"* discusses the development of NOrel surfaces and characterization of microbial and mammalian cell response towards them to validate their utility in biomedical and tissue engineering applications.

INDEX WORDS: Advanced Biopolymers; Nitric Oxide (NO); Biomedical Devices; Cell Culture; Device Infection; Clotting; 3D bone scaffolds; Wound Dressings; Catheters; Device Topcoats

DEVELOPMENT AND CHARACTERIZATION OF NITRIC OXIDE-RELEASING PLATFORMS FOR BIOMEDICAL DEVICE AND TISSUE ENGINEERING APPLICATIONS

by

JITENDRA PANT

B. Tech, ICFAI University, India, May 2010

M. E, Birla Institute of Science and Technology, India May 2015

A Dissertation Submitted to the Graduate Faculty of The University of Georgia in Partial Fulfillment of the Requirements for the Degree

DOCTOR OF

PHILOSOPHY

ATHENS, GEORGIA

2018

“DEVELOPMENT AND CHARACTERIZATION OF NITRIC OXIDE-RELEASING PLATFORMS FOR BIOMEDICAL DEVICE AND TISSUE ENGINEERING APPLICATIONS”

by

JITENDRA PANT

Major Professor:	Hitesh Handa
Committee:	William S. Kisaalita
	Ramana M. Pidaparti

Electronic Version Approved:

Suzanne Barbour
Dean of the Graduate School
The University of Georgia
December 2018

DEDICATION

My. Ph.D. dissertation is dedicated to my father Mr. Umesh Chandra Pant who taught me the importance of education and will-power and my mother Mrs. Devki Devi who showed me the power of faith and patience.

ACKNOWLEDGMENTS

Firstly, I would like to express my sincere gratitude to my advisor Dr. Hitesh Handa for giving me the wings to work on my research ideas. His valuable support was instrumental in reaching my research goals in a stress-free culture.

I would also like to thank my advisory committee: Dr. William S. Kisaalita and Dr. Ramana M. Pidaparti for their insightful comments and encouragement, but also for the hard question which incented me to widen my research from various perspectives.

My sincere thanks go to Dr. Marcus Goudie, my first colleague in the lab who answered a long list of doubts I had and helped me greatly in preparing my dissertation. I would also like to thank Ms. Dieu Thao Nguyen, Dr. Sean Hopkins, Dr. James Manuel, Mr. Arnab Mondal, Ms. Juhi Mancha, and Mr. Martin Tran who helped me with various experiments from time to time.

Above all, I would like to thank my loving family in India. My father Mr. Umesh Chandra Pant, who always emphasizes the power of honesty, hard work and commitment in achieving any goal in life; my mother Mrs. Devki Devi Pant, whose love and affection keeping me believing in good things in life, my sisters: Meenakshi, Manju, and Himani who are my ideal. Finally, I feel fortunate to have the support of my best friend, Dr. Manali Dimri, who has always shown faith in my decisions.

TABLE OF CONTENTS

LIST OF TABLES

LIST OF FIGURES

Chapter 1

Chapter 2

Chapter 3

Chapter 4

Chapter 5

Chapter 6

CHAPTER 1

INTRODUCTION AND LITERATURE REVIEW

Pant, Jitendra. Accepted by Advances in Polyurethanes (book)
Partially Reprinted here with permission of the publisher

Abstract

The healthcare sector is growing rapidly with a growth rate of 5.3%. The annual healthcare revenue generated by Biomedical devices in 2017 was US $513 billion. Biomedical devices like catheters, stents, extracorporeal circuits, sensors, and vascular grafts are inevitable in hospital care but unfortunately, they are also the leading cause of hospital acquired infections and thrombosis.

During my doctoral research, I worked towards the development of nitric oxide (NO) releasing biomedical devices and tissue engineering applications that imitates the body's natural way of NO release. The biomaterials are triggered in the presence of heat, moisture, and metals ions to release NO. Since these triggers are readily available in human body, the NO releasing biomaterials are excellent candidate for making invasive biomedical devices.

Leveraging on the antimicrobial, cell proliferating and noncytotoxic properties of NO, I developed NO releasing platforms for applications including wound dressings, catheters, 3D bone scaffolds, device topcoats and antimicrobial polymers during my Ph.D. These applications are discussed in detail in the forthcoming chapters.

1. Introduction

Infection, thrombosis, cytotoxicity, and foreign body response (FBR) are among the significant problems faced by long-term use of indwelling medical devices. This can lead to device failures, add to the healthcare cost while adding to the suffering of the patients.

The mechanism of bacterial adhesion is a very complex process. Bacterial adhesion involves initial reversible physicochemical interactions, followed by time-dependent irreversible molecular and cellular interactions.[1] Due to various physical forces, such as Brownian movement, van der Waals forces, and hydrophobic and electrostatic interactions, bacteria move to the implant surface. In the second phase, molecular and cellular interactions become predominant where bacteria attach irreversibly to the surface using various bacterial polymeric structures including

fimbriae, capsules, and slimes.[1] At this time, most bacteria multiply and produce extracellular polymeric substances (EPS) to stabilize the biofilm structure. This accumulation of bacterial biomass and EPS on a surface leads to biofilm formation over time (Figure 1.1). In a biofilm, bacteria are protected from adverse environmental conditions, including the application of antiseptics as well as host defense, which makes them difficult to eradicate. The presence of fibrinogen and thrombus on the surface also promotes bacterial adhesion.[2] The interaction of

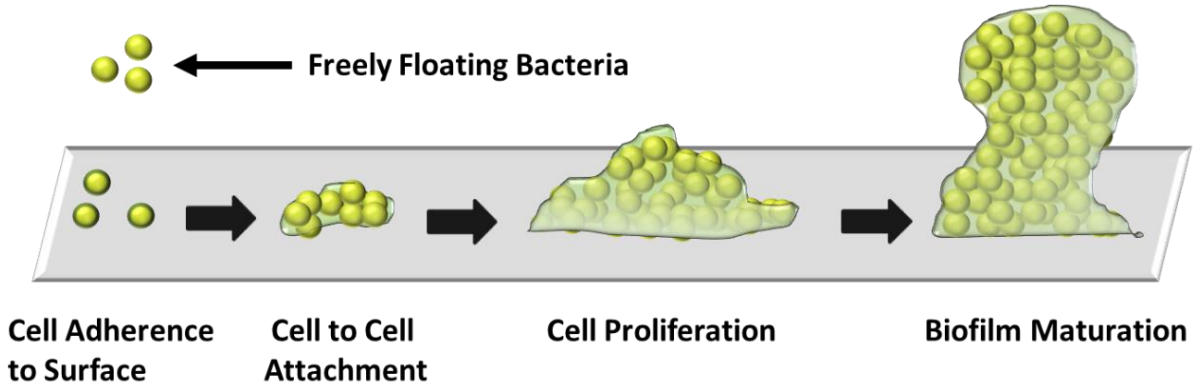

Figure 1.1. Series of events leading to biofilm formation on an implant surface. These events include (a) cell adherence to the implant's surface with the help of a specialized structure on the bacterial cell wall, (b) cell to cell attachment, (c) cell proliferation leading to growth and aggregation, and (d) biofilm maturation and development of resistance against antibacterial agents.

blood proteins with an implant surface is not only a fundamental phenomenon but is also key to several important medical complications. Plasma proteins binding on the surface of the implant can promote bacterial adhesion leading to the risk of local and systemic complications such as catheter-related blood infections (CRBIs). The incidences of CRBIs in the United States amount to more than 250,000 cases/year with an attributable mortality of up to 35% and an annual healthcare expenditure of $2.3 billion approximately.[3]In a biofilm, bacteria are protected from adverse environmental conditions, including the application of antiseptics as well as host defense, which makes them difficult to eradicate. The presence of fibrinogen and thrombus on the surface also promotes bacterial adhesion.[2] The interaction of blood proteins with an implant surface is not only a fundamental phenomenon but is also key to several important medical complications.

Plasma proteins binding on the surface of the implant can promote bacterial adhesion leading to the risk of local and systemic complications such as catheter-related blood infections (CRBIs). The incidences of CRBIs in the United States amount to more than 250,000 cases/year with an attributable mortality of up to 35% and an annual healthcare expenditure of $2.3 billion approximately.[3]

Another major complication related to the invasive device usage, is thrombosis that can cause life-threatening complications for patients. The blood coagulation cascade is a complex process, where protein adsorption occurs within a few seconds to minutes when blood comes in contact with a foreign surface (Figure 1.2) This is followed by platelet adhesion and activation that finally leads to thrombus formation. Adsorbed plasma proteins, such as fibrinogen, bind to glycoprotein GPIIb/IIIa receptors on activated platelets.[4] The activation of platelets also leads to conformation changes and the excretion of intracellular granulates containing adhesion molecules (P-selectin, coagulation factor V and VII, calcium ions, etc.), leading to additional adhesion and activation of platelets. Between 1955 and 2015, much has been learned about blood–surface interactions, and many approaches have been studied to prevent thrombosis with systemic anticoagulation and surface modification. In a clinical setting, many of these devices require the use of anticoagulant therapies (e.g., heparin) to avoid device failure. Unfortunately, the long-term use of systemic anticoagulation can be harmful to the patient and can result in bleeding, increased thrombosis, and thrombocytopenia.

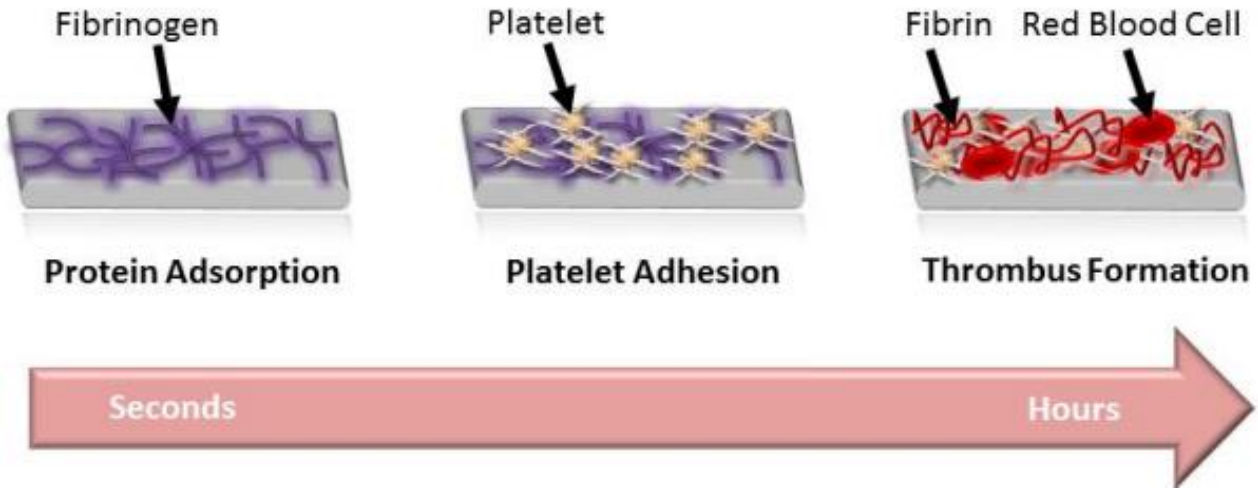

Figure 1.2. Series of steps involved in thrombus formation on an implanted surface. These events include fibrinogen adsorption, platelet adhesion, and activation, finally leading to a clot formation.

2. Nitric Oxide to the rescue

Nitric oxide (NO) is a free radical, water-soluble, ubiquitous gas, which influences various biological functions. It is a cellular signaling molecule naturally secreted by vascular endothelial cells and is involved in many physiological and pathological processes. As shown in Figure 1.3, NO is enzymatically synthesized endogenously from l-arginine by nitric oxide synthase (NOS). There are three NOS synthase isoforms: eNOS (endothelial NOS, generates NO from the endothelial lining of blood vessels), nNOS (neuronal NOS, present in neurons and produces NO that acts as a neurotransmitter), and iNOS (inducible NOS, present in macrophages as a response to bacterial/viral infections).[5] The eNOS and nNOS isoforms are calcium-dependent and increased NO production occurs when there is an increase in Ca2+. The iNOS isoform is calcium independent and is involved in immune responses, including autoimmune diseases, and is the predominant cause of septic shock.[6] Radomski et al. first described NO as a potent vasodilator secreted by the normal endothelium that has the ability to inhibit platelet adhesion and aggregation to the blood vessel wall.[7] In 1992, the free radical NO received approbation as “molecule of the year” by the journal Science and was the subject of a Nobel Prize. Numerous

published reports including ours have been devoted to a comprehensive discussion of different NO-releasing/generating materials and their many potential biomedical applications.[8-13]

2.1 Physiological Importance

Nitric oxide offers great potential to be utilized in biomedical applications due to its impact on wide-ranging biological functions including infection, angiogenesis, inflammation, vasodilation, thrombosis, smooth muscle cell proliferation and migration, wound healing, cardiovascular diseases, nervous system diseases, mammalian cell growth, and tumor formation.[14] Nitric oxide

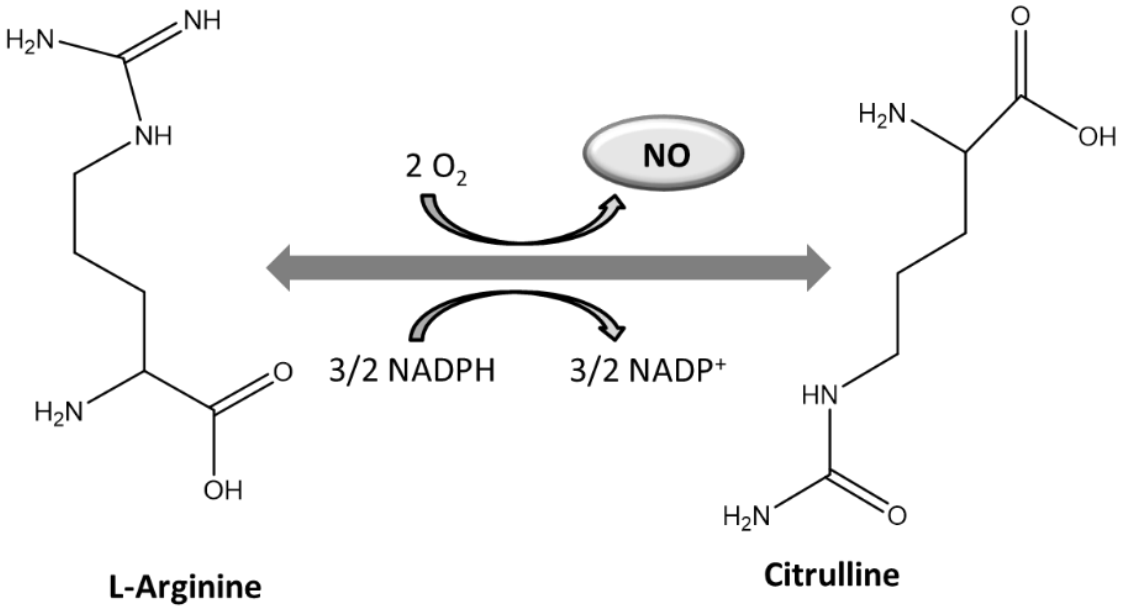

Figure 1.3. Enzymatic conversion of L-Arginine to Citrulline resulting in nitric oxide release

is known to be a potent inhibitor of platelet activation and adhesion. Healthy endothelial cells exhibit a NO flux of 0.5−4.0 × 10^{-10} mol/cm^2/min.[15] In addition, NO released within the sinus cavities and macrophages functions as a natural antimicrobial agent. In 2005, McMullin et al. showed that gaseous NO is bactericidal against several strains of bacteria derived from tracheal

aspirates of mechanically ventilated patients in the intensive care unit.[16] Therefore, using NO-releasing polymers that can locally deliver NO at or above physiologically relevant levels has the advantage of creating implantable devices that can possess both antithrombotic and antibacterial properties. Since NO is highly reactive under physiological conditions, many molecules with functional groups that can store, and release NO have been studied. Among various NO donors, diazeniumdiolates and S-nitrosothiols (RSNOs) have been studied widely. Diazeniumdiolates are synthetic NO donors that undergo proton or thermally driven mechanisms to release 2 mol of NO per diazeniumdiolate molecule. However major concern with diazeniumdiolated-based polymers, is the formation of potentially toxic decomposition products such as N-nitrosamines, which can lead to cancer.

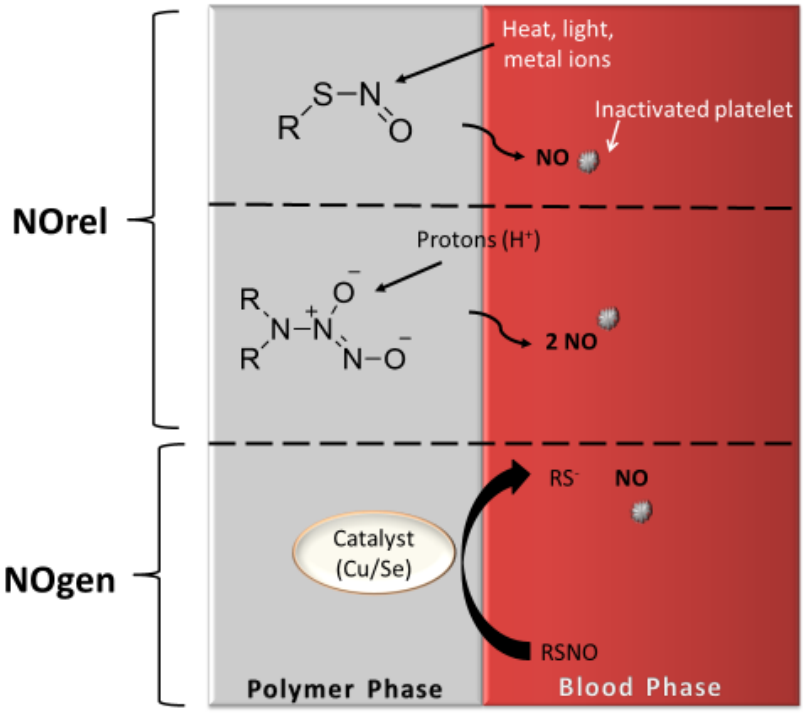

Figure 1.4. Two examples of NO-releasing (NORel) polymers where NO donor molecules (e.g., RSNOs or diazeniumdiolates) can be covalently or noncovalently incorporated into the PU. NO-generating (NOGen) polymers consist of immobilized catalysts that can generate NO from endogenous RSNO species.

To address this stability issue, several NO-generating polymers both endogenous and synthetic RSNOs have been studied widely. Some of the endogenous RSNOs include S-

nitrosoglutathione (GSNO), S-nitrosocysteine (CysNO), and S-nitrosoalbumin. S-nitroso-N-acetylpenicillamine (SNAP) and S-nitroso-N-acetylcysteine are two examples of synthetic RSNOs. These RSNOs can release NO via thermal decomposition, catalysis (using metals ions such as Cu+), or by exposure to light (wavelengths of 340 and/or 590 nm), resulting in disulfide species (RSSR) formation. The two commonly used approaches to release NO from polymeric surface are: (1) NO-releasing polymers (NORel), where NO donor molecules (e.g., diazeniumdiolates or RSNOs) that can release NO under physiological conditions are incorporated into the polymer; and (2) NO-generating (NOGen) polymers, where catalysts that can react with endogenous RSNOs to generate NO are incorporated into the polymers (Figure 1.4).

2.2 Nitric oxide-releasing/generating polymers

Many strategies have been studied to create localized NO release/generation from various polymeric materials. As discussed above, NORel polymers are prepared by covalently or noncovalently incorporating NO donor molecules into polymer matrices. Diazeniumdiolates have been incorporated into polymers for a variety of potential applications. Reynolds et al. suggested two novel strategies for the synthesis of NO-releasing polymers with covalently linked diazeniumdiolated secondary amines.[17] However, the NO-releasing polymers resulting from this synthetic strategy required incorporation of countercations to stabilize the diazeniumdiolates. In the second approach, the polymer was derivatized to contain pendant polyamine sites, which act as a linker to covalently bind the diazeniumdiolates. These diazeniumdiolates were found to be stable without additives, likely because the pendant amines are less rigid than the polymer backbone and allow the zwitterionic diazeniumdiolate to form more easily. Covalently bound NO donors have the advantage that the by-products remain covalently bound to the polymer matrix. The results showed an initial NO flux of 14 pmol/cm^2/s when immersed in pH 7.4 buffer at 37 °C for up to 6 days. Other diazeniumdiolate-based NO-releasing implants have proved helpful in

decreasing the local chronic inflammation and foreign body response by 33% and enhancing formation of blood vessels by >77% in vivo in adult male Sprague–Dawley rats.[18] In addition, NO release helped in reducing collagen capsule thickness in rat models by >50% around the implant as compared to controls. Success in using NO donors for preventing thrombosis either by covalently linking NO donors to the polymer or by embedding them within the polymers (NORel polymers) has been reported.[19] However, the utility of NORel polymers can be limited by their sensitivity toward heat, light, and moisture, leading to decrease NO release lifetimes. One of the obstacles in delivering NO from the polymers is rapid leaching of the NO donor species, resulting in nonlocalized NO release. To address this stability issue, several NO-generating polymers have been studied. These NOGen polymers have the advantage that they could potentially generate NO for long periods, provided that there is a constant source of endogenous RSNOs. One approach has been the use of various covalently linked Cu(II)–cyclen moieties or Cu nanoparticles (Cu-NPs) topcoats that have been immobilized onto polymeric backbones.[20-21] Owing to these properties, the newly developed material possesses great potential to be utilized as a coating material for various blood-contacting device applications.

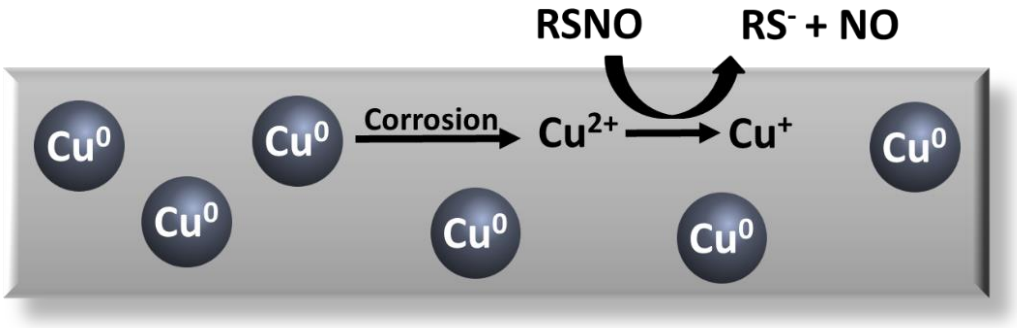

Figure 1.5. Scheme showing the mechanism of localized NO generation from polymer containing Cu (0) nanoparticles.

3. Conclusion

To improve the clinical applications of implantable devices, issues associated with their biocompatibility must be addressed. Over the years, there has been a significant advancement in

the medical device industry. In this regards, nitric oxide has emerged as a promising therapeutic agent with many potential applications in biomedical science due to its crucial role in cell proliferation, inflammation, infection, thrombosis, vasodilation, cell cycle regulation, and neurotransmission. It has been demonstrated that NO-releasing polymers have improved improve hemocompatibility via reduced platelet activation and infection. In this chapter, we discussed some of the applications of NO-releasing PUs that have been studied. The NO-releasing polymers are helpful in reducing the FBR, thrombosis, and microbial infection associated with biomedical devices. However, clinical applications of NO-releasing polymers have been limited by the potential loss of NO during storage and sterilization. Further addressing issues related to leaching of NO donors, NO shelf life, and sustaining the release of NO will help improve the potential for clinical applications of these materials and greatly improve patient outcomes.

This dissertation describes the development of nitric oxide-releasing polymers for various biomedical applications including top coats for biomedical devices (Chapter 2), nitric oxide combination with other therapeutic agents (Chapter 3), vascular catheters (Chapter 4), wound healing application of nitric oxide (Chapter 5), application of nitric oxide-releasing 3D scaffolds in bone tissue engineering (Chapter 6). Reprint permission has been granted for all the chapters.

References

(1) An, Y. H.; Friedman, R. J., *Handbook of bacterial adhesion: Principles, methods, and applications*. Springer Science & Business Media: **2000**; Vol. 204.

(2) Harris, L.; Tosatti, S.; Wieland, M.; Textor, M.; Richards, R. Staphylococcus aureus adhesion to titanium oxide surfaces coated with non-functionalized and peptide-functionalized poly (l-lysine)-grafted-poly (ethylene glycol) copolymers. *Biomaterials* **2004,** *25* (18), 4135-4148.

(3) Daniels, K. R.; Frei, C. R. The united states' progress toward eliminating catheter-related bloodstream infections: Incidence, mortality, and hospital length of stay from 1996 to 2008. *Am. J. Infect. Control* **2013,** *41* (2), 118-121.

(4) Gorbet, M. B.; Sefton, M. V. Biomaterial-associated thrombosis: Roles of coagulation factors, complement, platelets and leukocytes. *Biomaterials* **2004,** *25* (26), 5681-5703.

(5) Knowles, R. G.; Moncada, S. Nitric oxide synthases in mammals. *Biochem. J.* **1994,** *298* (Pt 2), 249.

(6) Stuehr, D. J. Mammalian nitric oxide synthases. *Biochimica et Biophysica Acta (BBA)-Bioenergetics* **1999,** *1411* (2-3), 217-230.

(7) Radomski, M. W.; Vallance, P.; Whitley, G.; Foxwell, N.; Moncada, S. Platelet adhesion to human vascular endothelium is modulated by constitutive and cytokine induced nitric oxide. *Cardiovasc. Res.* **1993,** *27* (7), 1380-1382.

(8) Pant, J.; Gao, J.; Goudie, M. J.; Hopkins, S. P.; Locklin, J.; Handa, H. A multi-defense strategy: Enhancing bactericidal activity of a medical grade polymer with a nitric oxide donor and surface-immobilized quaternary ammonium compound. *Acta Biomater.* **2017,** *58*, 421-431.

(9) Sundaram, J.; Pant, J.; Goudie, M. J.; Mani, S.; Handa, H. Antimicrobial and physicochemical characterization of biodegradable, nitric oxide-releasing nanocellulose–chitosan packaging membranes. *J. Agric. Food Chem.* **2016,** *64* (25), 5260-5266.

(10) Pant, J.; Goudie, M. J.; Chaji, S. M.; Johnson, B. W.; Handa, H. Nitric oxide releasing vascular catheters for eradicating bacterial infection. *Journal of Biomedical Materials Research Part B: Applied Biomaterials*.

(11) Frost, M. C.; Reynolds, M. M.; Meyerhoff, M. E. Polymers incorporating nitric oxide releasing/generating substances for improved biocompatibility of blood-contacting medical devices. *Biomaterials* **2005,** *26* (14), 1685-1693.

(12) Reynolds, M. M.; Frost, M. C.; Meyerhoff, M. E. Nitric oxide-releasing hydrophobic polymers: Preparation, characterization, and potential biomedical applications. *Free Radical Biol. Med.* **2004,** *37* (7), 926-936.

(13) Carpenter, A. W.; Schoenfisch, M. H. Nitric oxide release: Part ii. Therapeutic applications. *Chem. Soc. Rev.* **2012,** *41* (10), 3742-3752.

(14) Pant, J.; Goudie, M.; Brisbois, E.; Handa, H., Nitric oxide-releasing polyurethanes. In *Advances in polyurethane biomaterials*, Elsevier: **2016**, pp 417-449.

(15) Vaughn, M. W.; Kuo, L.; Liao, J. C. Estimation of nitric oxide production and reaction rates in tissue by use of a mathematical model. *Am. J. Physiol.: Heart Circ. Physiol* **1998,** *274* (6), H2163-H2176.

(16) Mcmullin, B. B.; Chittock, D. R.; Roscoe, D. L.; Garcha, H.; Wang, L.; Miller, C. C. The antimicrobial effect of nitric oxide on the bacteria that cause nosocomial pneumonia in mechanically ventilated patients in the intensive care unit. *Respir. Care* **2005,** *50* (11), 1451-1456.

(17) Reynolds, M. M.; Hrabie, J. A.; Oh, B. K.; Politis, J. K.; Citro, M. L.; Keefer, L. K.; Meyerhoff, M. E. Nitric oxide-releasing polyurethanes with covalently linked diazeniumdiolated secondary amines. *Biomacromolecules* **2006,** *7* (3), 987-994.

(18) Hetrick, E. M.; Prichard, H. L.; Klitzman, B.; Schoenfisch, M. H. Reduced foreign body response at nitric oxide-releasing subcutaneous implants. *Biomaterials* **2007,** *28* (31), 4571-4580.

(19) Brisbois, E. J.; Handa, H.; Major, T. C.; Bartlett, R. H.; Meyerhoff, M. E. Long-term nitric oxide release and elevated temperature stability with s-nitroso-n-acetylpenicillamine (snap)-doped elast-eon e2as polymer. *Biomaterials* **2013,** *34* (28), 6957-6966.

(20) Oh, B. K.; Meyerhoff, M. E. Spontaneous catalytic generation of nitric oxide from s-nitrosothiols at the surface of polymer films doped with lipophilic copper (ii) complex. *J. Am. Chem. Soc.* **2003,** *125* (32), 9552-9553.

(21) Pant, J.; Goudie, M. J.; Hopkins, S. P.; Brisbois, E. J.; Handa, H. Tunable nitric oxide release from s-nitroso-n-acetylpenicillamine via catalytic copper nanoparticles for biomedical applications. *ACS Appl. Mater. Interfaces* **2017,** *9* (18), 15254-15264.

CHAPTER 2

TUNABLE NITRIC OXIDE RELEASE FROM *S*-NITROSO-*N*-ACETYLPENICILLAMINE VIA CATALYTIC COPPER NANOPARTICLES FOR BIOMEDICAL APPLICATIONS

Pant, Jitendra. Accepted by ACS Applied Materials & Interfaces
Reprinted here with permission of the publisher

Abstract

The quest for novel therapies to prevent bacterial infections and blood clots (thrombosis) is of utmost importance in biomedical research due to exponential growth in cases of thrombosis, blood infections, and the emergence of multi-drug resistant strains of bacteria. Endogenous nitric oxide (NO) is a cellular signaling molecule that plays a pivotal role in host immunity against pathogens, prevention of clotting, and regulation of systemic blood pressure among several biological functions. The physiological effect of NO is dose-dependent that necessitates the need of tunable release kinetics which is the objective of this study. In the present study, polymer composites were fabricated by incorporating *S*-nitroso-*N*-acetylpenicillamine (SNAP) in a medical grade polymer, Carbosil, and top coated with varying levels of catalytic copper nanoparticles (Cu-NPs). The addition of Cu-NPs increased the NO release as well as the overall antimicrobial activity via its oligodynamic effect. The 10 wt% SNAP composites (without Cu-NPs coats) showed an NO flux of $1.32 \pm 0.6 \times 10^{-10}$ mol min^{-1} cm^{-2}, while Cu-NPs incorporated SNAP films exhibited a flux of $4.48 \pm 0.5 \times 10^{-10}$, $4.84 \pm 0.3 \times 10^{-10}$, and $11.7 \pm 3.6 \times 10^{-10}$ mol min^{-1} cm^{-2} with 1 wt%, 3 wt%, and 5 wt% Cu-NPs respectively. This resulted in a significant reduction (up to 99.8%) in both gram-positive and gram-negative bacteria with very low platelet adhesion (up to 92% lower) as compared to the corresponding controls. Copper leachates from the SNAP films were detected using ICP-MS technique and were found to be significantly lower than the recommended safety limit by the FDA. The cell viability test performed provided supportive evidences for the biocompatibility of the material *in vitro*.

1. Introduction

With over 8000 medical devices entering the market every year, the United States has the biggest medical device market in the world with an estimated market size of approximately $133 billion in 2016.[22] Unfortunately, infection and blood clotting (thrombosis) remain the major risks associated with the application of medical devices in humans. There is an exponential increase

in nosocomial infections due to the rapid development of multi-drug resistant strains and failure of the current antimicrobial strategies to prevent this. Similarly, blood clotting on the implants' surface is a complex medical problem, as they can break loose, and cause pulmonary embolism (blocked blood flow in lungs) by traveling to the lungs through the bloodstream. These two issues not only put the patient's life at risk but also delay their health recovery ultimately adding to the healthcare costs. The failure of currently available antimicrobials and antithrombotic agents to control these problems has spurred the development of new biocompatible and hemocompatible materials.

In the US alone there are over 1.7 million Hospital Acquired Infections (HAIs) cases annually resulting in 100,000 deaths.[22-24] Biofilm accumulation not only resists the action of bactericidal agents but can ultimately degrade the polymeric material used in device fabrication.[25-26] This can potentially lead to serious consequences like the release of toxic degradation products, bacteremia, and septicemia. The current state-of-the-art mainly uses antimicrobial agents like antibiotics or silver nanoparticles (Ag-NPs) with commercialized biomedical implants. Several studies have found Ag-NPs to be cytotoxic to human dermal fibroblast,[27] mice peritoneal macrophage cell products,[28] rat hepatocytes,[29] and both genotoxic and cytotoxic to human lung fibroblast cells.[30] These findings are in line with the cell membrane disruption and oxidative stress caused by Ag-NPs when tested on mouse fibroblast cells.[31] Similarly, the use of antibiotics has been a concern for the past few decade due to emerging issues of antibiotic resistance in bacteria.[32-33] Another important determinant for increasing chances of clinical success of a biomedical implant in the blood is the suppression of platelet activation which ultimately prevent thrombosis.[34-35] Even though heparin is a widely used and popular thrombotic agent to prevent blood clots, it can lead to side effects such as increased risk of hemorrhage and thrombocytopenia in addition to not being effective in 33% of the intensive unit care patients.[36-37] Recommendations from the studies suggest that there is a need to develop new biomaterials that should not only be

able to inhibit drug-resistant bacteria but should also be hemocompatible without causing the undesirable side effects such as cytotoxicity.

Multiple studies have reported the antibacterial and antithrombic success of NO obtained from various NO donors. The antibacterial effect of NO has been proven against infection causing agent pathogens such as *Staphylococcus aureus,*[38-39] *Staphylococcus epidermis,*[38] *Pseudomonas aeruginosa,*[40-41] *Escherichia coli,*[38-39, 42] *Acinetobacter baumanii,*[43-44] *Listeria monocytogenes,* and *Enterococcus faecalis*.[9] The antimicrobial mechanisms of NO include nitrosation of amines and thiols in the extracellular matrix, lipid peroxidation and tyrosine nitration in the cell wall, and DNA cleavage in the cellular matrix.[45] Moreover, the use of NO is unlikely to stimulate the production of resistant strains due to rapid reduction of microbial load.[40, 46-47] On the other hand, the ability of NO to prevent blood clots in the implants is due to its ability to inhibit platelet activation and adhesion of blood platelet cells on the surface which marks the initial phase of thrombosis.[48]

The potential role of endogenously released NO in controlling physiological processes has also led to the development of NO-releasing/generating materials which can provide an exogenous supply of NO to be utilized in biomedical applications.[35, 49-50] In general, the current NO releasing strategies can be achieved by two mechanisms: (i) NO generating materials (NOgen) that alters the endogenous NO production from the physiological NO donors such as nitrosothiols (RSNOs) using catalytic metal ions, heat, light or temperature as stimulants; and (ii) NO releasing (NOrel) exogenous NO donor molecules that actively release NO or its redox analogs.[13] The NOgen materials include several high and low molecular weight RSNOs including *S*-nitroso-albumin (high molecular weight), *S*-nitroso-cysteine, and *S*-nitroso-glutathione (both low molecular weight). The catalytic generation of NO from naturally occurring RSNOs has resulted in a number of NOgen materials, where material structures such as metal-organic frameworks or zeolites have been used to provide copper catalyzed generation of NO for both organic NO donors (such as nitrates and nitrites) as well as RSNOs.[11, 50-51]

Incorporation of external RSNOs within hydrophobic polymers has been shown to provide physiological NO release rates from the polymeric surface, reducing thrombus formation and bacterial adhesion both *in vitro* and *in vivo*.[52] Multiple studies have shown the use of NO donor systems like *S*-nitroso-*N*-acetylpenicillamine (SNAP), *N*-diazeniumdiolated dibutyl hexane diamine (DBHD/N_2O_2), *S*-nitroso-*N*-acetylcysteine (SNAC), and NO releasing metal-organic framework.[17, 34-35, 52] Out of these NO donors, SNAP has been used extensively for active NO release for multiple biomedical applications.[9, 53-56] Polymers with SNAP incorporation have been shown to release NO consistently for over 2 weeks but near the lower end of physiological levels.[57] Although very effective, the ability to maintain NO release at a level within the physiological limits (preferably at the upper end) would be beneficial for reproducibility, reliability, and increased efficacy for various biomedical applications. The ultimate effect of NO on pathogens, blood activity as well as mammalian cells is dose-dependent, therefore NO release can potentially be regulated via a catalyst/stimulant when using NO donors as therapeutic agents.[58-59] One such mean to increase the release rate, such as the exposure to light, has shown an excellent control of NO release.[60] While these materials may be useful for applications such as extracorporeal circuits, where the device remains outside of the body, these materials may have a limited applicability for implanted medical devices that remain inside the body as applying light to these areas is not feasible. Therefore, developing materials where NO release at the material/tissue interface can be controlled with an incorporated catalyst, such as copper nanoparticles (Cu-NPs), will be highly advantageous for long-term *in vivo* medical applications. From the application point of view, this strategy will not only ensure the long-term active supply of exogenous NO via SNAP at the site of application but will also provide the stimulation for enzymatic NO release via the action of copper ions on endogenous RSNOs in the blood.[51] In addition, copper ions possess oligodynamic effect i.e. they have inherent antibacterial properties which would work synergistically with NO to bring enhance the antibacterial effect.[61] To summarize, the addition of the Cu-NPs will not only provide a method to catalytically control the level of NO released from the physically blended NO donor

but also provides NO generating capabilities by utilizing endogenous NO donors in the blood when used in blood-contacting applications besides its oligodynamic effect. In this study, we fabricated a novel composite material with the incorporation of SNAP in a medical grade polymer, Carbosil™. The resulting composite was coated with varying concentrations of the Cu-NPs layer to catalyze the *in-situ* release of NO from the synthetic NO donor SNAP via copper ions. These materials were then examined for NO release kinetics, platelet adhesion, bacterial inhibition, and cytotoxicity besides other physical and chemical characterizations.

2. Materials and Methods

2.1 Materials

N-Acetyl-*D*-penicillamine (NAP), potassium chloride, sodium chloride, potassium phosphate monobasic, sodium phosphate dibasic, tetrahydrofuran (THF), ethylenediaminetetraacetic acid (EDTA), sulfuric acid and *N*, *N*-dimethylacetamide (DMAc) were purchased from Sigma-Aldrich (St. Louis, MO). Carbosil™ 20 80A (here on will be referred to as Carbosil) was obtained from DSM (Berkeley, CA). LB broth and LB Agar were obtained from Fisher Bioreagents (Fair Lawn, NJ). Phosphate buffered saline (PBS), pH 7.4, containing 138 mM NaCl, 2.7 mM KCl, 10 mM sodium phosphate, was used for all *in vitro* experiments. Dulbecco's modification of Eagle's medium (DMEM) and trypsin-EDTA were purchased from Corning (Manassas, VA 20109). The Cell Counting Kit -8 (CCK-8) was obtained from Sigma-Aldrich (St Louis MO 63103). The antibiotic Penicillin-Streptomycin (Pen-Strep) and fetal bovine serum (FBS) were purchased from Gibco-Life Technologies (Grand Island NY 14072). The LDH kit was purchased from Roche Life Sciences (Indianapolis, IN). The Copper nanoparticles (99%, 40-60 nm) were obtained from SkySpring Nanomaterials, Inc. (Houston, TX). The bacterial strains *Pseudomonas aeruginosa* (ATCC 27853) and *Staphylococcus aureus* (ATCC 5538) and mouse 3T3 cells (ATCC 1658) were originally obtained from American Type Culture Collection (ATCC).

2.2 Experimental Section

2.2.1 Synthesis of SNAP

Synthesis of SNAP was done through a modified version of a previously reported method.[62] Sodium nitrite and NAP were added in an equimolar ratio to a 1:1 mixture of methanol and water containing 2M H_2SO_4 and 2M HCl. The mixture was stirred in dark (to protect from NO release by light stimulation) for 40 min using a magnetic stirrer. Thereafter, the reaction vessel was placed in an ice bath to precipitate the SNAP crystals. The resulting crystals were filtered, rinsed, and dried under vacuum in the dark, and were stored at -20°C before their use in the experiment.

2.2.2 Fabrication of Copper-NPs doped NO generating composites

SNAP composites were prepared by initially dissolving 70 mg of Carbosil-2080A per mL of THF in an amber vial by stirring for 1h at room temperature using a magnetic stirrer. Once completely dissolved, 10 wt% SNAP (7mg/mL) was added and quickly dissolved for 2 min. The resulting solution was cast in Teflon™ molds (diameter = 2.5cm) and dried overnight in the dark to prevent undesired light-induced NO release from the SNAP. To ensure that there were no traces of residual THF, the films were further vacuum dried using a desiccator at room temperature. The control Carbosil films were prepared in a similar manner but excluded the addition of SNAP. The SNAP and Carbosil films were dip-coated twice with Carbosil (50 mg/mL) or the Cu-NPs (1, 3, or 5 wt% Cu-NPs (w/w)) dispersed in 50mg/mL of Carbosil solution. All the films were finally top coated with a layer of Carbosil (50 mg/mL) to prevent leaching of SNAP and/or Cu-NPs from the films. A representative cartoon of Cu-SNAP films is shown in Figure 2.1. Altogether four different types of polymeric composites and their respective controls (without SNAP) were fabricated:

1. SNAP composite: Carbosil (70 mg/mL) incorporating 10 wt% SNAP along with three top coats of Carbosil (50 mg/mL) to reduce leaching of SNAP
2. 1 wt% Cu-SNAP composite: SNAP composite with two intermediate coats of 1 wt% Cu-NPs and one top coat of (50 mg/mL) Carbosil
3. 3 wt% Cu-SNAP composite: SNAP composite with two intermediate coats of 3 wt% Cu-NPs and one top coat of (50 mg/mL) Carbosil
4. 5 wt% Cu-SNAP composite: SNAP composite with two intermediate coats of 5 wt% Cu-NPs and one top coat of (50 mg/mL) Carbosil

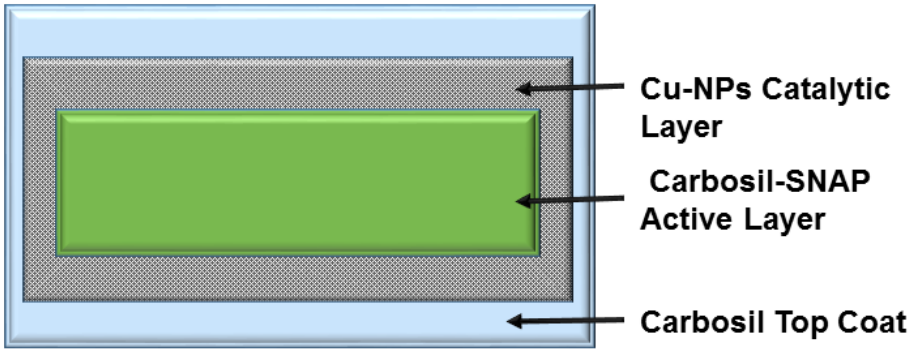

Figure 2.1. A representative schematic of the polymeric composites with SNAP and copper nanoparticles (Cu-NPs) coating. The innermost active layer is made by incorporating 10 wt% SNAP in the CarboSil polymer. After completely drying the films, two coats of Cu-NPs (1, 3, or 5 wt%) blended in CarboSil were applied. A final top coat of CarboSil (50g/L) was layered to prevent leaching of SNAP and Cu-NPs.

2.2.3 Surface morphology characterization (SEM)

All configurations of the Cu-SNAP composite films were examined under a scanning electron microscope (SEM) (FEI Inspect F FEG-SEM) to study the surface morphology of the polymeric composite. The topcoat solution of 3 wt% Cu-NPs in Carbosil (50 mg/mL) was cast into a film in a Teflon mold (d = 2.5 cm), dried, and examined for roughness using SEM. Dried film samples were mounted on a metal stub with double-sided carbon tape and sputter coated with 10 nm gold-palladium using a Leica EM ACE200 sputter coater. Images were taken at accelerating voltage 5 kV.

2.2.4 NO release kinetics

Nitric oxide released from the polymeric composites was measured using a Sievers Chemiluminescence Nitric Oxide Analyzer (NOA) 280i (Boulder, CO). Polymeric films were placed in the sample vessel immersed in PBS (pH 7.4) and maintained at 37 °C. Buffer for control samples also contained 100 µM EDTA to quench all metal ion activity in the buffer solution. Buffer samples containing films with copper top coats contained no EDTA to allow for the catalytic activity of copper. Nitric oxide was continuously purged from the buffer and swept from the headspace using nitrogen sweep gas and bubbler into the chemiluminescence detection chamber. Films were submerged in PBS in glass vials and kept at 37 °C between NO release measurements. The fresh buffer was used for each NO release measurement, and films were kept in fresh buffer for storage after each measurement. Nitric oxide release measurements were also conducted after exposure of the films to bacterial suspensions to confirm that NO was continued to be released throughout the entire exposure, as well as demonstrate the presence of bacteria and the medium had an insignificant effect on the release kinetics.

2.2.5 In vitro platelet adhesion

Fresh porcine blood was drawn into a BD 60 mL syringe with 3.4% sodium citrate at a blood: citrate ratio of 9:1 through a blind draw at the Large Animal Research Unit at the University of Georgia School of Animal and Dairy Science, Athens, GA. Immediately following the draw, the anticoagulated blood was centrifuged at 1200 rpm for 12 min using the Eppendorf Centrifuge 5702. The platelet-rich plasma (PRP) portion was collected carefully with a pipette as to not disturb the buffy coat. The remaining samples were then spun again at 4000 rpm for 20 min to achieve platelet poor plasma (PPP). Total platelet counts in both the PRP and PPP fractions were determined using a hemocytometer (Fisher). The PRP and PPP were combined in a ratio to give a final platelet concentration ca. 2×10^8 platelets/mL. Calcium chloride ($CaCl_2$) was added

to the final platelet solution to achieve a final concentration of 2.5 mM to reverse the effect of the anticoagulant during the experiment.

The degree of platelet adhesion was determined using a Roche lactate dehydrogenase (LDH) Cytotoxicity Detection Kit in a 96-well format as per the supplier's specifications. Each well was coated with the respective combination of control/NO releasing and control/Cu particle solutions. Coating of the wells was done in three stages: 1) a base layer of Carbosil (200 µL of 70 mg/mL), 2) copper layer (100 µL of 0, 1, 3 wt% Cu particles in 50 mg/mL Carbosil), 3) a top coat of 50 µL of 50 mg/mL Carbosil. The ratio of the copper layer to the top coat was done 2:1 as to mimic the number of dip coats used for film-based studies. For NO-releasing samples, 10 wt% SNAP in the Carbosil base layer was used; a total of n=16 samples were used for each material. The wells were dried for 6 hours between coats, followed by 24 hours drying under vacuum to ensure all THF had been removed from the wells.

Exposure to the PRP solution was done using 300 µL of the calcified PRP and incubated at 37°C for 2 hours with mild rocking (25 rpm) on a Medicus Health blood tube rocker. Following the incubation, the wells were infinitely diluted with 10 mM PBS. Lysing of the adhered cells was done using 200 µL Triton-PBS buffer (2% v/v Triton-X-100 in PBS). Briefly, 100 µL of the lysing buffer for each sample was combined with 100 µL of the detection agent and incubated for 25 min protected from light. A calibration curve was constructed using known dilutions of the final PRP, and the platelet adhesion on the polymeric composite was determined. The absorbance of each well was then measured using a 96 well plate reader (Biotek), and the number of platelets adhered was determined using the calibration curve. All protocols pertaining to the use of whole blood and platelets were approved by the University of Georgia.

2.2.6 In vitro analysis of inhibition of bacterial adhesion on the polymer surface

In order to evaluate the effectiveness of copper, nanoparticle assisted NO release from SNAP as a potent antibacterial strategy, a modified version of standard bacterial adhesion test was performed.[63] Antibacterial activity of the Cu-SNAP composites was investigated using common causative agents of blood infections: gram-positive *Staphylococcus aureus* (*S. aureus*) and gram-negative *Pseudomonas aeruginosa* (*P. aeruginosa*). These bacteria are among the most common causes of nosocomial bloodstream infection that can form embedded biofilm matrices on indwelling biomedical devices.[64] To investigate the antibacterial attribute of the fabricated films, single isolated colonies of *P. aeruginosa* and *S. aureus* strains were obtained from pre-culture LB agar Petri dishes, inoculated in 5 mL of LB medium, and incubated for 14 h at 120 rpm and 37°C. To ensure that the bacteria was in actively dividing phase, the optical density of the culture was measured at 600 nm ($O.D_{600}$) using UV-vis spectrophotometer (Thermo scientific Genesys 10S UV-Vis). To wash off the traces of the LB medium, the culture was centrifuged for 8 min at 2500 rpm, the supernatant was discarded, and an equivalent amount of sterile phosphate buffer saline (PBS, pH 7.4) was added and centrifuged again for 8 min at 2500 rpm. Fresh PBS was then added to the formed cell pellet and was vortexed for 30 secs to suspend the cells to be used in the study. The $O.D_{600}$ of the cell suspension in PBS was measured, using PBS as blank, and adjusted to get 10^8-10^{10} CFU/mL. Each of the test films (SNAP, 1 wt% Cu-NPs, 3 wt% Cu-NPs, 1 wt% Cu-SNAP, 3 wt% Cu-SNAP) and the control films (Carbosil) were exposed to 2 mL of *S. aureus* suspension and *P. aeruginosa* individually in 15 mL sterile tubes (n=3). This was followed by incubating the films at 37 °C for 24 h at a shaking speed of 120 rpm. After 24 h films were taken out of suspended bacterial culture and rinsed with sterile PBS to remove any loosely bound bacteria. To ensure that all the bound bacteria are detached from the films, the films were transferred to 2 mL of fresh PBS, sonicated with Omni-TH sonicator for 1 min followed by 30 s of vortex mixing. The resulting bacterial suspension was serially diluted (10^{-1} to 10^{-5}) and plated in Petri dishes with LB agar medium and incubated at 37 °C for 24 h. Post

incubation, the CFUs were counted and the attached viable CFU per surface area (cm^2) of the films were compared to the control and test films. The CFU per surface area of the films were counted and compared with controls to evaluate their efficacy to inhibition bacterial adhesion on the surface of the films. All protocols pertaining to the use of bacterial strains were used in a BSL-2 facility approved by the University of Georgia.

$$\%\ Bacterial\ inhibition = \frac{\left(\frac{CFU}{cm^2}\ in\ control\ samples - \frac{CFU}{cm^2} in\ test\ samples\right)\ X100}{\frac{CFU}{cm^2}\ in\ control\ samples}$$

2.2.7 Cu leaching studies using Inductively Coupled Plasma Mass Spectroscopy (ICP-MS)

Inductively coupled plasma mass spectrometry (ICP-MS) is an ultrasensitive method for the detection of specific elements. A VG ICP-MS Plasma Quad 3 instrument was used to detect the exact concentration of copper in sample leachates. The polymeric films with Cu-NPs (1 wt% Cu-NPs, 3 wt% NPs, 1 wt% Cu-SNAP and 3 wt% Cu-SNAP) were tested for potential copper diffusion. To obtain the leachate, 10 mg of the polymer films were soaked in 10 mL DMEM medium (concentration 1 mg per mL of medium) for 24 hours. Thereafter, the films were removed and the medium was tested for leached ^{65}Cu isotope following a previously established protocol.[65]

2.2.8 In vitro cytotoxicity assay

The cytotoxicity study was conducted to demonstrate any potential leaching from Cu-Carbosil, SNAP and Cu-SNAP film and its toxic effects on 3T3 mouse fibroblast cell line (ATCC-1658) in accordance with the ISO 10993 standard. The manufacturer's (Sigma-Aldrich) protocol was followed while using the Cell Counting Kit-8 (CCK-8) which utilizes highly water-soluble tetrazolium salt. WST-8 [2-(2-methoxy-4-nitrophenyl)-3-(4-nitrophenyl)-5-(2,4-disulfophenyl)-2H-tetrazolium monosodium salt] is reduced by dehydrogenases in live cells to give formazan (an orange color product) detected at 450 nm. Thus, the number of living cells is directly proportional

to the amount of the formazan dye generated by dehydrogenases in cells. The detection sensitivity of CCK-8 solution is higher than other tetrazolium salts such as MTT, MTS, XTT or WST-1 and unlike MTT it does not require the killing of cells for the assay. All protocols pertaining to the use of mammalian cells were approved by the University of Georgia

Cell culture: Mouse fibroblast cells were cultured in 75 cm^2 T-flask DMEM medium with 4.5g/L glucose and L-glutamine, 10% fetal bovine serum (FBS) and 1% penicillin-streptomycin and incubated at 37^oC in a humidified atmosphere with 5% CO_2. After the confluency reached 90%, the cells were trypsinized (0.18% trypsin and 5 mM EDTA) and 5000 cell/mL were seeded in 96 well plates.

Preparation of leachates: The polymeric films were allowed to leach in the DMEM medium by following the ISO standards (ISO 10993-5:2009 Test for in vitro cytotoxicity) to collect the extract (if any). Extracts from control and test films were obtained by soaking 10 mg of the sterilized films in 10 mL DMEM medium (concentration of 1 mg/mL of medium) in an amber color vial (to prevent NO release by light stimulation) and incubated for 24 h at 37^oC. After 24 h, the films were removed, and the resulting extracts were kept in the refrigerator (4^oC) prior to using them in the cell culture experiment.

Determination of degree of cytotoxicity: The suspension of cultured cells (5000 cell/mL) was inoculated (100 µL /well) in a 96-well plate. The 96-well plate was then pre-incubated in a humidified incubator at 37^oC, 5% CO_2 for 24 h. After 24 h, 10 µL of the different leachates were added (n=5) and incubated for another 24 h to allow the potential toxicants to act on cells. To each of the wells, 10 µL of the CCK-8 solution was added and incubated for 3 h. To avoid the background interference, 100 µL of the DMEM medium was added in 4 of the wells. The absorbance was measured at 450 nm and compared to cells grown in the leachate containing culture. Results were reported as percentage of cell viability (percentage of control) after subtracting the average absorbance of the medium (without cells) as follows.

$$\%\ Cell\ Viability = \frac{\text{Absorbance of the test samples}}{\text{Absorbance of the control samples}} \times 100$$

2.2.9 Statistical analysis

All data is reported as a mean ± standard deviation. All statistical comparisons were done using standard two-*tailed* *t*-test with unequal variance. The significance is stated for comparisons with $p < 0.05$.

3. Results and Discussion

3.1 NO flux analysis

As demonstrated in Figure 2.1, the NO release from the SNAP containing polymeric composites was enhanced by applying two layers of copper nanoparticles (Cu-NPs) and finally top-coated with Carbosil to prevent leaching of Cu-NPs and SNAP. The NO release mechanism involves oxidation of Cu^0 nanoparticles to Cu^{2+} ions in the presence of moisture. The resulting Cu^{2+} ions reduce to the active species, Cu^+ ions in the presence of reducing agents like thiolates (RS^-) that exist in the physiological environment (Figure 2.2). Ultimately, the Cu^+ ions catalyze the generation of NO from RSNOs such as SNAP.[34, 66] The NO flux from the SNAP films with and without Cu-NPs was measured using Nitric oxide analyzer (NOA) at different time points. Thiolate stability and formation at physiological pH has been investigated in an earlier study by D. Lyn. H. Williams.[67] The NO flux from the SNAP films with and without Cu-NPs was measured using Nitric oxide analyzer (NOA) at different time points. Thiolate stability and formation at physiological pH has been investigated in an earlier study by D. Lyn. H. Williams.[67] Theoretically, all the buffers (including PBS, DMEM, and blood) when properly adjusted to a pH of 7.4, will produce similar NO release via the previously discussed reaction mechanism (Figure 2.2).

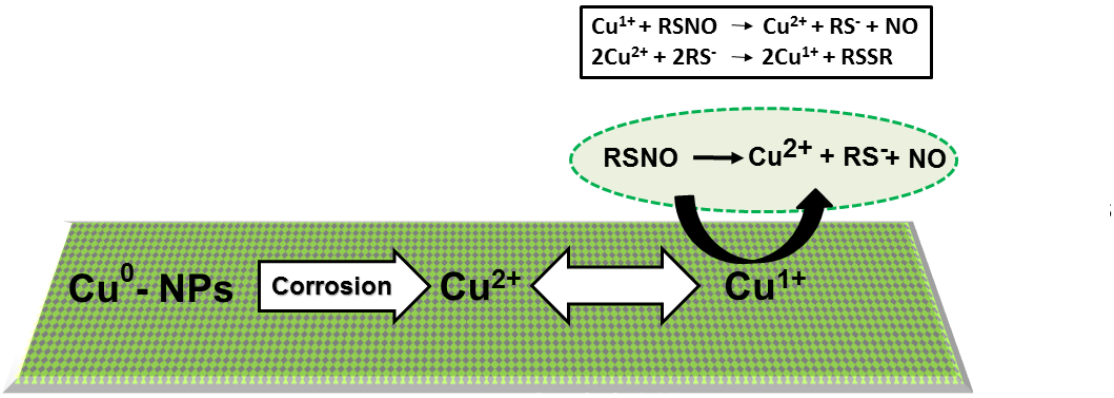

Figure 2.2. The schematic representing the mechanism of nitric oxide (NO) release from an RSNO such as SNAP. The mechanism involves oxidation of Cu^0 nanoparticles to Cu^{2+} ions in the presence of water.

Films containing 1 wt% Cu-SNAP and 3 wt% Cu-SNAP had increased flux values of 4.48 ± 0.5 × 10^{-10} $mol^{-2}min^{-1}$ and 4.84 ± 0.3 × 10^{-10} $mol^{-2}min^{-1}$, respectively. This NO flux corresponds to the higher end of physiological levels of NO released by endothelial cells that line the blood vessels. Incorporation of 5 wt% Cu-NPs in the SNAP films showed a drastic increase in the NO-release (11.7 ± 3.6 x10^{-10} mol min^{-1} cm^{-2}) from these materials was almost two times higher than the physiological levels, and therefore not used in the following *in vitro* studies. While the release of NO from 1 wt% and 3 wt% Cu-NPs films are similar initially, 3 wt% films sustained a higher release rate over the first 24-hour period. Films containing 5 wt% Cu-NPs showed similar release rates to those containing 3 wt% Cu after the first 24-hour period. These results demonstrate that the optimal concentration of Cu-NPs in the polymeric NO releasing composites presented in this study lies between 0-3 wt% for physiological release rates. Higher Cu-NPs concentrations, however, can provide increased NO fluxes well within physiological limits after 24 h. The decrease in NO flux for all composition can theoretically be explained on the basis of the ability of the Cu^{2+} to be reduced back to Cu^{1+} which acts as the ultimate catalyst enhancing NO release from SNAP, as Cu^{2+} does not contribute to the catalytic release of NO.[68] Initially, the films contain both crystallized regions of SNAP, as well as SNAP that is homogeneously incorporated within

the polymer matrix.[69] This combination of monodisperse SNAP and crystallized regions contribute to the higher initial release rates of NO, followed by extended release rates that can be maintained for > 20 d.[52]

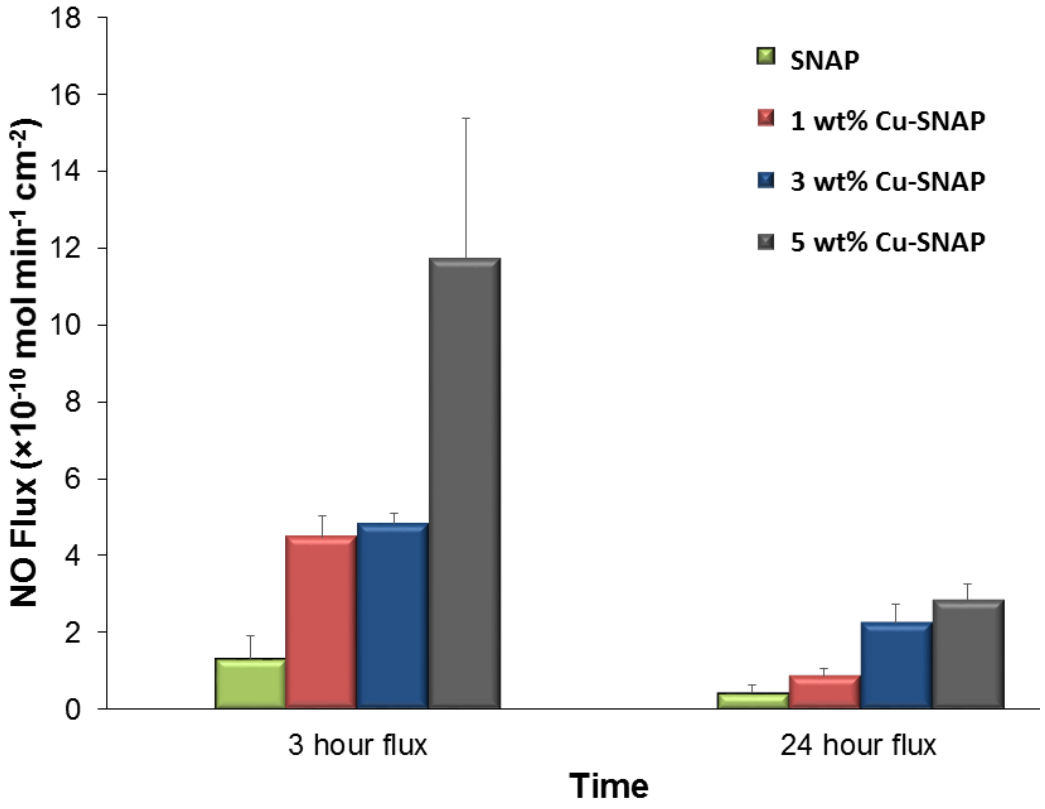

Figure 2.3. Nitric oxide (NO) flux analysis of SNAP composites with or without copper nanoparticles (Cu-NPs) at different time points. As illustrated in the figure, there is a proportional increase in the NO flux release from the composites with increase in Cu-NPs concentration. The 1 wt% Cu-SNAP and 3 wt% Cu-SNAP films possess NO flux in the upper end of the physiological NO flux range while 5 wt% Cu-SNAP films showed almost two times NO flux than physiological range. P-values < 0.05 were used for comparison. The error bar represents standard deviation.

The initial state of the composites allows for SNAP and Cu-NPs within the film to have minimum separation, leading to the reactive species (RS^-) being readily available for the reduction of Cu^{2+} to Cu^{1+}, where the catalytic activity can be maintained. Once SNAP from the homogeneous region is depleted and NO release is only from the crystallized regions, the catalytic ability of Cu ions to continue NO release can be limited by diffusion of Cu^{2+} to the crystallized regions to be reduced by the free thiols. Therefore, increasing the concentration of Cu-NPs will

increase the available Cu^{2+} ions to diffusion to these crystallized regions, which is observed in the 24-hour measurements. In the past, when used *in vivo,* we demonstrated that polymeric materials with incorporated NO donors could achieve higher levels of NO release due to the availability of free ascorbic acid in the blood to reduce Cu^{2+} to Cu^{1+},[20, 70] and could provide NO release from systemic RSNOs as well.[34] Control over this reduction reaction would result in lower concentrations of Cu-NPs required in the films to sustain increased NO release while lowering the initial release rate.

3.2 Surface morphology analysis of copper coats on polymeric composites

Surface morphology is an important parameter to decide the translational success of an antimicrobial polymer for medical application as surface morphologies can alter blood protein and bacterial adhesion on the surface of the polymer. No significant Cu-NPs traces were found on film's surface with 3 wt% copper observed as illustrated by the images captured from Surface Electron Microscopy (SEM) at an accelerating voltage of 5 kV. At a magnification of 225X, the surface of carbosil control looked very similar to the Surface with 3 wt% Cu-NPs. This assures that the presence of a top coat of the Cu-NPs does not alter surface morphology of the polymeric composite (Figure 2.4).

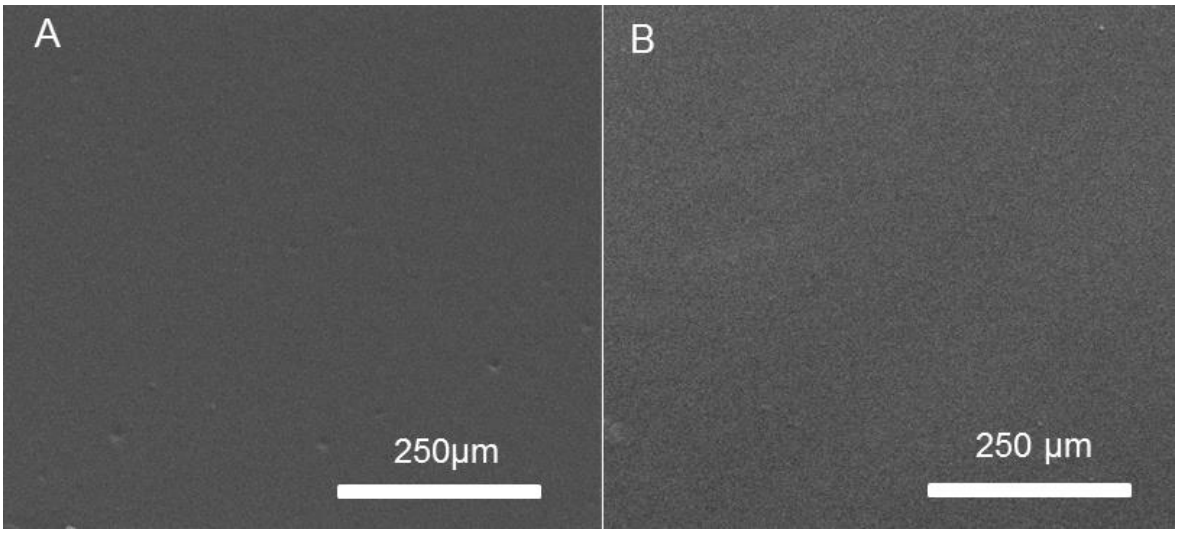

Figure 2.4. Representative image of A) Carbosil (control) and B) Carbosil films with 3 wt% Cu-NPs taken at an accelerating voltage of 5 kV (225x magnification). Scale bar represents 250 microns. As depicted, the top layer of films with and without copper coats are similar in their surface morphologies.

3.3 Detection of copper leaching

Detection of the amount of copper leaching from the polymeric composites is crucial for the preclinical success of biomaterial since a high diffusion of copper ions from the polymers will highly influence cell cytotoxicity and bacterial adhesion studies. After 24 h of soaking 10 mg of the polymer films in 5 mL DMEM medium (concentration 2 mg per mL of medium) to allow any potential leaching, the standard ICP-MS method was performed to monitor copper leaching from the films. The results of the detected copper leaching are shown in Table 1. The Cu-SNAP films showed a slightly higher amount of leached copper than films only containing Cu-NPs but still much below the recommended limit. The increase for the Cu-SNAP films is most likely due to the formation of nitric acid from the conversion of NO to nitrites within the medium.[71] Copper is known to be highly soluble in nitric acid, so the presence of even trace amounts could dissolve a portion of the copper within the polymer matrix. The highest recorded levels (306.9 ± 99.5 ppb) from the

films leachate in this study were well below cytotoxic concentrations towards mammalian cells. Earlier *in vitro* reports on copper cytotoxicity on a variety of mammalian cell lines have shown that cell viability stays at 100% until the concentration of copper reaches approximately 1000 ppb.[72-74] In a previous study, 10 wt% of copper nanoparticles have been blended within blood contacting polymers that demonstrated the negligible amount of leaching.[34] This demonstrates even further the negligible amount of copper being leached into the medium and its innocuous impact on biocompatibility.

3.4 Effects of Cu/SNAP on platelet adhesion

Many blood contacting devices such as vascular catheters have issues with blood compatibility due to the formation of a blood clot on device surface after implantation, therefore, the ability of a biomaterial to prevent platelet adhesion is an important parameter to validate the hemocompatibility. The ability for Cu-NPs incorporating SNAP films to prevent platelet adhesion was determined using an LDH assay after exposure to porcine platelet-rich plasma (PRP) for 2 h. Freshly drawn porcine blood was drawn 9:1 into 3.4% sodium citrate and processed to give a final recalcified platelet-rich solution with a total platelet count ca. 2×10^8 platelets/mL as

Table 2.1. The copper leachate concentration from polymeric composite and the relative leaching in DMEM medium as compared to the original amount of copper present in each film type.

Sample	Measured Copper Leachate (PPB)	% Copper Leaching (Relative to Initial Cu concentration)
1 wt% Cu-NPs	100.3±17.48	1.06±0.185
1 wt% Cu-SNAP	221.5±47.80	2.34±0.506
3 wt% Cu-NPs	93.37±5.995	0.329±0.0212
3 wt% Cu-SNAP	306.9±99.50	1.08±0.351

described in methods section 2.2.5. Total platelet adhesion to each composite composition is shown in Figure 2.5. The combination of 10 wt% SNAP with 3 wt% Cu nanoparticles (3% Cu-SNAP) provides the largest decrease in platelet adhesion, showing a 92% reduction when compared to Carbosil controls. This is expected as the combination of SNAP with 3 wt% Cu particles provided the highest level of NO release (p = 0.003). Similarly, as the little difference was observed between 1 wt% Cu-SNAP films and 3 wt% Cu-SNAP films in NO release, insignificant changes in the platelet adhesion was observed. However, the higher level of NO release provided by the 3 wt% Cu composites was observed to have slightly decreased platelet adhesion. The presence of Cu particles alone provides significant reduction in platelet adhesion when compared to Cu-Carbosil controls without SNAP (1 wt% Cu-Carbosil: 72% reduction, p = 0.006; 3 wt% Cu-Carbosil: 82% reduction, p = 0.003). The ability for low levels of NO generated by the reaction of the endogenous RSNOs present in the plasma (10 μM) with Cu-NPs demonstrate that while low levels of NO can reduce platelet adhesion drastically (>70%), the release of NO at the upper limit of the physiological release rates does significantly reduce platelet activation and adhesion when compared to lower levels of NO release.

The ability for the Cu assisted the generation of NO from natural RSNOs has been shown *in vivo,* reducing thrombus formation in a rabbit extracorporeal circuit model after 4 h ca. 40%.[34] Larger reductions in platelet adhesion seen in this study may result from using PRP, while the previous work was conducted *in vivo,* where hemoglobin present in the red blood cells may bind to NO, limiting the efficacy to prevent platelet adhesion. While Cu particle size for generation of NO from natural RSNOs has yet to be optimized, the focus of this work was to provide catalytic control of NO released from blended RSNOs within the polymer film, and not the generation of NO from naturally occurring RSNOs within the blood. However, this result shows that while the physical blending of NO donors into polymeric materials is limited in the lifetime of the NO release, the NO generating capability of the Cu ions within the polymer can continue to provide activity to prevent the adhesion of platelets to the material surface, providing controlled and predictable

release rates from both regimes (NOrel and NOgen), making this material ideal for long term blood contacting devices such as vascular catheters.

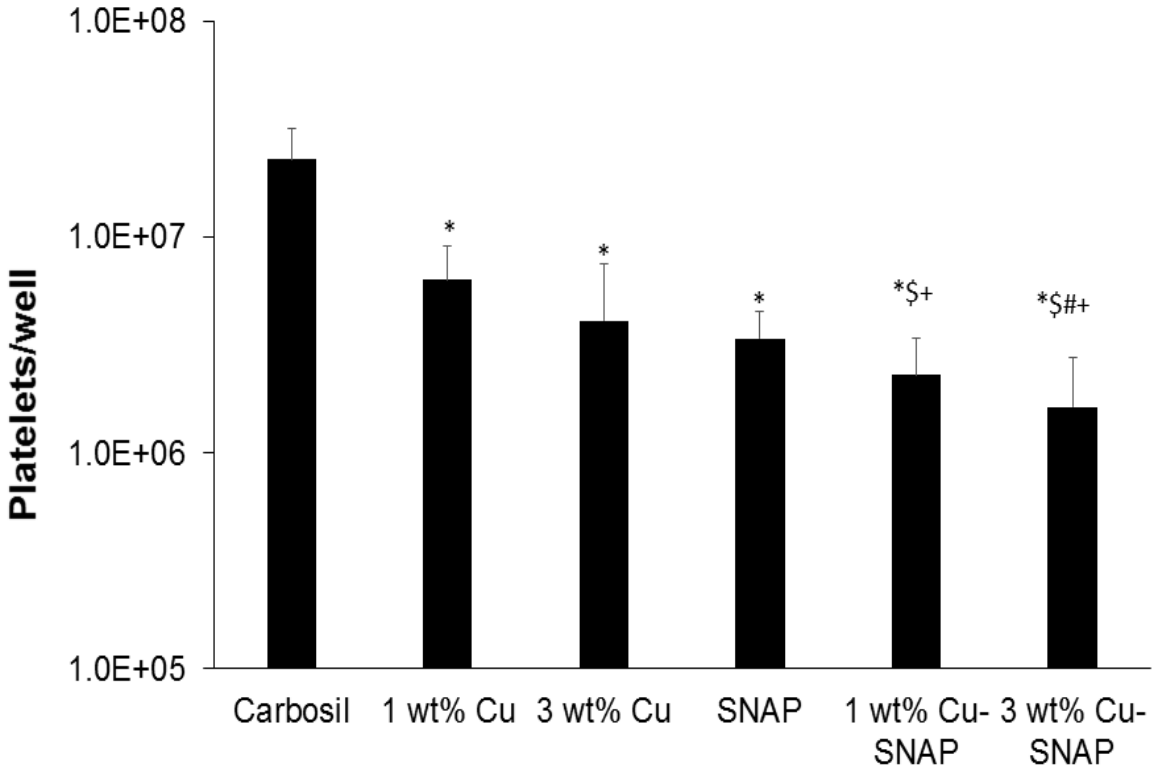

Figure 2.5. The graphical representation of the LDH assay results. P-values < 0.05 were considered significantly different. Note: * indicates significant difference with respect to (w.r.t) the control; $ indicates significant difference w.r.t 1 wt% Cu-Carbosil films; # indicates significant difference w.r.t the 3 wt% Cu-Carbosil films and + indicates significant difference w.r.t the SNAP films. The error bar stands for standard deviation.

3.5 Inhibition of gram positive and negative bacteria adhesion on the polymer surface

Biomedical device-related infections (BDRIs) are one of the major causes of morbidity and the associated healthcare cost. The gram-positive *S. aureus* and gram-negative *P. aeruginous* are among the most common causative agents of hospital-acquired infections.[74] *Invitro* bacteria, testing demonstrates that the Cu-NPs assisted NO release is effective in reducing the population of viable bacterial cells on polymeric films against both grams positive and negative bacteria (Figure 2.6). Even individually NO donor (SNAP), as well as Cu-NP controls, inhibited

both gram positive and gram-negative bacteria. The antibacterial properties of copper are due to its oligodynamic effect while the bactericidal properties of NO are due to denaturation of enzymes, deamination of DNA and lipid oxidation in pathogens.[45] In the presence of Cu-NPs coats the catalytic activity of copper increase the NO release from the SNAP thus enhancing the bacterial inhibition as compared to SNAP films alone. The NO flux release was directly proportional to the amount of Cu-NPs present and hence more bacteria-killing on the surface of the film. Table 2 shows the bacterial colony forming units per surface area of the composite (CFU/cm^2) that were present on the surface of each of the films. The NO flux is inversely proportional to the bacterial CFU/cm^2 showing that the enhanced NO release by Cu-SNAP films inhibited the bacterial growth significantly.

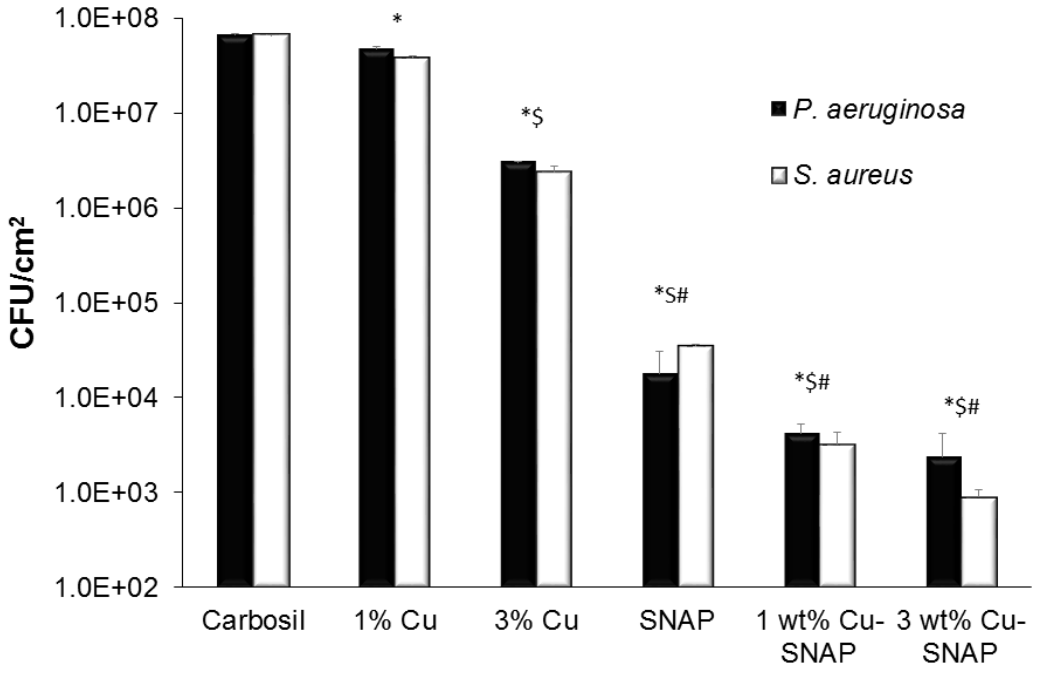

Figure 2.6. Graphical representation of inhibition of viable gram-negative (*P. aeruginosa*) and gram-positive (*S. aureus*) bacteria strains on the surface of control and test composites P-values < 0.05 were considered significantly different. Note: *, $, and # indicate significant difference in CFU/cm^2 of both bacteria compared to control, 1 wt% Cu, and 3 wt% Cu-Carbosil composites, respectively. The error bar represents standard deviation.

Overall there was a marked reduction of up to 2 logs by SNAP films while Cu-NPs coated films showed bacterial inhibition up to 5 logs. Among all the tested films, the 3wt% Cu-SNAP films with allowed the least amount of bacterial colony forming to grow per unit surface area of the composite (CFU/cm^2) as shown in Figure 2.6. The observed difference between the antibacterial effect of NO on gram-negative and gram-positive bacteria can be attributed to differences in their cell membrane properties. In the presence of Cu-NPs coats, the catalytic activity of copper increases the NO release from SNAP thus enhancing the bacterial inhibition as compared to the SNAP films alone. Table 2 shows a comparative quantification of the bacterial colony forming units per surface area of the composite (CFU/cm^2) that were present on the surface of each type of the films.

Table 2.2. The comparative analysis of bacterial CFU/cm^2 grown on with Carbosil, Cu-NPs, SNAP, and Cu-SNAP composites.

Films	NO Flux ($\times 10^{-10}$ mol^{-2}min^{-1}cm^{-2}) 0h	24h post bacteria	CFU/cm^2 *(S. aureus)*	CFU/cm^2 (*P. aeruginosa*)
Control (Carbosil)	--	--	6.7± 0.1 x 10^7	6.8 ± 0.1 x 10^7
1 wt% Cu	--	--	3.8 ± 0.22 x 10^7	4.8 ± 0.22 x 10^7
3 wt% Cu	--	--	2.4 ± 0.33 x 10^6	3.1 ± 0.33 x 10^6
SNAP	1.31 ± 0.6	0.43 ± 0.1	3.5 ±1.3 x 10^4	1.8 ± 1.3 x 10^4
1 wt% Cu-SNAP	4.48 ± 0.5	0.87± 0.1	3.2 ±1.1 x 10^3	4.2 ± 1.1 x 10^3
3 wt% Cu-SNAP	4.84 ± 0.2	2.25 ± 0.3	8.9 ±1.8 x 10^2	2.4 ± 1.8 x 10^2

The NO flux is inversely proportional to the bacterial CFU/cm^2 showing that the enhanced NO release by Cu-SNAP films inhibited the bacterial growth significantly. This is clear from the results that the higher NO flux can result in better bacterial inhibition as compared to the controls.

The NO flux is inversely proportional to the bacterial CFU/cm^2 showing that the enhanced NO release by Cu-SNAP films inhibited the bacterial growth significantly. This is clear from the results that the higher NO flux can result in better bacterial inhibition as compared to the controls. In a biofilm, the antibiotic-resistant bacteria can encase themselves in a hydrated matrix of polysaccharide and protein thus defending themselves effectively against the action of antibiotics.[32, 75] The low molecular weight of NO allows penetrating through the matrix in the biofilm which gives it an extra advantage over antibiotics and silver-based antibacterial strategies.[76-77] Having a higher influx of NO allows a higher penetration of the NO through the biofilm and thus killing the bacteria with comparatively significantly lesser dose in situations where other antibacterials are mostly ineffective. Furthermore, the use of NO is unlikely to stimulate the production of resistant strains due to rapid reduction of microbial load.[40, 46-47] In the past, we have shown the antibacterial attributes of NO releasing membrane against *A.baumanni*, *S. aureus*, *E. coli*, *L. monocytogenes, and E. faecalis.*[44-53] In addition, other published reports have also shown a significant reduction in bacterial growth (1-24 h studies) owing to the antibacterial properties of NO.[38, 41, 43] However, these studies have reported the effect of bacterial exposure on NO flux profile. Hence NO release was also measured from films after the bacterial studies to confirm NO was still being released from the residual SNAP in the films. The results showed that the residual NO flux after the bacterial exposure was still maintained within the physiological levels demonstrating that these films can be used beyond 24 h to kill bacteria if needed (Figure 2.7). As Cu-NPs has also been demonstrated to provide antibacterial properties, further optimization can be done to not only tune the NO release for the specific application but also provide the highest antibacterial activity between the level of Cu and NO release.

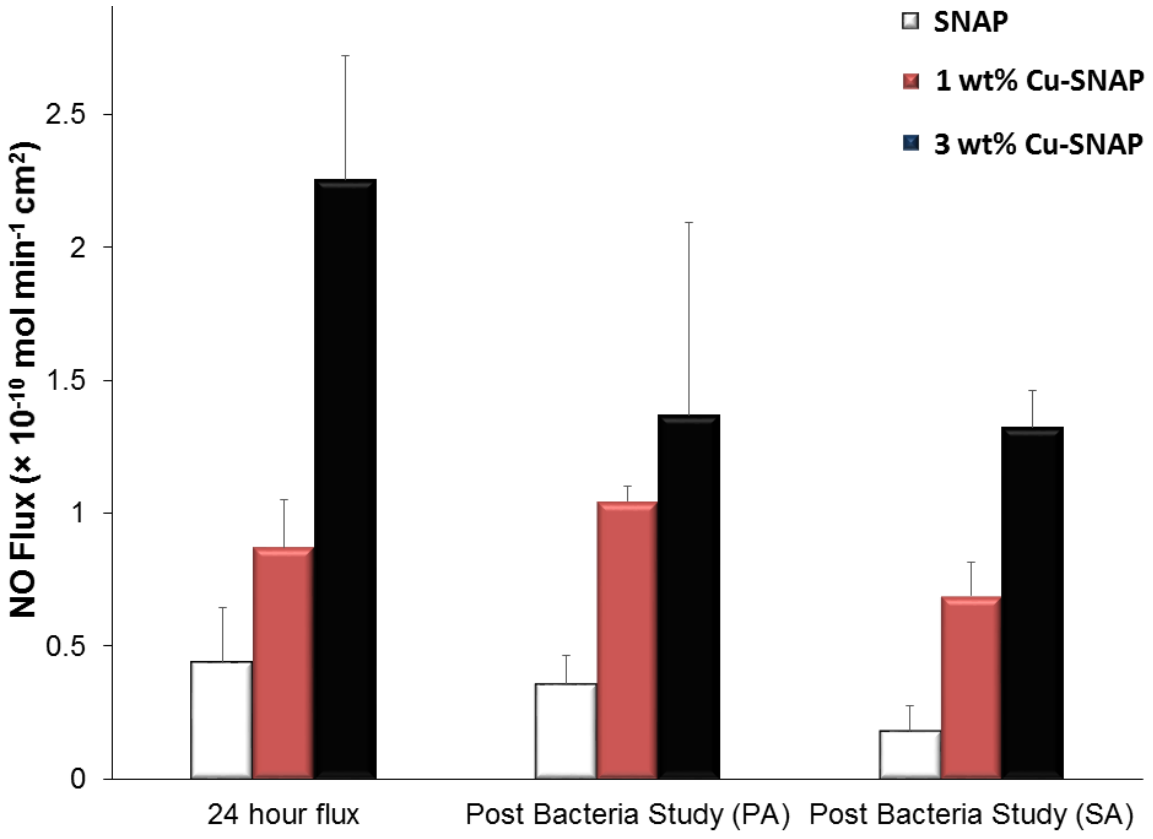

Figure 2.7. The NO flux release from the SNAP, 1 wt% Cu-SNAP and 3 wt% Cu-SNAP films at 24th hour prior to exposing them to the bacteria (left most bars). Post bacterial exposure individually with *Pseudomonas aeruginosa* (PA) and *Staphylococcus aureus* (SA) for a period of 24 h, the NO flux released was measured again and found to be in the physiological range. P-values < 0.05 were used for comparison. The error bar represents standard deviation.

3.5 Cytotoxicity of polymeric films leachates

As per the ISO 10993 standards, the purpose of performing biocompatibility testing of the medical device is to investigate its undesirable physiological effects such as cytotoxicity and to validate its fitness for human use. Recent studies have shown NO releasing strategies to be highly effective for controlling bacterial infection but the NO flux was much higher than the upper range of physiological NO flux.[78] Although antibacterial characteristic and platelet inactivation are one of the most important parameters for developing medical devices, it should not be at the cost of the host mammalian cells due to cytotoxicity. Hence achieving maximum bacterial inhibition and platelet activation while ensuring that these NO releasing composites are

not toxic to mammalian cells was another important objective of the present study. In the present study, we evaluated the relative cytotoxicity of potential leachates from the films with SNAP and/or Cu-NPs with respect to the control Carbosil films using cell counting kit-8 (CCK-8) assay after soaking the films in the medium for 24 h. The number of viable cells in the composites with SNAP, 1 wt%, and 3 wt% Cu-NPs are very similar relative to the control Carbosil composites demonstrating that these composites are biocompatible to the mammalian fibroblast cells (Figure 2.8). Morphologically, the fibroblast cells maintained their regular dendritic shapes as demonstrated by optical images obtained at 10X magnification using EVOS XL microscope. These results are in line with the Cu leachate detection analysis (Section 3.3) which demonstrated the negligible amount of copper (306.9 ppb) in the leachates from films, which is much below the recommended safety limit (2000 ppb) by the WHO. Furthermore, any leaching of SNAP, or more likely NAP (N-acetyl-penicillamine) and possibly dimers of NAP, would ultimately hydrolyze to penicillamine (and acetic acid). Low level of penicillamine (FDA approved) is widely used for heavy metal poising in humans as per FDA recommendation.[13] The NO flux exhibited by the endothelial cells in the blood vessels lining is in the range of 0.5-4.0 x 10^{-10} mol min^{-1} cm^{-2} [15] Theoretically, a flux closer to physiological range should not exhibit a cytotoxic response to the host. cells. The NO flux released by 1 wt% Cu-SNAP and 3% Cu-SNAP were reported to be very close to the upper range of endogenous NO flux, i.e 4.48 ± 0.5 x 10^{-10}, 4.8 4± 0.3 x 10^{-10} mol min^{-1} cm^{-2} respectively, and hence justify the absence of cytotoxicity by the polymeric films as a response to SNAP or its by-products leaching (if any) in the medium. In the past, polymeric films with 10 wt% SNAP are shown to be hemocompatible and biocompatible with mammalian cells.[55, 79] Overall this *in vitro* study showed these NO releasing polymeric composite containing 1 wt% or 3 wt% Cu-NPs in combination with 10% SNAP are safe towards mammalian cells through the negligible amount of leaching. Further testing in animal models would be helpful to establish *in vivo* data to reconfirm the efficacy of these composite in pre-clinical settings.

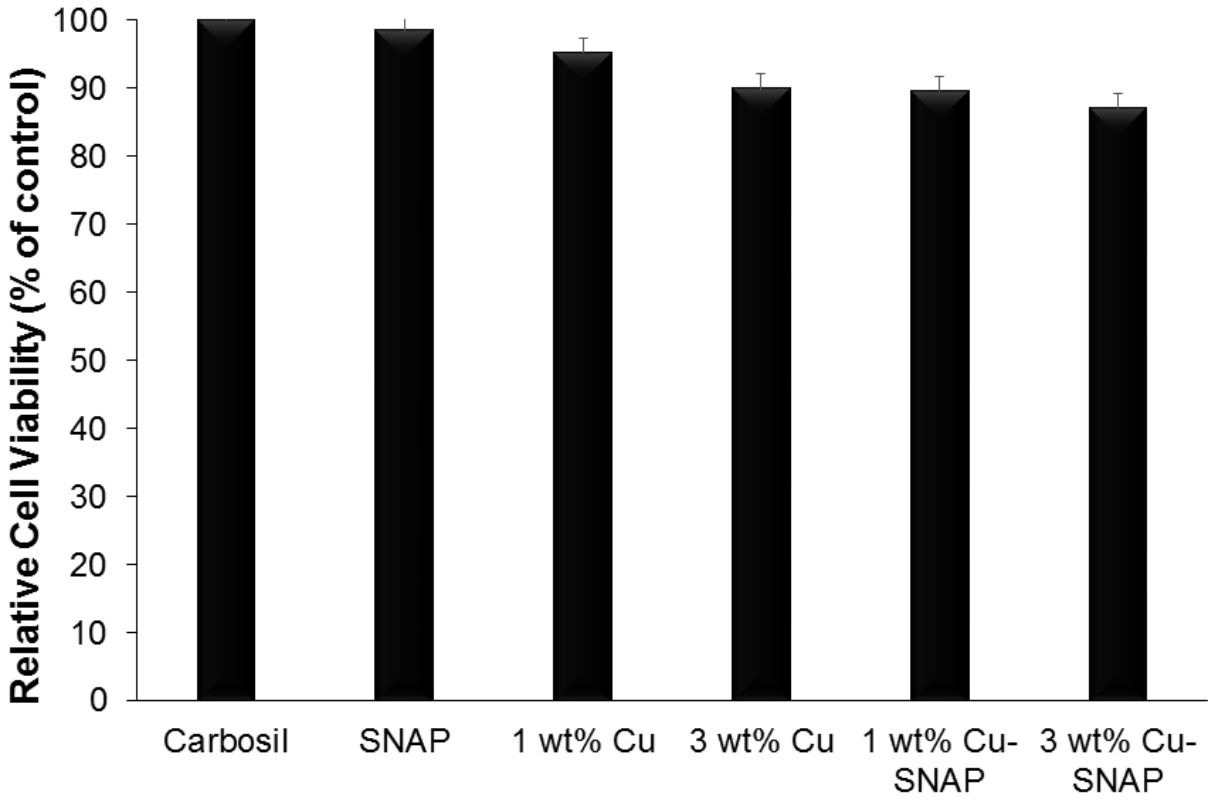

Figure 2.8. Graph showing the non-cytotoxic nature of the films using CCK-8 assay performed *in vitro* on mouse fibroblast 3T3 cell line with 24 h leachable from the composites. P-values < 0.05 were used for comparison. The error bar represents standard deviation.

4. Conclusions

Due to the dose-dependent effect of NO, achieving a local and continuous release of NO from the biomedical implants is a desirable attribute for their clinical success. In this study, controlled NO release from SNAP containing Carbosil films was achieved by incorporating Cu-NPs coatings on the SNAP films. Concentrations of Cu-NPs above 3 wt% were found to increase the release rate of NO from the polymer above physiological levels. While the SNAP films exhibit a NO flux of $1.32 \pm 0.6 \times 10^{-10}$ mol min^{-1} cm^{-2}, utilizing the Cu-NPs increases the NO release up to $4.84 \pm 0.3 \times 10^{-10}$ due to the catalytic activity of copper. This resulted in a significant reduction (up to 5 logs) in bacterial growth on the polymer surface. The Cu-SNAP combination could prevent >92% of platelet adhesion upon exposure to porcine PRP for 2 h. The ICP-MS study

showed that the leaching of copper from these films is below the toxicity limit. Furthermore, the Cu-SNAP combination was found to be non-cytotoxic to mammalian cells as demonstrated by the cytotoxicity assay performed on the mouse fibroblast 3T3 cell line. Overall the leaching and cytotoxicity studies combinedly provide evidence that these treatments may be safe for clinical use. Overall, when compared with the conventional approaches, the study recommends that the Cu-SNAP composites can provide an increased antibacterial activity for biomedical device coatings without causing drug resistance and cytotoxicity associated with currently available antimicrobial agents. The amount of NO release can be tuned by varying the copper concentration, thus expanding the use of Cu-SNAP combination for multiple biomedical applications. Overall, these composites are exceptionally promising to fabricate a new generation of medical devices with controlled NO release, reduced platelet adhesion and superior degree of microbial inhibition with potential biocompatibility.

References

(1) An, Y. H.; Friedman, R. J., *Handbook of bacterial adhesion: Principles, methods, and applications*. Springer Science & Business Media: **2000**; Vol. 204.

(2) Harris, L.; Tosatti, S.; Wieland, M.; Textor, M.; Richards, R. Staphylococcus aureus adhesion to titanium oxide surfaces coated with non-functionalized and peptide-functionalized poly (l-lysine)-grafted-poly (ethylene glycol) copolymers. *Biomaterials* **2004,** *25* (18), 4135-4148.

(3) Daniels, K. R.; Frei, C. R. The united states' progress toward eliminating catheter-related bloodstream infections: Incidence, mortality, and hospital length of stay from 1996 to 2008. *Am. J. Infect. Control* **2013,** *41* (2), 118-121.

(4) Gorbet, M. B.; Sefton, M. V. Biomaterial-associated thrombosis: Roles of coagulation factors, complement, platelets and leukocytes. *Biomaterials* **2004,** *25* (26), 5681-5703.

(5) Knowles, R. G.; Moncada, S. Nitric oxide synthases in mammals. *Biochem. J.* **1994,** *298* (Pt 2), 249.

(6) Stuehr, D. J. Mammalian nitric oxide synthases. *Biochimica et Biophysica Acta (BBA)-Bioenergetics* **1999,** *1411* (2-3), 217-230.

(7) Radomski, M. W.; Vallance, P.; Whitley, G.; Foxwell, N.; Moncada, S. Platelet adhesion to human vascular endothelium is modulated by constitutive and cytokine induced nitric oxide. *Cardiovasc. Res.* **1993,** *27* (7), 1380-1382.

(8) Pant, J.; Gao, J.; Goudie, M. J.; Hopkins, S. P.; Locklin, J.; Handa, H. A multi-defense strategy: Enhancing bactericidal activity of a medical grade polymer with a nitric oxide donor and surface-immobilized quaternary ammonium compound. *Acta Biomater.* **2017,** *58*, 421-431.

(9) Sundaram, J.; Pant, J.; Goudie, M. J.; Mani, S.; Handa, H. Antimicrobial and physicochemical characterization of biodegradable, nitric oxide-releasing nanocellulose–chitosan packaging membranes. *J. Agric. Food Chem.* **2016,** *64* (25), 5260-5266.

(10) Pant, J.; Goudie, M. J.; Chaji, S. M.; Johnson, B. W.; Handa, H. Nitric oxide releasing vascular catheters for eradicating bacterial infection. *Journal of Biomedical Materials Research Part B: Applied Biomaterials*.

(11) Frost, M. C.; Reynolds, M. M.; Meyerhoff, M. E. Polymers incorporating nitric oxide releasing/generating substances for improved biocompatibility of blood-contacting medical devices. *Biomaterials* **2005,** *26* (14), 1685-1693.

(12) Reynolds, M. M.; Frost, M. C.; Meyerhoff, M. E. Nitric oxide-releasing hydrophobic polymers: Preparation, characterization, and potential biomedical applications. *Free Radical Biol. Med.* **2004,** *37* (7), 926-936.

(13) Carpenter, A. W.; Schoenfisch, M. H. Nitric oxide release: Part ii. Therapeutic applications. *Chem. Soc. Rev.* **2012,** *41* (10), 3742-3752.

(14) Pant, J.; Goudie, M.; Brisbois, E.; Handa, H., Nitric oxide-releasing polyurethanes. In *Advances in polyurethane biomaterials*, Elsevier: **2016**, pp 417-449.

(15) Vaughn, M. W.; Kuo, L.; Liao, J. C. Estimation of nitric oxide production and reactionrates in tissue by use of a mathematical model. *Am. J. Physiol.: Heart Circ. Physiol* **1998,** *274* (6), H2163-H2176.

(16) Mcmullin, B. B.; Chittock, D. R.; Roscoe, D. L.; Garcha, H.; Wang, L.; Miller, C. C. The antimicrobial effect of nitric oxide on the bacteria that cause nosocomial pneumonia in mechanically ventilated patients in the intensive care unit. *Respir. Care* **2005,** *50* (11), 1451-1456.

(17) Reynolds, M. M.; Hrabie, J. A.; Oh, B. K.; Politis, J. K.; Citro, M. L.; Keefer, L. K.; Meyerhoff, M. E. Nitric oxide releasing polyurethanes with covalently linked diazeniumdiolated secondary amines. *Biomacromolecules* **2006,** *7* (3), 987-994.

(18) Hetrick, E. M.; Prichard, H. L.; Klitzman, B.; Schoenfisch, M. H. Reduced foreign body response at nitric oxide-releasing subcutaneous implants. *Biomaterials* **2007,** *28* (31), 4571-4580.

(19) Hopkins, S. P.; Pant, J.; Goudie, M. J.; Schmiedt, C.; Handa, H. Achieving long-term biocompatible silicone via covalently immobilized s-nitroso-n-acetylpenicillamine (snap) that exhibits 4 months of sustained nitric oxide release. *ACS Appl. Mater. Interfaces* **2018,** *10* (32), 27316-27325.

(20) Oh, B. K.; Meyerhoff, M. E. Spontaneous catalytic generation of nitric oxide from s-nitrosothiols at the surface of polymer films doped with lipophilic copper (ii) complex. *J. Am. Chem. Soc.* **2003,** *125* (32), 9552-9553.

(21) Pant, J.; Goudie, M. J.; Hopkins, S. P.; Brisbois, E. J.; Handa, H. Tunable nitric oxide release from s-nitroso-n-acetylpenicillamine via catalytic copper nanoparticles for biomedical applications. *ACS Appl. Mater. Interfaces* **2017,** *9* (18), 15254-15264.

(22) Grahn, B.; Wilson, P.; Krepel, C.; Seabrook, G.; Johnson, C.; Edmiston, C. Biomedical device-associated infections in surgical-critical care patients. *Am. J. Infect. Control* **2004,** *32* (3), E33-E34.

(23) Welsh, C. A.; Flanagan, M. E.; Hoke, S. C.; Doebbeling, B. N.; Herwaldt, L. Reducing health care-associated infections (hais): Lessons learned from a national collaborative of regional hai programs. *Am. J. Infect. Control* **2012,** *40* (1), 29-34.

(24) Donlan, R. M. Biofilm formation: A clinically relevant microbiological process. *Clin. Infect. Dis.* **2001,** *33* (8), 1387-1392.

(25) O'gara, J. P.; Humphreys, H. Staphylococcus epidermidis biofilms: Importance and implications. *J. Med. Microbiol.* **2001,** *50* (7), 582-587.

(26) O'gara, J. P. Ica and beyond: Biofilm mechanisms and regulation in staphylococcus epidermidis and staphylococcus aureus. *FEMS Microbiol. Lett.* **2007,** *270* (2), 179-188.

(27) Lee, Y.-H.; Cheng, F.-Y.; Chiu, H.-W.; Tsai, J.-C.; Fang, C.-Y.; Chen, C.-W.; Wang, Y.-J. Cytotoxicity, oxidative stress, apoptosis and the autophagic effects of silver nanoparticles in mouse embryonic fibroblasts. *Biomaterials* **2014,** *35* (16), 4706-4715.

(28) Park, E.-J.; Yi, J.; Kim, Y.; Choi, K.; Park, K. Silver nanoparticles induce cytotoxicity by a trojan-horse type mechanism. *Toxicol. In Vitro* **2010,** *24* (3), 872-878.

(29) Baldi, C.; Minoia, C.; Di Nucci, A.; Capodaglio, E.; Manzo, L. Effects of silver in isolated rat hepatocytes. *Toxicol. Lett.* **1988,** *41* (3), 261-268.

(30) Asharani, P. V., Mun, G.L.K., Hande, M.P., Valiyaveettil. Cytotoxicity and genotoxicity of silver nanoparticles in human cells. *ACS Nano* **2009,** *3* (2), 279-290.

(31) Cheng, X., Zhang, W., Ji, Y., Meng, J., Guo, H., Liu, J., Wu, X., Xu, H. Revealing silver cytotoxicity using au nanorods/ag shell nanostructures: Disrupting cell membrane and causing apoptosis through oxidative damage. *RSC Advances* **2013,** *3* (7), 2296-2305.

(32) Stewart, P. S.; Costerton, J. W. Antibiotic resistance of bacteria in biofilms. *The lancet* **2001,** *358* (9276), 135-138.

(33) Davies, J. Inactivation of antibiotics and the dissemination of resistance genes. *Science* **1994,** *264* (5157), 375-382.

(34) Major, T. C.; Brant, D. O.; Burney, C. P.; Amoako, K. A.; Annich, G. M.; Meyerhoff, M. E.; Handa, H.; Bartlett, R. H. The hemocompatibility of a nitric oxide generating polymer that catalyzes s-nitrosothiol decomposition in an extracorporeal circulation model. *Biomaterials* **2011,** *32* (26), 5957-5969.

(35) Brisbois, E. J.; Major, T. C.; Goudie, M. J.; Meyerhoff, M. E.; Bartlett, R. H.; Handa, H. Attenuation of thrombosis and bacterial infection using dual function nitric oxide releasing central venous catheters in a 9day rabbit model. *Acta Biomater.* **2016,** *44*, 304-312.

(36) Robinson, T. M.; Kickler, T. S.; Walker, L. K.; Ness, P.; Bell, W. Effect of extracorporeal membrane oxygenation on platelets in newborns. *Crit. Care Med.* **1993,** *21* (7), 1029-1034.

(37) Dillon, P. A.; Foglia, R. P. Complications associated with an implantable vascular access device. *J. Pediatr. Surg.* **2006,** *41* (9), 1582-1587.

(38) Charville, G. W.; Hetrick, E. M.; Geer, C. B.; Schoenfisch, M. H. Reduced bacterial adhesion to fibrinogen-coated substrates via nitric oxide release. *Biomaterials* **2008,** *29* (30), 4039-4044.

(39) Cai, W.; Wu, J.; Xi, C.; Meyerhoff, M. E. Diazeniumdiolate-doped poly(lactic-co-glycolic acid)-based nitric oxide releasing films as antibiofilm coatings. *Biomaterials* **2012,** *33* (32), 7933-7944.

(40) Hetrick, E. M.; Schoenfisch, M. H. Antibacterial nitric oxide-releasing xerogels: Cell viability and parallel plate flow cell adhesion studies. *Biomaterials* **2007,** *28* (11), 1948-1956.

(41) Engelsman, A. F.; Krom, B. P.; Busscher, H. J.; Van Dam, G. M.; Ploeg, R. J.; Van Der Mei, H. C. Antimicrobial effects of an no-releasing poly (ethylene vinylacetate) coating on soft-tissue implants in vitro and in a murine model. *Acta Biomater.* **2009,** *5* (6), 1905-1910.

(42) Carlsson, S.; Weitzberg, E.; Wiklund, P.; Lundberg, J. O. Intravesical nitric oxide delivery for prevention of catheter-associated urinary tract infections. *Antimicrob. Agents Chemother.* **2005,** *49* (6), 2352-2355.

(43) Mihu, M. R.; Sandkovsky, U.; Han, G.; Friedman, J. M.; Nosanchuk, J. D.; Martinez, L. R. The use of nitric oxide releasing nanoparticles as a treatment against acinetobacter baumannii in wound infections. *Virulence* **2010,** *1* (2), 62-67.

(44) Brisbois, E. J.; Bayliss, J.; Wu, J.; Major, T. C.; Xi, C.; Wang, S. C.; Bartlett, R. H.; Handa, H.; Meyerhoff, M. E. Optimized polymeric film-based nitric oxide delivery inhibits bacterial growth in a mouse burn wound model. *Acta Biomater.* **2014,** *10* (10), 4136-4142.

(45) Fang, F. C. Perspectives series: Host/pathogen interactions. Mechanisms of nitric oxide-related antimicrobial activity. *J. Clin. Invest.* **1997,** *99* (12), 2818.

(46) Feelisch, M. The use of nitric oxide donors in pharmacological studies. *Naunyn-Schmiedeberg's Arch. Pharmacol.* **1998,** *358* (1), 113-122.

(47) Bogdan, C. Nitric oxide and the immune response. *Nat. Immunol.* **2001,** *2* (10), 907-916.

(48) Dimmeler, S.; Fleming, I.; Fisslthaler, B.; Hermann, C.; Busse, R.; Zeiher, A. M. Activation of nitric oxide synthase in endothelial cells by akt-dependent phosphorylation. *Nature* **1999,** *399* (6736), 601-605.

(49) Frost, M. C., Reynolds, M.M., Meyerhoff, M.E. Polymers incorporating nitric oxide releasing/generating substances for improved biocompatibility of blood-contacting medical devices. *Biomaterials* **2005,** *26* (14), 1685-1693.

(50) Riccio, D. A.; Schoenfisch, M. H. Nitric oxide release: Part i. Macromolecular scaffolds. *Chem. Soc. Rev.* **2012,** *41* (10), 3731-3741.

(51) Mccarthy, C. W.; Guillory, R. J.; Goldman, J.; Frost, M. C. Transition-metal-mediated release of nitric oxide (no) from s-nitroso-n-acetyl-d-penicillamine (snap): Potential applications for endogenous release of no at the surface of stents via corrosion products. *ACS Appl. Mater. Interfaces* **2016,** *8* (16), 10128-10135.

(52) Brisbois, E. J.; Handa, H.; Major, T. C.; Bartlett, R. H.; Meyerhoff, M. E. Long-term nitric oxide release and elevated temperature stability with s-nitroso-n-acetylpenicillamine (snap)-doped elast-eon e2as polymer. *Biomaterials* **2013,** *34* (28), 6957-6966.

(53) Sundaram, J.; Pant, J.; Goudie, M. J.; Mani, S.; Handa, H. Antimicrobial and physicochemical characterization of biodegradable, nitric oxide-releasing nanocellulose-chitosan packaging membranes. *J. Agric. Food Chem.* **2016**.

(54) Brisbois, E. J.; Kim, M.; Wang, X.; Mohammed, A.; Major, T. C.; Wu, J.; Brownstein, J.; Xi, C.; Handa, H.; Bartlett, R. H. Improved hemocompatibility of multilumen catheters via nitric oxide (no) release from s-nitroso-n-acetylpenicillamine (snap) composite filled lumen. *ACS Appl. Mat. & Interfaces* **2016,** *8* (43), 29270-29279.

(55) Goudie, M. J.; Brisbois, E. J.; Pant, J.; Thompson, A.; Potkay, J. A.; Handa, H. Characterization of an s-nitroso-n-acetylpenicillamine–based nitric oxide releasing polymer from a translational perspective. *International Journal of Polymeric Materials and Polymeric Biomaterials* **2016,** *65* (15), 769-778.

(56) Pant, J.; Goudie, M.; Brisbois, E.; Handa, H. Nitric oxide-releasing polyurethanes. *Advances in Polyurethane Biomaterials* **2016**, 417.

(57) Brisbois, E. J.; Davis, R. P.; Jones, A. M.; Major, T. C.; Bartlett, R. H.; Meyerhoff, M. E.; Handa, H. Reduction in thrombosis and bacterial adhesion with 7 day implantation of s-nitroso-n-acetylpenicillamine (snap)-doped elast-eon e2as catheters in sheep. *J. Mater. Chem. B* **2015,** *3* (8), 1639-1645.

(58) Stuehr, D. J.; Nathan, C. Nitric oxide. A macrophage product responsible for cytostasis and respiratory inhibition in tumor target cells. *J. Exp. Med.* **1989,** *169* (5), 1543-1555.

(59) Palmer, R. M.; Ferrige, A.; Moncada, S. Nitric oxide release accounts for the biological activity of endothelium-derived relaxing factor. *Nature* **1987,** *327* (6122), 524-526.

(60) Frost, M. C.; Meyerhoff, M. E. Controlled photoinitiated release of nitric oxide from polymer films containing s-nitroso-n-acetyl-dl-penicillamine derivatized fumed silica filler. *J. Am. Chem. Soc.* **2004,** *126* (5), 1348-1349.

(61) Flinn, F. B.; Inouye, J. Some physiological aspects of copper in the organism. *J. Biol. Chem.* **1929,** *84* (1), 101-114.

(62) Chipinda, I.; Simoyi, R. H. Formation and stability of a nitric oxide donor: S-nitroso-n-acetylpenicillamine. *The Journal of Physical Chemistry B* **2006,** *110* (10), 5052-5061.

(63) Torres, N.; Oh, S.; Appleford, M.; Dean, D. D.; Jorgensen, J. H.; Ong, J. L.; Agrawal, C. M.; Mani, G. Stability of antibacterial self-assembled monolayers on hydroxyapatite. *Acta Biomater.* **2010,** *6* (8), 3242-3255.

(64) Otto, M. Staphylococcal infections: Mechanisms of biofilm maturation and detachment as critical determinants of pathogenicity. *Annu. Rev. Med.* **2013,** *64*, 175-188.

(65) Vanhoe, H.; Vandecasteele, C.; Versieck, J.; Dams, R. Determination of iron, cobalt, copper, zinc, rubidium, molybdenum, and cesium in human serum by inductively coupled plasma mass spectrometry. *Anal. Chem.* **1989,** *61* (17), 1851-1857.

(66) Williams, D. L. H. The mechanism of nitric oxide formation from s-nitrosothiols (thionitrites). *Chem. Commun.* **1996,** (10), 1085-1091.

(67) Williams, D. L. H. The chemistry of s-nitrosothiols. *Acc. Chem. Res.* **1999,** *32* (10), 869-876.

(68) Harding, J. L.; Reynolds, M. M. Metal organic frameworks as nitric oxide catalysts. *J. Am. Chem. Soc.* **2012,** *134* (7), 3330-3333.

(69) Wo, Y.; Li, Z.; Brisbois, E. J.; Colletta, A.; Wu, J.; Major, T. C.; Xi, C.; Bartlett, R. H.; Matzger, A. J.; Meyerhoff, M. E. Origin of long-term storage stability and nitric oxide release behavior of carbosil polymer doped with s-nitroso-n-acetyl-d-penicillamine. *ACS Appl. Mater. Interfaces* **2015,** *7* (40), 22218-22227.

(70) Wonoputri, V.; Gunawan, C.; Liu, S.; Barraud, N.; Yee, L. H.; Lim, M.; Amal, R. Copper complex in poly (vinyl chloride) as a nitric oxide-generating catalyst for the control of nitrifying bacterial biofilms. *ACS Appl. Mater. Interfaces* **2015,** *7* (40), 22148-22156.

(71) Squadrito, G. L.; Pryor, W. A. Oxidative chemistry of nitric oxide: The roles of superoxide, peroxynitrite, and carbon dioxide. *Free Radical Biol. Med.* **1998,** *25* (4), 392-403.

(72) Fahmy, B.; Cormier, S. A. Copper oxide nanoparticles induce oxidative stress and cytotoxicity in airway epithelial cells. *Toxicol. In Vitro* **2009,** *23* (7), 1365-1371.

(73) Seth, R.; Yang, S.; Choi, S.; Sabean, M.; Roberts, E. In vitro assessment of copper-induced toxicity in the human hepatoma line, hep g2. *Toxicol. In Vitro* **2004,** *18* (4), 501-509.

(74) Valodkar, M.; Rathore, P. S.; Jadeja, R. N.; Thounaojam, M.; Devkar, R. V.; Thakore, S. Cytotoxicity evaluation and antimicrobial studies of starch capped water soluble copper nanoparticles. *J. Hazard. Mater.* **2012,** *201*, 244-249.

(75) Costerton, J.; Stewart, P. Biofilms and device-related infections. *Persistent Bact. Infect.* **2000**, 423-437.

(76) Barraud, N.; Hassett, D. J.; Hwang, S.-H.; Rice, S. A.; Kjelleberg, S.; Webb, J. S. Involvement of nitric oxide in biofilm dispersal of pseudomonas aeruginosa. *J. Bacteriol.* **2006,** *188* (21), 7344-7353.

(77) Hetrick, E. M.; Shin, J. H.; Paul, H. S.; Schoenfisch, M. H. Anti-biofilm efficacy of nitric oxide-releasing silica nanoparticles. *Biomaterials* **2009,** *30* (14), 2782-2789.

(78) Pegalajar-Jurado, A.; Wold, K. A.; Joslin, J. M.; Neufeld, B. H.; Arabea, K. A.; Suazo, L. A.; Mcdaniel, S. L.; Bowen, R. A.; Reynolds, M. M. Nitric oxide-releasing polysaccharide derivative exhibits 8-log reduction against escherichia coli, acinetobacter baumannii and staphylococcus aureus. *J. Controlled Release* **2015,** *217*, 228-234.

(79) Yapor, J.; Lutzke, A.; Pegalajar-Jurado, A.; Neufeld, B.; Damodaran, V.; Reynolds, M. Biodegradable citrate-based polyesters with s-nitrosothiol functional groups for nitric oxide release. *J. Mater. Chem. B* **2015,** *3* (48), 9233-9241.

CHAPTER 3

A MULTI-DEFENSE STRATEGY: ENHANCING BACTERICIDAL ACTIVITY OF A MEDICAL GRADE POLYMER WITH A NITRIC OXIDE DONOR AND SURFACE-IMMOBILIZED QUATERNARY AMMONIUM COMPOUND

Pant, Jitendra. Accepted by Acta Biomaterilia
Reprinted here with permission of the publisher

Abstract

Although the use of biomedical devices in hospital-based care is inevitable, unfortunately, it is also one of the leading causes of the nosocomial infections, and thus demands development of novel antimicrobial materials for medical device fabrication. In the current study, a multi-defense mechanism against Gram-positive and Gram-negative bacteria is demonstrated by combining a NO releasing agent with a quaternary ammonium antimicrobial that can be covalently grafted to medical devices. Antibacterial polymeric composites were fabricated by incorporating a nitric oxide (NO) donor, *S*-nitroso-*N*-acetyl-penicillamine (SNAP) in CarboSil® polymer and top coated with surface immobilized benzophenone based quaternary ammonium antimicrobial (BPAM) small molecule. The results suggest that SNAP and BPAM have a different degree of toxicity towards Gram-positive and Gram-negative bacteria, and the SNAP-BPAM combination is effective in reducing both types of adhered viable bacteria equally well. SNAP-BPAM combinations reduced the adhered viable *Pseudomonas aeruginosa* by 99.0% and *Staphylococcus aureus* by 99.98% as compared to the control CarboSil films. Agar diffusion tests demonstrate that the diffusive nature of NO kills bacteria beyond the direct point of contact which the non-leaching BPAM cannot achieve alone. This is important for potential application in biofilm eradication. The live-dead bacteria staining shows that the SNAP-BPAM combination has more attached dead bacteria (than live) as compared to the controls. The SNAP-BPAM films have increased hydrophilicity and higher NO flux as compared to the SNAP films useful for preventing blood protein and bacterial adhesion.

1. Introduction

Invasive medical devices predispose patients to more than 850,000 biomedical device-related infections (BDRIs) annually.[1] Out of various biomedical devices that are frequently used in clinical practices, intravenous infusion devices, and urinary catheters represent a major

source of nosocomial septicemia.[1-2] For instance, the incidences of catheter-related bloodstream infections in the United States are approximately 80,000 cases/year in intensive care units alone and up to 250,000 cases/year in total with an attributable mortality of up to 35% .[3] Medical devices or implants create high risks for infections through several modes including (i) infecting patients directly by serving as a substrate for microorganisms' growth and colonization (biofilm), and/or (ii) damaging or invading epithelial layer in the host, which is a barrier to infection. It is evident that incorporation of microbicides in the medical devices would prevent BDRIs and ultimately bring down the cost associated with prolonged hospital stays. Presently, antibiotics and silver nanoparticles-based approaches are used to kill microorganisms; however, the emergence of antibiotic resistance and the issue of cytotoxicity and genotoxicity raises alarming concerns.[4-7] Most of the BDRIs involve multiple strains of microorganisms, and hence treatment with a single antibiotic is not effective.[8] It has been shown that tolerance level for antibiotics is 1000 times higher for biofilms when compared to bacterial suspensions.[9] This demands immediate attention as the use of multiple antibiotics and high doses only exacerbate the existing issues of antibiotic resistance and cytotoxicity. These challenges necessitate the exploration of alternative approaches to overcome the challenges of BDRIs caused by a wide variety of bacteria. In this regard, the combination of novel bactericidal agents such as surface-bound poly quaternary ammonium cations and nitric oxide (NO) donors can be advantageous due to their distinctive biocidal actions. This would not only assure high bactericidal efficiency but will also minimize the emergence of antibiotic resistance in pathogens due to their non-specific actions.

Membrane-disrupting poly "-onium" (quaternary ammonium) cations with various alkyl chain lengths have drawn considerable interest as a class of antimicrobial reagents because of their facile synthesis, broad application, outstanding antimicrobial activity, low cost, and low bacterial resistance [10-14]. Designing surfaces containing covalently bound poly "oniums" is one of the most successful strategies to date used to overcome surface microbial infections. [15-18] Among these polycations, the benzophenone chromophore has been utilized to develop photochemically

grafted quaternary ammonium coatings.[19-20] Benzophenone based quaternary ammonium cations (BPAM) has been shown to exhibit instant contact killing and high biocidal activity against both Gram-positive and Gram-negative bacteria. BPAM also exhibits rapid surface attachment (within 1 min) to the polymer with mild UV irradiation and good mechanical durability (survives Taber abrasion testing) due to the high photochemical efficiency of benzophenone and cross-linked network structure with polymer post irradiation.[20]

The generally accepted hypothesis for the biocidal mechanism of surface-immobilized quaternary ammoniums suggests that the positively charged "-onium" replaces the bacteria's natural counterions (Mg^{2+} and Ca^{2+}) and disrupt the ionic integrity of the membrane.[21-22] In addition, the alkyl chains of polycations intercalate into the phospholipid bilayer structure which disturbs its organization, forming holes in the membrane. [23-24] An alternative mechanism bacteria killing by quaternary ammoniums hypothesized that phospholipids are drawn out of bacterial lipid bilayer where they can permeate into cationic films. [25-26] Klibanov *et al*. have reported that bacteria fail to develop resistance to the lethal action of surface-bound quaternary ammonium because such surface acting antibacterial agent permeates bacterial membranes non-selectively via a 'brute-force' mechanism.[11] Although widely accepted as a highly efficient antibacterial agent, BPAM has several disadvantages that can limit its applications. The charge density of surface-bound quaternary ammonium might be eliminated by neutralization with anionic cellular components in the cytoplasm that is expelled out of the dead bacteria or screened by the layer of negatively charged dead bacterial cells covering the material's surface. [27-28] Moreover, due to its inability to act on bacteria that are not in intimate contact, BPAM cannot act on bacteria deeply embedded in a matrix of biofilm on a polymer surface. Furthermore, in the case of blood-contacting materials, fouling of the surface through the adsorption of protein can potentially hinder the surface-contact effect of quaternary ammonium cations such as BPAM on adhered bacteria. These limitations of the BPAM can be overcome by combining it with a nitric oxide (NO) donor as NO can diffuse through the biofilm matrix. Owing to its antimicrobial and antithrombotic potential,

NO can provide antibacterial activity even if the surface of the material is compromised due to aforementioned reasons.[29-30] Schoenfisch group has done multiple studies in the past to demonstrate that the combination of NO donors with other antimicrobials agents results in a significant improvement in the overall bactericidal activity of the material. [31-33]

In nature, nitric oxide (NO) is an endogenously produced (macrophages, endothelial cells, neurons) free radical gas with a very short half-life of fewer than 5 second.[34-39] Healthy endothelium lining in the inner wall of blood vessels releases an estimated NO flux of 0.5 to 4.0 × 10^{-10} mol min^{-1} cm^{-2}. [40-43] Endogenous NO is catalytically released by nitric oxide synthase in mammals and plays an important role in the immune response to infections caused by bacteria, fungus or viruses. [44-45] The NO released within the sinus cavities and macrophages functions as a natural antimicrobial agent to non-specifically combat pathogen invasion in mammals including humans.[37] Over the past two decades, NO-based therapies have emerged as a potential bactericidal agent to kill even the most prevalent pathogens causing hospital-acquired infection such as methicillin-resistant *Staphylococcus aureus* (MRSA) *and Pseudomonas aeruginosa,* and other bacteria including *Escherichia coli*, *Acinetobacter baumanii*, *Listeria monocytogenes,* and *Enterococcus faecalis.* [29, 46-54] The nonspecific innate immune response of NO results from lipid peroxidation and tyrosine nitration in the cell wall, nitrosation of amines and thiols in the extracellular matrix, and DNA cleavage in the cellular matrix.[55] Due to the non-specific action of NO and rapid reduction of bacteria load at the infection locale, the possibility of NO resistant strains remains limited. [48, 52, 56-58] In addition, NO based material can be used in blood-contacting device applications because it temporarily inhibits the activation of platelets on the polymer's surface which BPAM alone cannot. [59] The realization of the immense potential of NO in creating

biomimetic materials has encouraged researchers to synthesize several NO donor molecules to allow the storage and local delivery of NO at the material surface. S-nitroso-N acetylpenicillamine (SNAP) is one such NO donor that has widely been used in developing NO-releasing materials.43, 52, 60-63 In the past, Worley et al., have demonstrated the (NO)-releasing quaternary ammonium (QA)-functionalized generation 1 (G1) and generation 4 (G4) poly(amidoamine) (PAMAM) dendrimers using N-diazonium diolate NO donors. The present study demonstrates the enhanced bactericidal effect by permanent photocrosslinking and surface immobilization of BPAM on a CarboSil based polymeric composite with SNAP embedded as a NO donor.

This study investigated, the combined effect of the NO-releasing donor (SNAP) and non-leaching quaternary ammonium (BPAM) to prevent the adherence of bacterial cells on the polymeric surface in addition to killing bacteria beyond the direct point of contact. Briefly, polymeric films were prepared by incorporating SNAP in CarboSil® 20 80A (a medical grade silicone–polycarbonate-urethane copolymer). The BPAM was surface immobilized as a top-coat onto SNAP-CarboSil films by UV based photocrosslinking. The SNAP-BPAM based strategy to kill bacteria on the polymer surface was characterized physically and chemically and validated for its antibacterial efficiency.

2. Materials and Methods

2.1 Materials

CarboSil® 20 80A thermoplastic silicone–polycarbonate-urethane (hereafter will be referred to as CarboSil) was obtained from DSM Biomedical (Berkeley, CA). N-Acetyl-D-penicillamine (NAP), methanol, sodium chloride, potassium chloride, potassium phosphate monobasic, sodium phosphate dibasic, dimethylacetamide (DMAc), tetrahydrofuran (THF),

ethylenediaminetetraacetic acid (EDTA), and sulfuric acid were obtained from Sigma-Aldrich (St. Louis, MO). N-Bromosuccinimide (NBS), 2, 2'-azo-bis(2-methylpropiontirle) (AIBN), and N, N-dimethyl dodecyl amine were purchased from Alfa-Aesar. LB broth, Lennox, and LB Agar, miller media were purchased from Fischer Bioreagents (Fair Lawn, NJ). 4-Methylbenzophenone (Oxchem), cyclohexane (Honeywell), that-amyl alcohol (JT Baker), isopropyl alcohol (IPA) (JT Baker) sodium chloride (EMD Chemical), and peptone (HiMedia) were used without further purification. Phosphate buffered saline (PBS), pH 7.4, containing 138mM NaCl, 2.7mM KCl, 10mM sodium phosphate, was used for all *in vitro* experiments including bacteria testing. The two-color fluorescent live/dead BacLight bacterial viability kit L7012 (Molecular Probes, Life Technologies) which contains SYTO® 9 green fluorescent nucleic acid stain and the propidium iodide red fluorescent nucleic acid stain was utilized to evaluate the bacterial viability. Gram-negative *Pseudomonas aeruginosa* (ATCC 27853) and Gram-positive *Staphylococcus aureus* (ATCC 6538) were originally obtained from American Type Tissue Collection (ATCC).

2.2 Instrumental Methods

UV-vis spectroscopy was performed on a Cary Bio Spectrophotometer (Varian). Two irradiation wavelengths, 254 and 365 nm, were utilized in this study. The UV light sources were a Compact UV lamp (UVP) and FB-UBXL-1000 UV Crosslinker (Fisher Scientific) with bulbs of 254 nm wavelength for small (1 × 1 cm) and larger (2.5 × 2.5 cm) substrates, respectively. The substrates were held at 0.5 cm from the light source during irradiation to obtain a power of 6.5 mW/cm^2. Another UV light source was an OmniCure, Series 1000 with 365 nm bandpass filter, equipped with a liquid-filled fiber optic waveguide. The polymeric composite films were held 2 cm from the source for a power of 25 mW/cm^2. The thickness of the surface grafted BPAM film was measured using an M-2000 spectroscopic ellipsometer (J.A. Woollam Co., Inc). Water contact angles were measured by a DSA 100 drop shape analysis system (KRŰSS) with a computer-controlled liquid dispensing system. Water droplets with a volume of 1 µL were used to measure

the static contact angle. A fluorescent microscope (EVOS FL, Thermo-Scientific) equipped with a 100× objective was used for live/dead bacterial viability photomicrographs. A GFP FITC filter cube (excitation: 490 nm, emission: 503 nm) was used for SYTO® 9 and a Texas Red filter cube (excitation: 577 nm, emission: 620 nm) was used for the propidium iodide. The NO release study was performed using nitric oxide analyzer (NOA) 280i.

2.3 Synthesis of Bactericidal Agents and fabrication of polymeric films

2.3.1 *S*-Nitroso-*N*- acetylpenicillamine (SNAP) synthesis

A method reported by Chipinda et al. was modified for synthesizing SNAP from NAP. [64] Briefly, sodium nitrite and NAP were added in an equimolar ratio to a 1:1 mixture of methanol and water containing 2 M H_2SO_4 and 2 M HCl. The mixture was stirred in the dark (to protect NO release by light stimulation) for 40 min using a magnetic stirrer. Thereafter, the reaction vessel was placed in an ice bath to precipitate the SNAP crystals. The resulting crystals were filtered out of the solution and allowed to air dry in dark followed by vacuuming to remove traces of any solvent. SNAP crystals were stored in a freezer prior to use.

2.3.2 Benzophenone based antimicrobial molecule (BPAM) synthesis

The benzophenone based antimicrobial molecule (BPAM) was prepared using the previously reported procedure of Gao et al.,.[20] Briefly, 4-methylbenzopheone (6.0 g, 30.6 mM), NBS (6.0 g, 33.6 mM), AIBN (1.0 g, 6.1 mM), and cyclohexane (100 mL) were added to a round-bottom flask under nitrogen atmosphere. The suspension was stirred under reflux overnight. After stirring, the mixture was cooled and filtered to remove any solid residues and the filtrate was concentrated under reduced pressure. The solid mixture was dissolved in diethyl ether and washed with water, brine and dried over magnesium sulfate. The mixture was filtered and concentrated under reduced pressure. The recovered solid was recrystallized from absolute

ethanol to give fine white crystals. Yield: 7.1 g, 89 %. ^{1}H NMR: δ, 7.80 (t, 2H, J = 3.0 Hz); 7.78 (t, 2H, J = 1.4 Hz); 7.60 (t, 1H, J = 7.0 Hz); 7.50 (d, 2H, 8.2 Hz); 7.49 (t, 2H, 7.6 Hz); 4.53 (s, 2H). ^{13}C NMR ($CDCl_3$): δ, 195.93, 142.09, 137.39, 132.54, 130.52, 129.99, 128.92 128.33, 128.16, 32.25.

N-(4-benzoylbenzyl)-N,N-dimethylbutan-1-aminium iodide (BPAM): (4-bromomethyl) benzophenone (1.7 g, 6.2 mM), N, N-demethyldodecylamine (1.7 mL, 6.2 mM), and tert-amyl alcohol (5 mL) were added to a sealable pressure flask. The mixture was stirred and heated in the sealed vessel at 95 °C for 24 h. The flask was cooled to room temperature and the solvent was removed under reduced pressure. The resulting brown waxy solid was recrystallized in hexane/ethyl acetate (7:4) to give a waxy white solid. Yield: 1.7 g, 67 %. ^{1}H NMR ($CDCl_3$): δ, 7.84 (dd, 4H, J = 8.2, 23.9 Hz); 7.75 (d, 2H, J = 7.0 Hz); 7.59 (t, 1H, J = 7.6 Hz); 7.47 (t, 2H, 7.7 Hz); 3.57 (m, 2H); 3.35 (s, 6H); 1.80 (bs, 2H); 1.31 (bs, 4H); 1.21 (bs, 16H); 0.84 (t, 3H, J= 6.6 Hz). ^{13}C NMR ($CDCl_3$): δ, 210.33, 139.75, 136.70, 133.53, 133.24, 131.53, 130.54, 130.24, 120.66, 66.63, 64.12, 49.85, 32.06, 29.69, 29.58, 29.46, 29.37, 26.42, 22.82, 14.29.

2.3.3 Fabrication of antimicrobial SNAP-CarboSil polymer films

To begin making the polymeric SNAP films, 70mg/mL of CarboSil was dissolved in tetrahydrofuran (THF) as a solvent and stirred for 1 h at room temperature using a magnetic stirrer. After complete dissolution, 10 % (w/w) of SNAP was quickly added and dissolved for 2 min in the Carbosil-THF solution. The SNAP films (10 wt %) were cast in Teflon molds (diameter = 2.5 cm) and dried overnight in dark to prevent undesired loss of NO from the films using 3 ml of resulting SNAP-CarboSil-THF solution. The films were coated twice with 50 mg/ml CarboSil solution (in THF). This outer coating ensures that SNAP does not leach out from the films and also generates a smooth surface. The control CarboSil films were prepared and coated in a similar manner, without the addition of SNAP.

2.3.4 Surface immobilization of BPAM on SNAP-CarboSil films

The BPAM film was immobilized onto SNAP-CarboSil film surfaces using spray coating. BPAM/isopropanol solution (5 mg/mL) was sprayed using an airbrush spray gun from a distance of 20 cm onto a vertically placed substrate to achieve uniform coating. Upon solvent evaporation, a thin film of BPAM remained on the surface. Then BPAM coated films were subsequently irradiated with UV light (254 nm, 6.5 mW/cm^2) for 2 min to covalently immobilize BPAM to the surface. The films were sonicated with isopropanol for 1 min to rinse off any residual, physisorbed BPAM and dried under a stream of nitrogen. Figure 3.1 shows the fabrication procedure to make SNAP-BPAM CarboSil films (hereafter will be called SNAP-BPAM films).

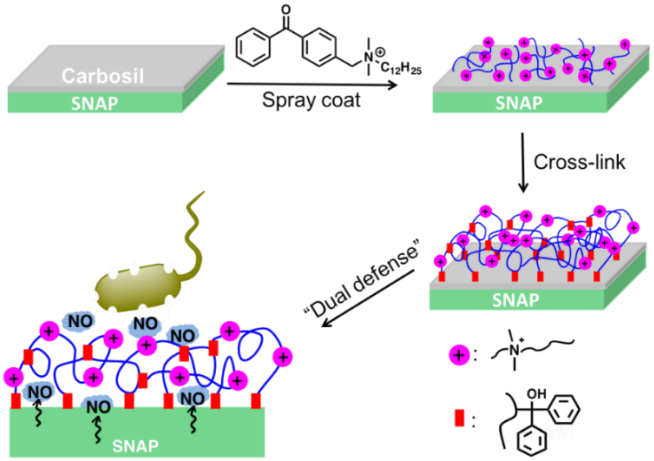

Figure 3.1. The fabrication of the SNAP-BPAM CarboSil film and its biocidal action. Antibacterial polymeric composites were fabricated by incorporating a NO donor, *S*-nitroso-*N*-acetyl-penicillamine (SNAP) in CarboSil polymer and top coated with surface immobilized benzophenone based quaternary ammonium antimicrobial (BPAM) small molecule via photocrosslinking.

2.4 Nitric Oxide release kinetics

Nitric oxide release from the SNAP and SNAP-BPAM films was measured using a Sievers Chemiluminescence Nitric Oxide Analyzer (NOA) 280i (Boulder, CO). The Sievers chemiluminescence NOA is considered as the gold standard for detecting *in vitro* nitric oxide release from the substrate. It is widely used for measurement of nitric oxide released from

materials due to the ability to limit interfering species, such as nitrates and nitrites, as they are not transferred from the sample vessel to the reaction cell. Prior to NO release measurements, the films (n = 3) were incubated for 1 h (PBS containing 100 mM EDTA, room temperature) to avoid the burst release associated with NO-releasing materials.[43, 61] Films were then placed in the sample vessel immersed in PBS (pH 7.4) containing 100 mM EDTA. Nitric oxide was continuously purged from the buffer and swept from the headspace using nitrogen sweep gas and a bubbler into the chemiluminescence detection chamber. Films were submerged in PBS with EDTA and stored in glass vials and kept at 37°C between NO-release measurements. Fresh PBS solution was used for each NO-release measurement, and films were kept in fresh PBS solution for storage after each measurement.

2.5 UV-vis spectrophotometry

All UV-Vis spectra were recorded in the wavelength range of 200-700 nm using a UV-Vis spectrophotometer Cary Bio Spectrophotometer (Varian) at room temperature. CarboSil films and SNAP CarboSil films were developed on quartz glass substrates by spin coating with 200 µL of CarboSil/THF solution (50 mg/mL) at 1000 rpm for 30 s. BPAM was top coated on CarboSil/quartz substrates by spray coating with BPAM/IPA solution (10 mg/mL). The UV-vis spectrum of CarboSil was measured as the background. The presence of the S-NO group of SNAP provides characteristic absorbance maxima at 340 and 590 nm.[43, 65] CarboSil films were dissolved in DMAc and absorbance values were measured at 340 nm. The amount of SNAP was then determined using a calibration curve from known molar concentrations of SNAP in DMAC and compared to untreated control CarboSil films.

2.6 Quantification of adhered and viable colony forming units on polymeric surface

In this study, the ability of the CarboSil polymer with SNAP-BPAM combination to kill the adhered bacteria on the polymer surface was tested using the Gram-negative *Pseudomonas aeruginosa* and Gram-positive *Staphylococcus aureus* bacteria which are amongst the most common causes of hospital-acquired infections (HAIs). A modified protocol of standard bacterial adhesion tests was used to quantify the viable colony forming units of bacteria per surface area of the films (CFU/cm^2). [66-68] A single colony of bacteria was isolated from a previously cultured LB-agar plate and incubated in LB medium for 14 h at 37°C at a rotating speed of 150 rpm. The optical density of the culture was measured at a wavelength of 600 nm ($O.D_{600}$) using UV-vis spectrophotometer (Thermo scientific Genesys 10S UV-Vis) to ensure that bacteria is in log phase of their growth. The bacteria culture was then centrifuged at 3500 rpm for 7 min, the supernatant was discarded. And sterile phosphate buffer saline (PBS), pH 7.4 was added to the bacterial pellet. This procedure was repeated twice to remove all traces of LB medium and to suspend bacteria in PBS solution. In parallel, serial dilutions of the bacteria were prepared and plated in LB agar Petri dishes in order to verify the consistency of concentration of viable cells between experiments. The OD_{600} of the cell suspension in PBS was measured and adjusted to the CFU/ml in the range of 10^7-10^9 based on the standard calibration curve. CarboSil control, SNAP films, BPAM coated CarboSil films and SNAP-BPAM films (n = 3 for each type; surface area = 0.94 cm^2) were exposed to bacterial cells (CFU: 10^9-10^7) at 37 °C for 24 h in a shaker incubator (150 rpm) after soaking them in PBS for 1 h to account for the burst effect. The 24 h incubation allows the bacteria to adhere to the surface of the films and the adhered bacteria were acted upon by BPAM and NO. After 24 h, films were removed from the solution and any loosely bound bacteria were washed by gently rinsing them with continuously flowing PBS (5 ml) using a pipette. The films were sonicated for 45 sec using an Omni-Tip homogenizer followed by vortexing for 30 seconds to collect the adhered bacteria into a 2 ml PBS solution. The PBS solution with bacteria was serially diluted (10^{-1} -10^{-5}), plated in the solid LB agar medium and incubated for 20 h at 37°C.

After 20 h, the CFUs of the adhered viable bacteria on the surface of the polymer were counted keeping in account the dilution factor.

2.7 Analysis of residual NO flux post bacteria exposure

To ensure that fabricated film releases enough levels of nitric oxide after exposure to Pseudomonas *aeruginosa* or *Staphylococcus aureus strain* for 24 h (Section 2.6), the residual NO release was confirmed following the same procedure as explained in Section 2.4 using the Sievers Nitric Oxide Analyzer (NOA). Triplicates of each film types (n = 3) were analyzed for measuring the residual NO flux.

2.8 Zone of inhibition (ZOI) analysis

A standard agar diffusion protocol was followed to conduct zone of inhibition (ZOI) study to demonstrate the diffusive nature of NO molecule released from SNAP and SNAP-BPAM films in the surrounding agar. This study was designed to prove that the NO release from the polymeric composite can kill bacteria which are not in direct contact with the polymeric films which BPAM alone fails to achieve. As a proof of concept, Gram-positive *S. aureus* and Gram-negative *P. aeruginosa* bacteria strains were used for the study. A single colony of each bacterium was suspended individually in LB and incubated at 37°C for 14 h at a rotating speed of 150 rpm. Using *UV-Vis spectrophotometer* (Genesis 10S-Thermo Scientific), the optical density (OD) of each of the bacterial cultures was measured at 600 nm (OD_{600}). The observed OD_{600} was adjusted to $1x10^7$ colony forming units per mL (CFUs/mL) based on a calibration curve based on the known concentration of *S. aureus* and *P. aeruginosa.* A sterile cotton swab was placed into each of the strain cultures and then gently pressed and rotated against pre-made LB-agar Petri dishes (14 cm) to spread the bacteria aseptically and uniformly. Circular disks (diameter: 22 mm) of control, SNAP, BPAM, and SNAP-BPAM films were placed on top of bacterial culture and pressed gently.

The Petri dishes were incubated overnight at 37°C in inverted position. The ZOI diameters were compared to evaluate the antimicrobial efficacy of NO releasing SNAP and SNAP-BPAM films.

2.9 Live/dead staining assay

While the bacterial adhesion test allows counting the viable CFUs on the surface of the polymer, it doesn't provide any quantitative or qualitative information on how many cells were initially attached and died due to SNAP-BPAM biocidal activity. Using live/dead staining, we observed both live and dead bacterial cells that were bound to the surface of the polymer. This qualitative study was then combined with Cell Profiler software to quantify the live and dead bacteria on the polymeric surface. SYTO® 9 dye, yields green fluorescence and labels all bacteria in a population with intact membranes. In contrast, propidium iodide, which yields red fluorescence, penetrates only the bacteria with damaged membranes and replaces SYTO® 9 stains, causing a reduction in green fluorescence and the appearance of red fluorescence. Consequently, bacteria with damaged cell membranes can be distinguished from live bacteria. For each of the bacterial strains, 10 mL bacterial culture was grown to late log phase in broth (shaken at 100 rpm for 10 h at 37 °C). The culture was centrifuged at 4000 rpm for 10 min. The supernatant was removed and the pellet was suspended in sterile distilled water. Before staining, 10 µL bacterial suspension with a concentration around 10^8 CFU/mL was placed on the CarboSil, BPAM coated CarboSil, SNAP-blended CarboSil, and SNAP-BPAM CarboSil films and dried at 37 °C for 5 min to achieve quick and intimate contact. Equal volumes of SYTO® 9 and propidium iodide (1.5 µL) were combined, added to 1 mL of distilled water, and mixed thoroughly. Diluted dye mixture (10 µL) was trapped between the slide with adhered bacteria and 18 mm square coverslip. The sample was incubated in dark for 15 min at room temperature and imaged qualitatively with an EVOS fluorescence microscope. Both the live and dead bacteria from the fluorescent images were then quantified with Cell Profiler software by randomly selecting different spots (n = 3) on the films.

2.10 Statistical significance

For all the quantitative measurements n = 3 data points were taken into consideration unless otherwise mentioned. Standard two-*tailed t*-test with unequal variance is used to do all statistical comparisons. The data is reported as a mean ± standard deviation and the significance with a p-value < 0.05 is stated for comparisons.

3. Results

3.1 Photocrosslinking of BPAM on SNAP-CarboSil and quantification of total SNAP

The benzophenone moiety of BPAM photochemically reacts with C-H groups of the CarboSil polymer to form new C-C bonds at the interface. Upon absorption of UV light, the promotion of one electron from a nonbinding n orbital to the antibonding π* orbital of the carbonyl group yields a biradicaloid triplet state where the electron-deficient oxygen n orbital interacts with surrounding weak C-H δ bonds, resulting in H abstraction to complete the half-filled n orbital. The two resulting carbon radicals then combine to form a new C-C bond. This process was monitored by the decrease in absorbance of the n-π* transition of BP using UV-vis spectrometry (Figure 3.2 (A)).

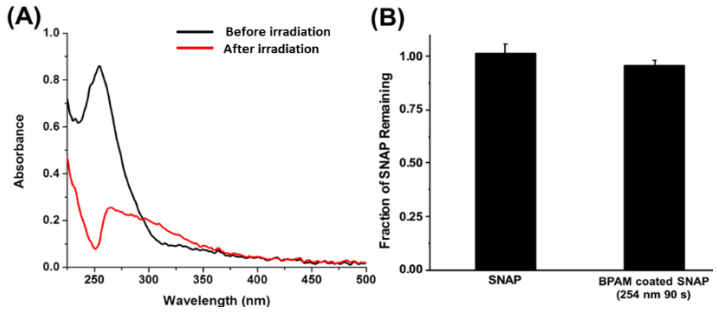

Figure 3.2. UV-mediated photocrosslinking study of BPAM on SNAP film: 2 (A). UV-Vis Spectra of SNAP-BPAM film before and after UV irradiation (254 nm, 90 s). After UV irradiation for 90 seconds, absorbance at 255 nm decreased, indicating the completion of the crosslinking reaction. Figure 2 (B). Total SNAP content after UV irradiation that was reported to be around 95.44 ± 2.5% of the initial SNAP content**.**

Before exposure to UV light, the λ_{max} absorbance at 255 nm was observed, which is the characteristic n-π* transition of BPAM.[20] A spectrum shoulder ranging from 310-350 nm is assigned to the UV absorbance (λ_{max}) of SNAP.[64] The low intensity of the SNAP absorbance is due to the low concentration of SNAP within the CarboSil polymer matrix. After UV irradiation for 90 seconds, absorbance at 255 nm decreased, indicating the completion of the crosslinking reaction. The broad shoulder at 250~300 nm could be due to slight photo-oxidation of the polycarbonate base. [69] The remaining SNAP content after UV treatment is shown in Figure 3.2 (B) and was confirmed to maintain 95.44 ± 2.5% of the initial SNAP content. This can be mainly due to the presence of a top coat of Carbosil in the SNAP films before the application of BPAM. In the past, the application of top coats of CarboSil which are in the order of 100 microns has been shown to significantly reduce leaching when compared to non-top coated films [43]. These results confirmed that surface immobilized BPAM doesn't adversely cause significant loss of SNAP from the polymeric composite.

3.2 Nitric oxide release from SNAP and SNAP-BPAM CarboSil films

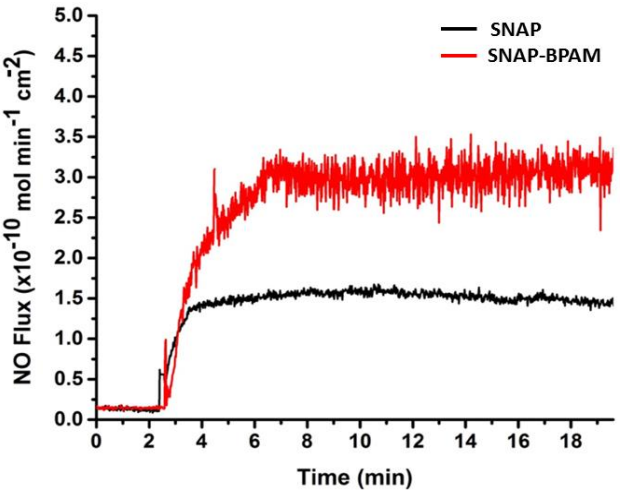

Figure 3.3. Real-time NO flux rate of SNAP doped CarboSil (black) and BPAM coated SNAP CarboSil films (red) analyzed at the physiological temperature using Sievers Nitric Oxide Analyzer (NOA). SNAP-BPAM (SNAP films with BPAM top coat) showed an increase in NO flux at different time points.

Incorporation of SNAP to CarboSil has shown to provide continuous and localized NO delivery to specific sites of interest.[70-71] The incorporation of SNAP in medical grade polymers have been shown to be hemocompatible and possesses stability during long-term storage at room temperature and physiological conditions. [63, 72-73]

In this study, release rates of NO were measured at physiological conditions (pH 7.4, 37°C) to demonstrate that the presence of the BPAM coating does not adversely affect the NO release profile. The release of NO from these compounds stems from the breaking of the S-NO bond that can be catalyzed using heat, light, moisture, or metal ions.[43, 60, 65] Representative real-time NO release profiles from SNAP and SNAP-BPAM films was recorded via NOA as shown in

Figure 3.3. SNAP films exhibited an initial release rate of $1.35 \pm 0.11 \times 10^{-10}$ mol min^{-1} cm^{-2} and release rate of $0.28 \pm 0.02 \times 10^{-10}$ mol min^{-1} cm^{-2} after 24 h. SNAP films with BPAM top coat showed an increase in NO flux both at the initial ($2.58 \pm 0.25 \times 10^{-10}$ mol min^{-1} cm^{-2}) and at the 24-hour time point ($0.59 \pm 0.04 \times 10^{-10}$ mol min^{-1} cm^{-2}) (Figure 3.4).

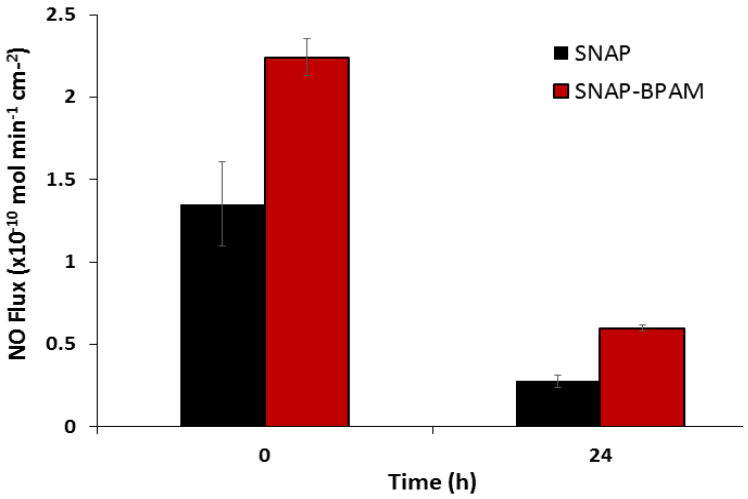

Figure 3.4. NO release flux with or without BPAM topcoat

This may be attributed to the increase in hydrophilicity of the films with the presence of BPAM topcoat as described above. The increased flux is still well within the physiological range

(0.5-4.0 × 10^{-10} mol $min^{-1}cm^{-2}$) making it relevant and effective for biomedical device applications.[40] The NO flux exhibited by the films is sufficient to kill bacteria beyond 24 h. This has been shown *in vivo* in a 7-day sheep catheter model using similar hydrophobic polymers with 10 wt. % SNAP.[74] These materials exhibit similar NO release characteristics over a 28-d period and demonstrate that NO release rates at the lower end of physiological limits are still effective in providing antibacterial activity. Another report has also shown that hydrophobic polymers with SNAP have extended NO-release at physiological levels (up to 20 days).[70] Furthermore, the incorporation of SNAP in medical grade polymers are not only hemocompatible and biocompatible but also stable during long-term storage (6 months) at room temperature and physiological conditions. [63, 72-73]

3.3. Coating thickness and contact angle analysis

The thickness and static contact angle measurements are among the most relevant physical characterizations for a polymeric coating. The results of these characterizations are illustrated in Table 1. The thickness of the crosslinked BPAM coatings on CarboSil and SNAP CarboSil films after UV irradiation were 45.7 ± 0.3 nm and 47.9 ± 0.5 nm, respectively, indicating successful grafting of a BPAM coating. Water contact angles of control CarboSil, SNAP CarboSil, BPAM CarboSil, and SNAP-BPAM CarboSil surfaces are also listed in Table 1. We have previously shown that blending SNAP into the CarboSil polymeric matrix does not affect the hydrophobicity of the polymer [71]. The study showed that due to lower water uptake of CarboSil, limited leaching of SNAP has been seen from SNAP doped CarboSil. Leaching is further reduced with the use of a top coat (< 10% of total SNAP loading in first 24 h) as compared to the non-coated films. A change in the topcoat of Carbosil is much thicker than photocrosslinked BPAM coat (100 µm vs 50 nm for BPAM) and hence little or no changes to the leaching kinetics of SNAP is expected. Blending SNAP into the CarboSil polymeric matrix does not affect the hydrophobicity

of the polymer. The CarboSil control surface was found to be hydrophobic with contact angle (CA) of 119.3 ± 0.4°. The surface grafted layer of BPAM significantly decreases the hydrophobicity of the CarboSil based polymer film, reducing the CA to 63.5° ± 0.5°, resulting from the positively charged ammonium functional groups.

Table 3.1. Physical characterization of antibacterial films

Sample	CarboSil	SNAP CarboSil	BPAM CarboSil	SNAP-BPAM CarboSil
Thickness (nm)	N/A	N/A	45.7 ± 0.3	47.9 ± 0.5
Contact Angle (˚)	119	115	67.9 ± 0.6	63.5 ± 0.5

The increase in the surface hydrophilicity is expected to increase the antibacterial efficacy of the SNAP-BPAM polymer films as studies have shown a marked increase in NO release from the hydrophilic surface when compared to the hydrophobic surfaces.[43] This is in line with the results obtained from the NO release kinetics study (Section 3.2). Furthermore, increased hydrophilicity helps in the repulsion of non-specific protein adsorption, and ultimately bacterial adhesion[75-76] as confirmed by the bacterial adhesion test (Section 3.4) and Live/Dead staining (Section 3.6).

3.4 Quantification of adhered viable bacteria (CFU/cm^2)

Biofilm formation is a major cause of morbidity and mortality associated with hospital acquired infection (HAIs). *Staphylococcus aureus,* a Gram-positive bacterium, and *Pseudomonas aeruginosa*, a Gram-negative bacterium are among the most common causes of nosocomial bloodstream infections that can form embedded biofilm matrices on indwelling biomedical

devices.[77-79] As shown in Figure 3.5, the amount of viable *P. aeruginosa and S. aureus* adhered on SNAP-BPAM film surfaces are significantly lower than that of control films.

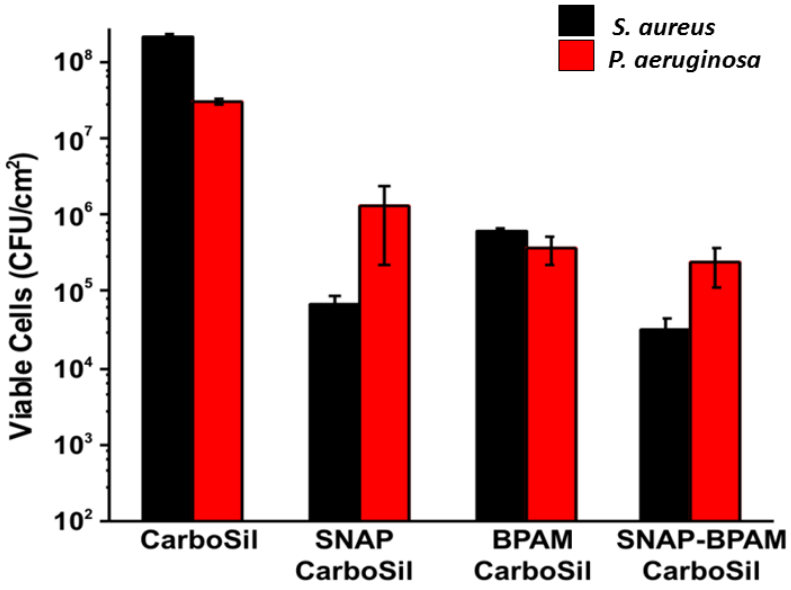

Figure 3.5. Comparative graphs to show the differences in inhibition of viable colony forming units of Gram-positive *S. aureus* and Gram-negative *P. aeruginosa* on the unit surface area (CFU/cm^2) of SNAP films, BPAM films and SNAP-BPAM films as compared to control CarboSil. Overall SNAP-BPAM combination showed a significant reduction in bacterial CFU/cm^2. The synergistic effect thus enhances the bactericidal activity due to synergistic effect of SNAP and BPAM. P-value < 0.05 were considered statistically significant.

While BPAM and SNAP are excellent antimicrobial agents, the combination offers several advantages not possessed by an individual antimicrobial agent. BPAM by itself has a superior antibacterial potential towards Gram-negative *P. aeruginosa* as compared to SNAP, and SNAP is superior with respect to its bactericidal action against Gram-positive *S. aureus*. The combination is very effective against both Gram-positive and negative bacteria. Overall the SNAP-BPAM films reduced the adhered viable bacteria (both Grams positive and negative) to the maximum extent as compared to the control films. SNAP-BPAM films showed a 4-log reduction in Gram-positive *S. aureus* and 3-log reduction for Gram-negative *P. aeruginosa* as compared to the CarboSil control. Figure 3.5 and Table 3.2 represents the respective graphs and the data for the reduction in the adhered CFU of both the bacteria per surface area of the polymeric composites. The difference in the results between the two bacteria can be attributed to the

difference in the cell wall and membrane composition of Gram-positive and Gram-negative bacteria.[80] Non-leaching BPAM can only act on bacteria in intimate contact while NO can act beyond the direct point of contact because of diffusion. The activity of BPAM is also diminished with time by the layer of bacterial cells (live or dead) on polymeric composites as they tend to neutralize the charge on quaternary ammonium. This problem can be addressed by the application of NO. The small molecular size of NO allows it to diffuse through the bacterial biofilm and kill the bacterial cells which are otherwise resistant to bactericidal agents.[53-54]

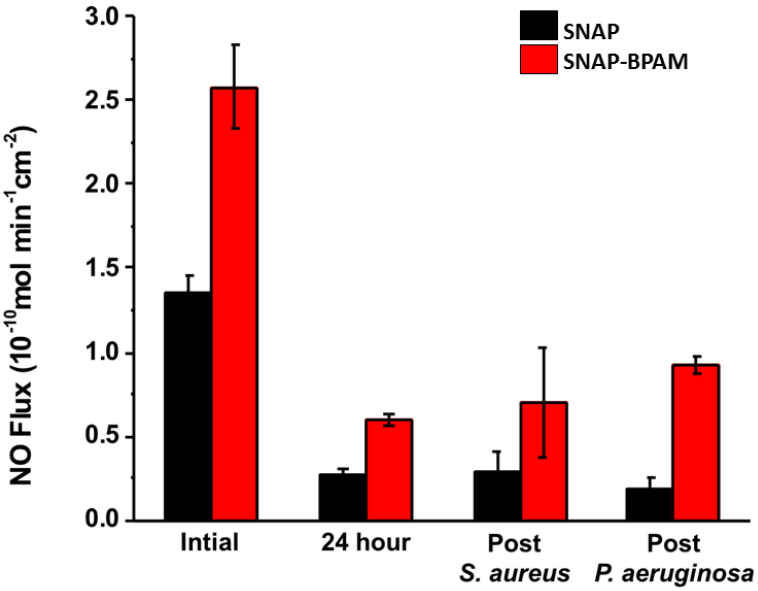

Figure 3.6. Effect of immobilized BPAM top coats on NO release kinetics of the SNAP-BPAM films as measured by chemiluminescence before (0h and 24 h) and after bacterial exposure (24 h study). The residual NO flux was observed to be in the physiological range even after 24 h of bacteria exposure indicating the antibacterial effect can be extended beyond the 24 h. P-value < 0.05 were considered statistically significant.

In other words, the gradually released NO extended the life of BPAM by lowering the concentration of surrounding bacteria near the surface. The SNAP-BPAM films have relatively higher hydrophilicity (due to BPAM coat) than SNAP films alone which increased the NO flux release from the SNAP-BPAM films.The residual NO analysis after exposing films to bacteria

suspension (Figure 3.6) showed an abundance of NO up to 0.92 ±0.05 × 10^{-10} mol min^{-1} cm^{-2} flux, suggesting that these films can

BPAM coat) than SNAP films alone which increased the NO flux release from the SNAP-BPAM films. The residual NO analysis after exposing films to bacteria suspension (Figure 3.6) showed an abundance of NO up to 0.92 ±0.05 × 10^{-10} mol min^{-1} cm^{-2} flux, suggesting that these films can continue to exhibit antibacterial properties beyond 24 h. The combined action of these bactericidal agents via multiple mechanisms of bacteria killing warrants a significant reduction in viable bacterial load for both Gram-positive and negative strains.

3.5 Bacterial killing via NO diffusion

While BPAM is an excellent antimicrobial agent, due to its non-diffusive nature, it cannot kill the bacteria protected within the biofilm matrix. Moreover, the charge density of surface-bound BPAM might be neutralized with anionic cellular components in the cytoplasm that is expelled out of the dead bacteria or screened by the layer of negatively charged dead bacterial cells covering the material's surface.[26-28] Therefore, the diffusive nature of NO can be beneficial in biofilm eradication beyond the close vicinity of the material which otherwise can't be achieved via BPAM application. The standard agar diffusion test allowed us to show the bactericidal effect of the NO releasing films in the presence and absence of the BPAM. The CarboSil films with incorporated antimicrobial agents (SNAP-BPAM) and their combination resulted in a zone of inhibition (ZOI) of different diameters when exposed to LB agar plates with bacterial culture. As expected, the result demonstrated that BPAM has no ZOI, while the SNAP films and SNAP-BPAM films showed a clear ZOI due to the release of NO gas from SNAP when placed in an incubator at 37°C for 20 h (Figure 3.7).

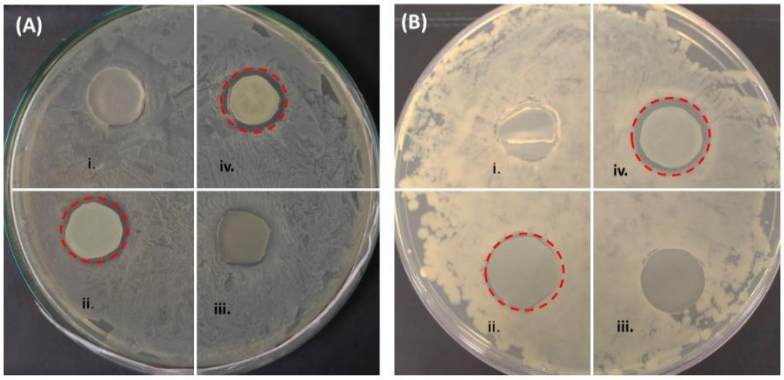

Figure 3.7. Zone of inhibition (ZOI) can be seen inside the dotted circle: (A) *S. aureus*; (B) *P. aeruginosa*; (i) Control, (ii) SNAP, (iii) BPAM, and (iv) SNAP-BPAM. The bigger ZOI with SNAP-BPAM combination is due to increase in NO flux with BPAM topcoat.

The explanation for this is the diffusive nature of NO that can penetrate in the LB agar and hence prevent the bacterial growth in the area around the film. The breaking of the S-NO bond in SNAP causes the release of NO. On the other hand, BPAM is non-diffusive in nature and hence can only act on bacteria which are in direct contact. From an application point of view, this will be beneficial for biofilm eradication as NO due to its small size would easily penetrate through the matrix of a bacterial biofilm. Even though BPAM didn't show any ZOI, it did prevent the growth of bacteria in direct contact underneath the film. The ZOI for *P. aeruginosa* was observed to be 24 mm for SNAP films and 26mm for SNAP-BPAM films. Similarly, the ZOI for *S. aureus* was observed to be 24 mm with SNAP films and 25 mm for SNAP-BPAM films. Overall SNAP-BPAM composites showed the largest ZOI for both *S. aureus* as well as *P. aeruginosa* strains among all the composites. The bigger ZOI with SNAP-BPAM combination is due to increase in NO flux with BPAM topcoat ($1.35 \pm 0.11 \times 10^{-10}$ in SNAP films vs $2.58 \pm 0.25 \times 10^{-10}$ mol min^{-1} cm^{-2} in SNAP-BPAM films) as observed by chemiluminescence NOA. Figure 3.7 shows the comparative ZOI diameter among the films for both the bacterial strains. The difference in antibacterial efficacy shown towards the two bacterial strains can be attributed to the membrane properties of Gram-positive and Gram-negative bacteria.[80]

3.6 Analysis and quantitation of live/dead stain test on CarboSil films

As mentioned above, the bacterial adhesion test (section 3.4) showed the reduction in adhered viable cells and zone of inhibition agar diffusion test (section 3.5) demonstrated the killing of bacteria through diffusion respectively. However, the relative number of live and dead bacteria on the films were not evaluated by either of these tests. Therefore, the antibacterial activity of the SNAP-BPAM hybrid CarboSil films was also evaluated using a live/dead fluorescent stain assay which stains the live cells as green and the dead cells as red.

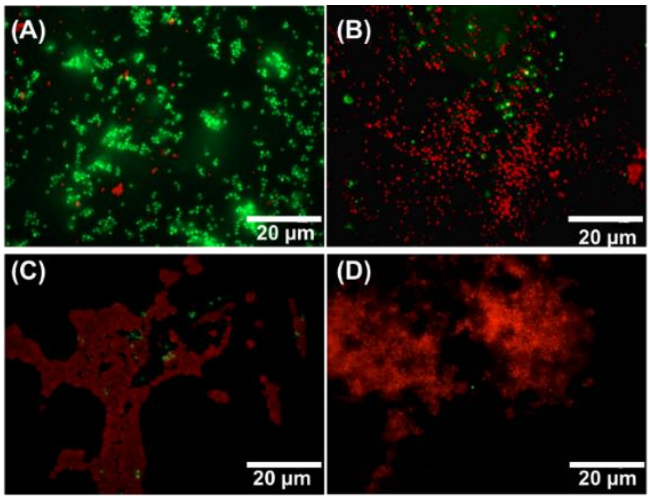

Figure 3.8. Fluorescent images of *S. aureus* in contact with (A) Control CarboSil film, (B) BPAM film, (C) SNAP film and (D) SNAP-BPAM film after live-dead staining observed fluorescence microscopy. The red color indicates dead cells while the green fluorescence indicates viable bacteria. As obvious from the image, SNAP-BPAM combination (D) showed the maximum bactericidal efficiency.

Figure 3.8 shows fluorescent images of *S. aureus* cells exposed on control CarboSil, BPAM, SNAP, and SNAP-BPAM films. The bacterial cell count for the live/dead assay was quantitatively estimated at three randomly selected spots by using Cell Profiler software as recommended by published reports.[81-82] On the control films (Figure 3.8A), 97.35 ± 0.72 % bacterial cells showed green fluorescence, evenly distributed across the surface, and retained intact spherical shape, suggesting that the tested bacterial cells were viable. On BPAM coated CarboSil films (Figure 3.8B), 94.41 ± 0.61 % of the total bacterial cells were stained red, indicating the cell membrane disruption caused by contact with surface-bound quaternary ammonium. On

SNAP films, 97.58 ± 0.44 % of the total bacteria showed red fluorescence indicating dead cells (Figure 3.8C). In the case of SNAP-BPAM CarboSil films (Figure 3.8D), a 99.62 ± 0.59 % killing efficacy was achieved, demonstrating that the hybrid method effectively enhances the antibacterial activity of the functionalized biocompatible polymer material.

This enhancement in bactericidal activity of SNAP-BPAM as compared to SNAP and BPAM films is in line with the viable bacteria adhesion test as well as the zone of inhibition testing. Notably, the pattern of aggregation of bacterial cells on the surface of the film was observed to be different and dependent on the antibacterial agent. The bacterial cells on control CarboSil and BPAM films have a regular pattern of bacterial cell distribution. On the other hand, the cells were aggregated together on SNAP Carbosil films, possibly due to the hydrophobicity of the CarboSil surface which caused repulsion to the negatively charged bacterial cells. On the SNAP-BPAM films, the dead cells dispersed across the surface which might be due to the relatively lower hydrophobicity (C.A = 63.5° ± 0.5) of the SNAP-BPAM films' surface as compared to SNAP films (C.A = 115° ± 0.2) resulting from the positively charged ammonium functional groups. Overall, lived/dead staining experiment combined with Cell Profiler software further validated that combined NO and surface-bound quaternary ammonium can provide dual antibacterial activities and thus significantly enhance the biocidal activity as compared to the individual agent. The authors suggest further *in vitro* testing and high-resolution image analysis on bacterial aggregation pattern to validate this plausible theoretical explanation.

4. Discussion

In the present study, a NO donor molecule (SNAP) and a surface immobilized benzophenone based antimicrobial molecule (BPAM) were used in combination and their combined effect to reduce microbial adhesion and viability on a medical grade polymeric surface

was evaluated. Since the λ_{max} of BPAM and SNAP are distinctly separated, this benefits the hybrid material in two ways: (1) BPAM can absorb photons efficiently for the photoreaction even in the presence of SNAP; (2) Photo-degradation of SNAP is limited in the crosslinking process since the irradiation wavelength is 254 nm for the maximum energy absorbance efficiency of BPAM.

The antibacterial potential of SNAP-BPAM films was tested via (i) Bacterial Adhesion test (ii) Agar diffusion test (iii) Live/Dead staining. Combined these three tests allowed to quantitatively assess the bacterial adhesion (both viable and non-viable) and their subsequent killing by NO and BPAM action. The antimicrobial properties of NO are due to denaturation of enzymes, deamination of DNA and lipid oxidation in bacteria matrix.[55] On the other hand, BPAM kills the bacteria that are in direct contact by damaging the bacterial cell membrane integrity due to electrostatic interactions.[21-22]

In the past, we have shown that SNAP based NO releasing polymers have many desirable properties from a translational perspective such as the long-term storage stability (6 months), ease of sterilization, and extended NO release (> 2 weeks) without negatively affecting the physical characteristics, bacterial inhibition, biocompatibility, and hemocompatibility of the polymer.[43, 53, 62-63] Similarly, the surface grafted BPAM has been reported to exhibit excellent antimicrobial activity against Gram-positive and Gram-negative bacteria on instant contact due to high surface charge density of the deposited BPAM thin film.[20] However, this is the first study that combines SNAP and BPAM together to demonstrate their antibacterial potential.

The study demonstrated that the SNAP-BPAM combination has better antibacterial properties than SNAP or BPAM alone. BPAM is highly regarded as a bactericidal agent, but, it can only act on bacteria that are in direct contact. NO molecule through its diffusive nature allows acting on bacteria that are beyond the direct contact. This property is useful to act on biofilm matrix that otherwise prevents the penetration of antibacterial agent and keeps the bacteria immune. BPAM however, imparts a relatively hydrophilic surface to SNAP-CarboSil as apparent from a decrease in the contact angle. Studies have shown higher NO release from the hydrophilic

surface when compared to the hydrophobic surfaces which in turn resulted in higher bacterial killing.[43] This is in line with the NO flux analysis as the SNAP-BPAM films showed higher NO flux as compared to the SNAP films. Furthermore, a hydrophilic surface helps in the repulsion of non-specific protein adsorption, and ultimately bacterial adhesion[75-76] as confirmed by the bacterial adhesion test and Live/Dead staining. From a translational perspective, a biomedical implant fabricated with a non-leaching, hydrophilic surface would be able to form a solvated, aqueous layer upon contact with body fluids and thus reduce bacterial adhesion.[83] In addition, NO also has the advantage in blood-contacting device applications of the localized effect of temporarily inhibiting the activation of platelets that approach the polymer surface.[59]

In vitro characterization of the SNAP-BPAM containing CarboSil polymer in the present showed that such polymeric composites can yield better antibacterial effect as compared to SNAP or BPAM individually (Figures 3.5, 3.7, and 3.8). Their distinct but very effective mode of bactericidal action assures that the bacteria that in contact with the polymeric composites are attacked via multiple bactericidal mechanisms. The NO release with the SNAP-BPAM combination was shown to be higher than with SNAP alone making their cooperation more effective in terms of diffusion of NO into the biofilm (Figures 3.3 and 3.4). These SNAP-BPAM-CarboSil composites continued to release NO flux in the physiological range past the bacteria exposure for 24 h (Figure 3.6). The sustained release of diffusible NO also extended the duration of localized action of BPAM by lowering the concentration of surrounding viable bacteria near the polymer surface allowing BPAM to kill any bacteria in local contact.

Overall, the combined action of these bactericidal agents via distinct mechanisms warrants a significant reduction in viable bacterial load for both Gram-positive and negative strains. Furthermore, the rapid action of NO (half-life < 5sec) and non-specific lethal action of surface-bound BPAM via physical membrane disruption limit the development of resistant bacterial strains.[48, 52, 56-58]

5. Conclusion

In the current study, a polymeric composite was fabricated by blending SNAP in the CarboSil polymer and BPAM was surface grafted via UV photocrosslinking and its ability to inhibit bacteria on the surface was tested both qualitatively and quantitatively. The SNAP-BPAM combination was more effective in maximizing the bacterial load on the surface of the polymeric composite as compared to SNAP or BPAM films individually. The bacterial adhesion test demonstrated that combination is equally effective in minimizing the adhered viable CFUs of both Gram-positive and Gram-negative bacteria whereas SNAP was more effective against *S. aureus* and BPAM alone was more effective against *P. aureginosa* when tested alone. As demonstrated by the agar diffusion test diffusive nature of NO allowed to kill the bacteria beyond the direct point of contact which BPAM can't achieve alone. This is important for potential application in biofilm eradication. The lived dead staining allowed to observe that SNAP-BPAM combination has a higher number of attached dead bacteria (than live) as compared to the controls. BPAM coat also increased the hydrophilicity and higher NO flux as compared to the SNAP films. In addition, NO based material can be used in blood-contacting device applications because it temporarily inhibits the activation of platelets on the polymer's surface which BPAM cannot.[59] Overall, all these characteristics are ideal for controlling biomedical device related infections, especially in preventing bacteria from developing antibiotic resistance due to the different killing mechanisms exhibited by SNAP and BPAM.

Acknowledgement

Funding for this work was supported by National Institutes of Health, USA grants K25HL111213, R01HL134899, and Centers for Disease Control and Prevention contract 200-2016-91933.

References

(1) Stamm, W. E. Infections related to medical devices. *Annals of Internal Medicine* **1978,** *89* (5_Part_2), 764-769.

(2) Brisbois, E. J.; Kim, M.; Wang, X.; Mohammed, A.; Major, T. C.; Wu, J.; Brownstein, J.; Xi, C.; Handa, H.; Bartlett, R. H. Improved hemocompatibility of multilumen catheters via nitric oxide (no) release from s-nitroso-n-acetylpenicillamine (snap) composite filled lumen. *ACS Appl. Mater. Interfaces* **2016,** *8* (43), 29270-29279.

(3) Warren, J. W. Catheter-associated urinary tract infections. *Infectious disease clinics of North America* **1997,** *11* (3), 609-622.

(4) Stewart, P. S.; Costerton, J. W. Antibiotic resistance of bacteria in biofilms. *The lancet* **2001,** *358* (9276), 135-138.

(5) Lee, Y.-H.; Cheng, F.-Y.; Chiu, H.-W.; Tsai, J.-C.; Fang, C.-Y.; Chen, C.-W.; Wang, Y.-J. Cytotoxicity, oxidative stress, apoptosis and the autophagic effects of silver nanoparticles in mouse embryonic fibroblasts. *Biomaterials* **2014,** *35* (16), 4706-4715.

(6) Park, E.-J.; Yi, J.; Kim, Y.; Choi, K.; Park, K. Silver nanoparticles induce cytotoxicity by a trojan-horse type mechanism. *Toxicol. In Vitro* **2010,** *24* (3), 872-878.

(7) Asharani, P.; Low Kah Mun, G.; Hande, M. P.; Valiyaveettil, S. Cytotoxicity and genotoxicity of silver nanoparticles in human cells. *ACS nano* **2008,** *3* (2), 279-290.

(8) Raad, I.; Darouiche, R.; Hachem, R.; Sacilowski, M.; Bodey, G. P. Antibiotics and prevention of microbial colonization of catheters. *Antimicrobial agents and chemotherapy* **1995,** *39* (11), 2397-2400.

(9) Jefferson, K. K.; Goldmann, D. A.; Pier, G. B. Use of confocal microscopy to analyze the rate of vancomycin penetration through staphylococcus aureus biofilms. *Antimicrobial agents and chemotherapy* **2005,** *49* (6), 2467-2473.

(10) Yatvin, J.; Gao, J.; Locklin, J. Durable defense: Robust and varied attachment of non-leaching poly"-onium" bactericidal coatings to reactive and inert surfaces. *Chemical Communications* **2014,** *50* (67), 9433-9442.

(11) Milović, N. M.; Wang, J.; Lewis, K.; Klibanov, A. M. Immobilized n-alkylated polyethylenimine avidly kills bacteria by rupturing cell membranes with no resistance developed. *Biotechnology and Bioengineering* **2005,** *90* (6), 715-722.

(12) Yudovin-Farber, I.; Beyth, N.; Nyska, A.; Weiss, E. I.; Golenser, J.; Domb, A. J. Surface characterization and biocompatibility of restorative resin containing nanoparticles. *Biomacromolecules* **2008,** *9* (11), 3044-3050.

(13) Koplin, S. A.; Lin, S.; Domanski, T. Evaluation of the antimicrobial activity of cationic polyethylenimines on dry surfaces. *Biotechnology Progress* **2008,** *24* (5), 1160-1165.

(14) Ferreira, L.; Zumbuehl, A. Non-leaching surfaces capable of killing microorganisms on contact. *Journal of Materials Chemistry* **2009,** *19* (42), 7796-7806.

(15) Park, D.; Wang, J.; Klibanov, A. M. One-step, painting-like coating procedures to make surfaces highly and permanently bactericidal. *Biotechnology Progress* **2006,** *22* (2), 584-589.

(16) Xie, Y.; Hill, C. a. S.; Xiao, Z.; Militz, H.; Mai, C. Silane coupling agents used for natural fiber/polymer composites: A review. *Composites Part A: Applied Science and Manufacturing* **2010,** *41* (7), 806-819.

(17) Yuan, S. J.; Pehkonen, S. O.; Ting, Y. P.; Neoh, K. G.; Kang, E. T. Inorganic−organic hybrid coatings on stainless steel by layer-by-layer deposition and surface-initiated atom-transfer-

radical polymerization for combating biocorrosion. *ACS Applied Materials & Interfaces* **2009,** *1* (3), 640-652.

(18) Locklin, J. J., Us pat. **2013**; Vol. US20130036558A1.

(19) Dhende, V. P.; Samanta, S.; Jones, D. M.; Hardin, I. R.; Locklin, J. One-step photochemical synthesis of permanent, nonleaching, ultrathin antimicrobial coatings for textiles and plastics. *ACS Applied Materials & Interfaces* **2011,** *3* (8), 2830-2837.

(20) Gao, J.; Huddleston, N. E.; White, E. M.; Pant, J.; Handa, H.; Locklin, J. Surface grafted antimicrobial polymer networks with high abrasion resistance. *ACS Biomaterials Science & Engineering* **2016**.

(21) Kügler, R.; Bouloussa, O.; Rondelez, F. Evidence of a charge-density threshold for optimum efficiency of biocidal cationic surfaces. *Microbiology* **2005,** *151* (5), 1341-1348.

(22) Sonenshein, A. L.; Hoch, J. A.; Losick, R., *Bacillus subtilis and other gram-positive bacteria: Biochemistry, physiology, and molecular genetics*. American Society for Microbiology: **1993**.

(23) Lewis, K.; Klibanov, A. M. Surpassing nature: Rational design of sterile-surface materials. *Trends in Biotechnology* **2005,** *23* (7), 343-348.

(24) Tiller, J. C., Antimicrobial surfaces. In *Bioactive surfaces*, Borner, H. G.; Lutz, J. F., Eds. **2011**, pp 193-217.

(25) Bieser, A. M.; Tiller, J. C. Mechanistic considerations on contact-active antimicrobial surfaces with controlled functional group densities. *Macromolecular bioscience* **2011,** *11* (4), 526-534.

(26) Gao, J.; White, E. M.; Liu, Q.; Locklin, J. Evidence for the phospholipid sponge effect as the biocidal mechanism in surface-bound polyquaternary ammonium coatings with variable cross-linking density. *ACS Appl. Mater. Interfaces* **2017,** *9* (8), 7745-7751.

(27) Bieser, A. M.; Tiller, J. C. Mechanistic considerations on contact-active antimicrobial surfaces with controlled functional group densities. *Macromolecular Bioscience* **2011,** *11* (4), 526-534.

(28) Lee, S. B.; Koepsel, R. R.; Morley, S. W.; Matyjaszewski, K.; Sun, Y.; Russell, A. J. Permanent, nonleaching antibacterial surfaces. 1. Synthesis by atom transfer radical polymerization. *Biomacromolecules* **2004,** *5* (3), 877-882.

(29) Nablo, B. J.; Prichard, H. L.; Butler, R. D.; Klitzman, B.; Schoenfisch, M. H. Inhibition of implant-associated infections via nitric oxide release. *Biomaterials* **2005,** *26* (34), 6984-6990.

(30) Carpenter, A. W.; Schoenfisch, M. H. Nitric oxide release: Part ii. Therapeutic applications. *Chem. Soc. Rev.* **2012,** *41* (10), 3742-3752.

(31) Carpenter, A. W.; Worley, B. V.; Slomberg, D. L.; Schoenfisch, M. H. Dual action antimicrobials: Nitric oxide release from quaternary ammonium-functionalized silica nanoparticles. *Biomacromolecules* **2012,** *13* (10), 3334-3342.

(32) Worley, B. V.; Slomberg, D. L.; Schoenfisch, M. H. Nitric oxide-releasing quaternary ammonium-modified poly (amidoamine) dendrimers as dual action antibacterial agents. *Bioconj. Chem.* **2014,** *25* (5), 918-927.

(33) Worley, B. V.; Schilly, K. M.; Schoenfisch, M. H. Anti-biofilm efficacy of dual-action nitric oxide-releasing alkyl chain modified poly (amidoamine) dendrimers. *Mol. Pharm.* **2015,** *12* (5), 1573-1583.

(34) Hou, Y.; Janczuk, A.; Wang, P. Current trends in the development of nitric oxide donors. *Current Pharmaceutical Design* **1999,** *5* (6), 417-442.

(35) Vodovotz, Y.; Bogdan, C.; Paik, J.; Xie, Q.; Nathan, C. Mechanisms of suppression of macrophage nitric oxide release by transforming growth factor beta. *The Journal of experimental medicine* **1993,** *178* (2), 605-613.

(36) Hibbs, J. B.; Taintor, R. R.; Vavrin, Z.; Rachlin, E. M. Nitric oxide: A cytotoxic activated macrophage effector molecule. *Biochem. Biophys. Res. Commun.* **1988,** *157* (1), 87-94.

(37) Macmicking, J.; Xie, Q.-W.; Nathan, C. Nitric oxide and macrophage function. *Annu. Rev. Immunol.* **1997,** *15* (1), 323-350.

(38) Halpenny, G. M., Heilman, B., Mascharak, P.K. Nitric oxide (no)-induced death of gram-negative bacteria from a light controlled no-releasing platform. *Chemistry & Biodiversity* **2012,** *9* (9), 1829-1839.

(39) Rouby, J. J. The nose, nitric oxide, and paranasal sinuses: The outpost of pulmonary antiinfectious defenses? *American Journal of Respiratory and Critical Care Medicine* **2003,** *168* (3), 265-266.

(40) Vaughn, M. W.; Kuo, L.; Liao, J. C. Estimation of nitric oxide production and reactionrates in tissue by use of a mathematical model. *Am. J. Physiol.: Heart Circ. Physiol* **1998,** *274* (6), H2163-H2176.

(41) Handa, H.; Brisbois, E. J.; Major, T. C.; Refahiyat, L.; Amoako, K. A.; Annich, G. M.; Bartlett, R. H.; Meyerhoff, M. E. In vitro and in vivo study of sustained nitric oxide release coating using diazeniumdiolate-doped poly (vinyl chloride) matrix with poly (lactide-co-glycolide) additive. *J. Mater. Chem. B* **2013,** *1* (29), 3578-3587.

(42) Handa, H.; Major, T. C.; Brisbois, E. J.; Amoako, K. A.; Meyerhoff, M. E.; Bartlett, R. H. Hemocompatibility comparison of biomedical grade polymers using rabbit thrombogenicity model for preparing nonthrombogenic nitric oxide releasing surfaces. *J. Mater. Chem. B* **2014,** *2* (8), 1059-1067.

(43) Brisbois, E. J.; Handa, H.; Major, T. C.; Bartlett, R. H.; Meyerhoff, M. E. Long-term nitric oxide release and elevated temperature stability with s-nitroso-n-acetylpenicillamine (snap)-doped elast-eon e2as polymer. *Biomaterials* **2013,** *34* (28), 6957-6966.

(44) Degroote, M. A.; Fang, F. C., Antimicrobial properties of nitric oxide. In *Nitric oxide and infection*, Springer: **2002**, pp 231-261.

(45) Pant, J.; Goudie, M.; Brisbois, E.; Handa, H., Nitric oxide releasing polyurethanes. In *Advances in polyurethane biomaterials*, Elsevier: **2016**, pp 471-550.

(46) Sundaram, J.; Pant, J.; Goudie, M. J.; Mani, S.; Handa, H. Antimicrobial and physicochemical characterization of biodegradable, nitric oxide-releasing nanocellulose-chitosan packaging membranes. *J. Agric. Food Chem.* **2016**.

(47) Brisbois, E. J.; Bayliss, J.; Wu, J.; Major, T. C.; Xi, C.; Wang, S. C.; Bartlett, R. H.; Handa, H.; Meyerhoff, M. E. Optimized polymeric film-based nitric oxide delivery inhibits bacterial growth in a mouse burn wound model. *Acta Biomaterialia* **2014,** *10* (10), 4136-4142.

(48) Heilman, B. J.; Halpenny, G. M.; Mascharak, P. K. Synthesis, characterization, and light-controlled antibiotic application of a composite material derived from polyurethane and silica xerogel with embedded photoactive manganese nitrosyl. *Journal of Biomedical Materials Research Part B: Applied Biomaterials* **2011,** *99* (2), 328-337.

(49) Nablo, B. J.; Chen, T.-Y.; Schoenfisch, M. H. Sol-gel derived nitric-oxide releasing materials that reduce bacterial adhesion. *J. Am. Chem. Soc.* **2001,** *123* (39), 9712-9713.

(50) Nablo, B. J.; Schoenfisch, M. H. Antibacterial properties of nitric oxide–releasing sol-gels. *Journal of Biomedical Materials Research Part A* **2003,** *67* (4), 1276-1283.

(51) Hetrick, E. M.; Schoenfisch, M. H. Reducing implant-related infections: Active release strategies. *Chem. Soc. Rev.* **2006,** *35* (9), 780-789.

(52) Hetrick, E. M.; Schoenfisch, M. H. Antibacterial nitric oxide-releasing xerogels: Cell viability and parallel plate flow cell adhesion studies. *Biomaterials* **2007,** *28* (11), 1948-1956.

(53) Pant, J.; Goudie, M. J.; Hopkins, S. P.; Brisbois, E. J.; Handa, H. Tunable nitric oxide release from s-nitroso-n-acetylpenicillamine via catalytic copper nanoparticles for biomedical applications. *ACS Appl. Mater. Interfaces*.

(54) Singha, P.; Pant, J.; Goudie, M. J.; Workman, C. D.; Handa, H. Enhanced antibacterial efficacy of nitric oxide releasing thermoplastic polyurethanes with antifouling hydrophilic topcoats. *Biomaterials Science* **2017**.

(55) Fang, F. C. Perspectives series: Host/pathogen interactions. Mechanisms of nitric oxide-related antimicrobial activity. *Journal of Clinical Investigation* **1997,** *99* (12), 2818-2825.

(56) Privett, B. J.; Broadnax, A. D.; Bauman, S. J.; Riccio, D. A.; Schoenfisch, M. H. Examination of bacterial resistance to exogenous nitric oxide. *Nitric Oxide* **2012,** *26* (3), 169-173.

(57) Feelisch, M. The use of nitric oxide donors in pharmacological studies. *Naunyn-Schmiedeberg's Arch. Pharmacol.* **1998,** *358* (1), 113-122.

(58) Bogdan, C. Nitric oxide and the immune response. *Nat. Immunol.* **2001,** *2* (10), 907-916.

(59) Hakim, T.; Sugimori, K.; Camporesi, E.; Anderson, G. Half-life of nitric oxide in aqueous solutions with and without haemoglobin. *Physiological measurement* **1996,** *17* (4), 267.

(60) Williams, D. L. H. The chemistry of s-nitrosothiols. *Accounts of Chemical Research* **1999,** *32* (10), 869-876.

(61) Brisbois, E. J.; Major, T. C.; Goudie, M. J.; Bartlett, R. H.; Meyerhoff, M. E.; Handa, H. Improved hemocompatibility of silicone rubber extracorporeal tubing via solvent swelling-impregnation of s-nitroso-n-acetylpenicillamine (snap) and evaluation in rabbit thrombogenicity model. *Acta biomaterialia* **2016,** *37*, 111-119.

(62) Brisbois, E. J.; Davis, R. P.; Jones, A. M.; Major, T. C.; Bartlett, R. H.; Meyerhoff, M. E.; Handa, H. Reduction in thrombosis and bacterial adhesion with 7 day implantation of s-nitroso-n-acetylpenicillamine (snap)-doped elast-eon e2as catheters in sheep. *Journal of Materials Chemistry B* **2015**.

(63) Goudie, M. J.; Brisbois, E. J.; Pant, J.; Thompson, A.; Potkay, J. A.; Handa, H. Characterization of an s-nitroso-n-acetylpenicillamine–based nitric oxide releasing polymer from a translational perspective. *Int. J. Polym. Mater. Polym. Biomater.* **2016,** *65* (15), 769-778.

(64) Chipinda, I.; Simoyi, R. H. Formation and stability of a nitric oxide donor: S-nitroso-n-acetylpenicillamine. *The Journal of Physical Chemistry B* **2006,** *110* (10), 5052-5061.

(65) Frost, M. C.; Meyerhoff, M. E. Controlled photoinitiated release of nitric oxide from polymer films containing s-nitroso-n-acetyl-dl-penicillamine derivatized fumed silica filler. *J. Am. Chem. Soc.* **2004,** *126* (5), 1348-1349.

(66) Nablo, B. J.; Schoenfisch, M. H. Poly (vinyl chloride)-coated sol− gels for studying the effects of nitric oxide release on bacterial adhesion. *Biomacromolecules* **2004,** *5* (5), 2034-2041.

(67) Nablo, B. J.; Rothrock, A. R.; Schoenfisch, M. H. Nitric oxide-releasing sol–gels as antibacterial coatings for orthopedic implants. *Biomaterials* **2005,** *26* (8), 917-924.

(68) Torres, N.; Oh, S.; Appleford, M.; Dean, D. D.; Jorgensen, J. H.; Ong, J. L.; Agrawal, C. M.; Mani, G. Stability of antibacterial self-assembled monolayers on hydroxyapatite. *Acta Biomater.* **2010,** *6* (8), 3242-3255.

(69) Diepens, M.; Gijsman, P. Photo-oxidative degradation of bisphenol a polycarbonate and its possible initiation processes. *Polymer Degradation and Stability* **2008,** *93* (7), 1383-1388.

(70) Wo, Y.; Li, Z.; Brisbois, E. J.; Colletta, A.; Wu, J.; Major, T. C.; Xi, C.; Bartlett, R. H.; Matzger, A. J.; Meyerhoff, M. E. Origin of long-term storage stability and nitric oxide release behavior of carbosil polymer doped with s-nitroso-n-acetyl-d-penicillamine. *ACS Appl. Mater. Interfaces* **2015,** *7* (40), 22218-22227.

(71) Goudie, M. J.; Brainard, B. M.; Schmiedt, C. W.; Handa, H. Characterization and in vivo performance of nitric oxide-releasing extracorporeal circuits in a feline model of thrombogenicity. *Journal of Biomedical Materials Research Part A* **2016**.

(72) Brisbois, E. J.; Major, T. C.; Goudie, M. J.; Meyerhoff, M. E.; Bartlett, R. H.; Handa, H. Attenuation of thrombosis and bacterial infection using dual function nitric oxide releasing central venous catheters in a 9day rabbit model. *Acta Biomater.* **2016,** *44*, 304-312.

(73) Brisbois, E. J.; Kim, M.; Wang, X.; Mohammed, A.; Major, T. C.; Wu, J.; Brownstein, J.; Xi, C.; Handa, H.; Bartlett, R. H. Improved hemocompatibility of multi-lumen catheters via nitric oxide (no) release from s-nitroso-n-acetylpenicillamine (snap) composite filled lumen. *ACS Appl. Mater. & Interfaces* **2016**.

(74) Brisbois, E. J.; Davis, R. P.; Jones, A. M.; Major, T. C.; Bartlett, R. H.; Meyerhoff, M. E.; Handa, H. Reduction in thrombosis and bacterial adhesion with 7 day implantation of s-nitroso-n-

acetylpenicillamine (snap)-doped elast-eon e2as catheters in sheep. *J. Mater. Chem. B* **2015,** *3* (8), 1639-1645.

(75) Rana, D.; Matsuura, T. Surface modifications for antifouling membranes. *Chem. Rev* **2010,** *110*, 2448–2471.

(76) Chen, S.; Li, L.; Zhao, C.; Zheng, J. Surface hydration: Principles and applications toward low-fouling/nonfouling biomaterials. *Polymer* **2010,** *51* (23), 5283-5293.

(77) Allan, N. D.; Giare-Patel, K.; Olson, M. E. An in vivo rabbit model for the evaluation of antimicrobial peripherally inserted central catheter to reduce microbial migration and colonization as compared to an uncoated picc. *BioMed Research International* **2012,** *2012*.

(78) Otto, M. Staphylococcal infections: Mechanisms of biofilm maturation and detachment as critical determinants of pathogenicity. *Annu. Rev. Med.* **2013,** *64*, 175-188.

(79) Kiedrowski, M. R.; Horswill, A. R. New approaches for treating staphylococcal biofilm infections. *Annals of the New York Academy of Sciences* **2011,** *1241* (1), 104-121.

(80) Roy, H. Tuning the properties of the bacterial membrane with aminoacylated phosphatidylglycerol. *IUBMB life* **2009,** *61* (10), 940-953.

(81) Carpenter, A. E.; Jones, T. R.; Lamprecht, M. R.; Clarke, C.; Kang, I. H.; Friman, O.; Guertin, D. A.; Chang, J. H.; Lindquist, R. A.; Moffat, J.; Golland, P.; Sabatini, D. M. Cellprofiler: Image analysis software for identifying and quantifying cell phenotypes. *Genome Biology* **2006,** *7* (10), 1-11.

(82) Kamentsky, L.; Jones, T. R.; Fraser, A.; Bray, M.-A.; Logan, D. J.; Madden, K. L.; Ljosa, V.; Rueden, C.; Eliceiri, K. W.; Carpenter, A. E. Improved structure, function and compatibility for cellprofiler: Modular high-throughput image analysis software. *Bioinformatics* **2011,** *27* (8), 1179-1180.

(83) Louie, J. S.; Pinnau, I.; Ciobanu, I.; Ishida, K. P.; Ng, A.; Reinhard, M. Effects of polyether–polyamide block copolymer coating on performance and fouling of reverse osmosis membranes. *Journal of Membrane Science* **2006,** *280* (1–2), 762-770.

CHAPTER 4

NITRIC OXIDE RELEASING VASCULAR CATHETERS FOR ERADICATING BACTERIAL INFECTION

Pant, Jitendra. Accepted by Journal of Biomedical Research-Part B
Reprinted here with permission of the publisher

Abstract

The interaction of blood proteins with an implant surface is not only a fundamental phenomenon but is also key to several important medical complications. Plasma proteins binding on the surface of intravascular catheters can promote bacterial adhesion leading to the risk of local and systemic complications such as catheter-related blood infections (CRBIs). The incidences of CRBIs in the United States amounts to more than 250,000 cases/year with an attributable mortality of up to 35% and an annual healthcare expenditure of $2.3 billion approximately. This demands the development of truly non-thrombogenic and antimicrobial catheters. In the present study, catheters were fabricated by incorporating a nitric oxide donor (NO) molecule, *S*-Nitroso-*N*-Acetyl-Penicillamine (SNAP) in a hydrophobic medical grade polymer, Elasteon-E2As. Nitric oxide (NO) offers antithrombotic and antibacterial attributes without promoting drug resistance and cytotoxicity. SNAP-E2As catheters were first coated with fibrinogen, a blood plasma protein plays a key role in clot formation and eventual bacterial adhesion to the implant surface. The suitability of the catheters for biomedical applications was tested *in vitro* for contact angle, NO release kinetics, inhibition of bacteria and absence of cytotoxicity towards mammalian cells. The highly hydrophobic catheters released NO in the physiological range that inhibited > 99 % bacterial viability on fibrinogen-coated catheters in a 24 h study. No toxic response of E2As-SNAP catheters leachate was observed using a standard cytotoxicity assay with mouse fibroblast cells. Overall, the results showed that the SNAP-E2As catheters can inhibit viable bacteria even in the presence of blood proteins without causing a cytotoxic response.

1. Introduction

Intravascular catheters are blood contacting devices that are used globally by millions of patients each year. In modern-day medical practices, intravascular catheters enabling direct

vascular access are indispensable for patient diagnosis and treatment, particularly in intensive care units (ICUs).[1] These catheters include peripheral vascular catheters, such as arterial and venous catheters, central venous catheters (CVCs) including tunneled (long-term) and percutaneous non-tunneled catheters, midline catheters, peripherally inserted central catheters (PICCs) and pulmonary artery catheters.[2-5] Although their importance in providing necessary vascular access cannot be denied, they also constitute a breach in the barrier between the outside milieu and the bloodstream, thus increasing the risk of hospital-acquired infections (HAIs). Their use can put the patient at a high risk of local and systemic infectious complications like catheter-related blood infections (CRBIs), septic thrombophlebitis, endocarditis, metastatic infections (e.g., lung abscess, brain abscess, osteomyelitis, and endophthalmitis).[6] The CRBIs rank among the most frequent and potentially lethal nosocomial infections.[7] More than 11% of all the hospital-acquired infections (HAIs) are caused by central venous catheters (CVCs). The incidences of CRBIs in the United States amounts to more than 250,000 cases/year with an attributable mortality of up to 35%.[8] With an additional cost of about $35,000 per episode, CRBIs increase annual healthcare expenditure up to $2.3 billion. Catheter-related blood infections can be attributed to contamination of venous catheter prior to insertion, failure to aseptic insertion or maintenance of the catheter exit site or end luminal site during hub manipulation. Reports have shown that biofilm formation can occur within three days of catheter insertion.[9]

Bacteria binding on the catheter surface can be exacerbated in the presence of blood proteins as they provide a favorable surface for bacteria to adhere. The bacterial adhesion on any indwelling device surfaces is a multi-step process that occurs in three phases and can be exacerbated by protein binding in the initial step.[10] In phase I, blood plasma proteins rapidly coat the device surface immediately after insertion, followed by bacterial adhesion. Initially, the non-specific interaction between the adsorbed protein layer and bacterial cells is mediated by a combination of forces such as gravitational force, Van der Waals force and Coulomb force.[11] This

is followed by specific binding between plasma proteins on the device surface, and bacterial membrane proteins and polysaccharides during phase II. In phase III, a protective layer of exopolysaccharide is secreted by certain bacteria, ultimately constituting a biofilm that resists the effect of bactericidal agents like antibiotics.[12] Approximately 60% of all hospital-associated infections (over one million cases per year) occur due to biofilm formation on indwelling medical devices.[3] Different approaches such as silver-doped material, anti-quorum sensing drugs, and antibiotics have been followed over the last few decades, yet CBRIs remain a problem.[13-15] Therefore, new approaches to reduce the possibilities of these complications, to create truly non-thrombogenic, and antimicrobial catheters are extremely necessary. The ideal catheter should serve two main purposes: (i) minimize blood protein adhesion and (ii) inhibit bacterial adhesion and/or promote bacterial killing. One of the potential approaches could be to fabricate vascular catheters by combining a hemocompatible polymer with a thromboresistant and antimicrobial agent. While the hemocompatible nature of the polymer will prevent the blood protein adhesion and ultimate clot formation, the antimicrobial agent will inhibit bacterial growth and biofilm formation on catheter surface.

To address the aforementioned problems, we developed antithrombic and antibacterial material for venous catheter application. Elaste-Eon-E2As was used as the base polymer and a nitric oxide donor, *S*-nitroso-*N*-acetyl-penicillamine (SNAP) was incorporated into it. E2As is a biomedical grade polymer which is highly hydrophobic in nature that demonstrates excellent hemocompatibility. In the past, a comparative study by Handa et al. on thrombus formation by different medical grade hydrophobic polymers suggested that Elaste-Eon-E2As has smaller thrombus area in a 4 h rabbit model than other polymers such as compared to Tecoflex SG80A, Tecophilic SP60D60, and plasticized poly(vinyl chloride) and hence making it suitable for making blood-contacting devices.[16] This is in line with other studies which demonstrated excellent hemocompatibility of E2As.[17-19]

Incorporation of a NO releasing donor molecule such as SNAP in a hydrophobic polymer such as E2As can significantly inhibit the attached viable bacteria on the polymer surface.[20-26] Nitric oxide (NO) has inherent antithrombotic and antibacterial properties. It is a cellular signaling molecule which is released at a flux of 0.5-4.0 x 10^{-10} mol $min^{-1}cm^{-2}$ in the human body by endothelial cells lining the blood vessels in addition to macrophages and sinus cavities.[16, 24-28] The unpaired NO electron is extremely reactive and has a very short half-life of < 5 sec. [29] The use of NO as an antibacterial agent is not expected to result in any resistance due to its short half-life, rapid reduction of microbial load and non-specific action.[27, 30-32] Furthermore, studies have shown that the SNAP-doped E2As polymer does not result in any cytotoxicity against mammalian cells *in vitro*.[19, 25] The absence of antibiotic resistance and cytotoxicity makes NO based antimicrobial therapy, a better alternative to other commonly used strategies such as antibiotics-based approaches.[33-37]

While the antithrombic and antibacterial properties of NO releasing polymer has been shown as two independent properties in the past. In the present study, the interdependence of fibrinogen binding on bacterial adhesion and how NO releasing catheter surface can overcome this problem is demonstrated. To achieve this, we developed E2As-SNAP based catheters with varying concentration of SNAP, coated them with blood protein fibrinogen and then characterize them in terms of their biomedical applications.

2. Materials and Methods

2.1 Materials

Elast-eon E2As was obtained from AorTech International, plc (Scoresby, Victoria, Australia). Potassium phosphate monobasic, sodium phosphate dibasic, potassium chloride and

sodium chloride, N-acetyl-D-penicillamine (NAP), sodium nitrite, tetrahydrofuran (THF), Ethylenediaminetetraacetic acid (EDTA), hydrochloric acid, sulfuric acid, fibrinogen from bovine plasma, and N, *N*-dimethylacetamide (DMAc) were obtained from Sigma-Aldrich (St. Louis, MO). Autoclaved phosphate buffered saline (PBS), pH 7.4, containing 138 mM NaCl, 2.7 mM KCl, and 10 mM sodium phosphate was used for all *in vitro* experiments. The bacterial strains *Escherichia coli* (ATCC 11303) and *Staphylococcus aureus* (ATCC 6538) and mouse fibroblast cells (ATCC 1658) were originally obtained from the American Type Culture Collection (ATCC).

2.2 Methods

2.2.1 Fabrication of nitric oxide-releasing catheters

A total of thirty-six catheters with a length of 1 cm were fabricated by blending the Elaste-Eon-E2As polymer with SNAP. Elaste-Eon-E2As is a copolymer of mixed soft segments including polydimethylsiloxane and poly hexamethylene oxide. All catheters were prepared by dip-coating stainless-steel mandrels of 2.37 mm diameter in the E2As polymer solutions. The control polymer solution consisted of the E2As in THF (70 mg/mL). To prepare the control catheters, the stainless-steel mandrels were dipped into the control solution 35 times with a drying time of 2 minutes between each coat. The SNAP-doped E2As catheters had a tri-layer configuration consisting of an E2As base layer, SNAP-doped middle layer, and E2As top layer. Top/base layers were composed of 70 mg/mL E2As in THF. Two active solutions were prepared to contain varying weight percentages of SNAP: 5 wt% and 10 wt%. The SNAP-E2As catheters were prepared by dip-coating 4 base layers of the E2As solution, 27 layers of the active, E2As-SNAP solution and 4 top layers of the E2As solution. The top layer not only maintains the hydrophobicity of the surface but prevents any possible leaching of the SNAP from E2As polymer. A drying time of 2 minutes was allowed between each dip coating. All the catheters were dried for a minimum of 24

h at room temperature under a fume hood in ambient lighting. After drying, the catheters were removed from the mandrels and stored in the freezer to prevent NO loss through thermal stimulation.

2.2.2 Contact angle analysis via drop shape analyzer

Owing to the smaller surface area and 3D structure of venous catheter, E2As-SNAP films with similar concentrations as that of E2As-SNAP catheters (tri-layer configuration) were created to have a flat 2D surface for contact angle measurement. The polymeric films of E2As with and without 5 wt% and 10 wt% SNAP were cast in a Teflon mold having a diameter of 2.5 cm. The films were top-coated with E2As and dried similarly to that of catheters. For contact angle analysis, films were placed on top of a glass slide and placed under Kruss DA 100 drop shape analyzer and a ~1 µl drop was placed on films surface. The contact angles for each film type was measured from each frame of the recorded files using the sessile drop approximation.

2.2.3 Binding of fibrinogen protein on the catheter surface

The catheters (length = 1 cm, diameter = 3.27 mm) were soaked in a phosphate buffer solution without chloride salts to bind the plasma protein fibrinogen. Meanwhile, a high concentration fibrinogen protein solution of 20 mg/mL was prepared in PBS as the stock. 100 µL of concentrated fibrinogen solution was added under the surface of 900 µL buffer solution to ensure minimal protein was trapped at the air-water interface. The final concentration of the fibrinogen solution in the buffer was 2 mg/mL. The catheters soaked in the protein solution were kept in an incubator at 37°C for 2h. After 2h, the well was infinitely diluted with deionized water to remove any loosely bound protein. The catheters with bound fibrinogen were used to examine the NO release kinetics and bacterial inhibition.

2.2.4 Nitric oxide release analysis with and without blood protein fibrinogen

The NO release profile was tested with and without exposure to blood protein fibrinogen using a Sievers chemiluminescence Nitric Oxide Analyzer (NOA) 280i (Boulder, CO). The SNAP-doped catheters were placed in a sample cell and immersed in PBS at pH 7.4 containing 100 µM EDTA (to avoid metallic ions assisted NO release). NO released by the catheter sections in the buffer solution was swept into the NOA chemiluminescence detection chamber using N_2 sweep gas and bubbler. Amber color sample cells were used to avoid NO release via light stimulation. Prior to analysis, E2As-SNAP catheter sections with and without fibrinogen exposure were soaked in a 2 mg/mL solution of blood protein fibrinogen for 90 minutes. All catheters were incubated in PBS at 37 °C for the NO release measurement by the NOA. The results were reported as NO flux released per surface area of the catheter sections ($x10^{-10}$ mol min^{-1} cm^{-2}).

2.2.5 Bacterial adhesion test

In the past, multiple studies have been done to show the antibacterial effect of NO but in the absence of blood protein fibrinogen.[23, 25,26] One crucial aspect of the present study was to demonstrate the antibacterial effect of NO on fibrinogen-coated catheters which somewhat imitate the catheter-related blood infection *in vitro*. In, in real-life situations also, the attached blood plasma protein fibrinogen can facilitate bacterial adhesion at a tissue-implant interface, leading to blood infections.[38-40] In the current study, we intended to show the combined effects of E2As and NO to cause a significant reduction in bacteria bound on fibrinogen-coated catheters.

Using a standard bacteria adhesion test, the potential of the E2As-SNAP catheters to inhibit bacterial growth was tested following standard aseptic techniques [23, 41]. Fibrinogen was allowed to bind on the catheter's surface by soaking the catheters in a 20 mg/mL blood protein fibrinogen solution. The gram-positive *Staphylococcus aureus* (*S. aureus*) and gram-negative *Escherichia coli* (*E. coli*) were selected for the study as they are among the most common

pathogens responsible for biofilm formation in vascular catheters.[42] In fact, *S. aureus* is one of the most common causes of catheter-related bloodstream infections (CRBIs) specifically biofilm-associated infections on indwelled biomedical devices.[43-44] The procedure begins with growing 10 mL liquid suspension of bacteria in a 50 mL tube incubated at 37°C for 14 h at a shaking speed of 120 rpm. The optical density of the grown bacteria was measured at 600 nm (OD_{600}) using the UV-vis spectrophotometer (Thermo Scientific Genesys 10S UV-Vis). To remove the traces of LB medium, the bacteria culture was centrifuged for 7 min at 3500 rpm, the supernatant was discarded and 10 mL of sterile phosphate buffer saline (PBS) was added to the bacterial pellet. This step was once again repeated; optical density was measured and readjusted to get the cell count in the range of 10^{-7}-10^{-9} colony forming units per mL of suspension (CFU/mL). The catheters were UV illuminated for 30 min to sterilize their surface prior to using them in the experiment. Thereafter, catheters were exposed to the resulting bacterial suspension for 24 h in a 150-rpm shaker incubator at 37°C. After the 24 h period, the catheters were rinsed with PBS to wash off the bacteria that was not tightly adhered to the catheters' surface. The catheters were placed in 2 mL of sterile PBS solution and homogenized for 45 s. Serial dilutions in the range of 10^{-1}-10^{-5} were made and bacteria solutions were plated on solid LB agar plates. The LB agar plates with the bacteria were incubated for approximately 20 h at 37°C. After 20 h, the CFUs per unit surface area (CFU/cm^2) were counted using the following formula; dilution and working volumes were considered to back-calculate the exact number.

$$\%\ Bacterial\ inhibition = \frac{\left(\frac{CFU}{cm^2}\ in\ control\ samples - \frac{CFU}{cm^2} in\ test\ samples\right) X100}{\frac{CFU}{cm^2}\ in\ control\ samples}$$

2.2.6 Cytotoxicity Assay

To provide a proof of concept on the noncytotoxic behavior of the SNAP-E2As polymer, a standard cell culture assay was conducted in accordance with the ISO 10993 standard. 3T3 Mouse fibroblast cells (ATCC 1658) were exposed to the leachates obtained from SNAP-E2As catheter in a sterile environment in a stepwise manner following standard protocol.[25, 41]

Cell culture: In a 75 cm^2 T-flask containing complete DMEM medium with 1% penicillin-streptomycin antibiotic solution and 10% fetal bovine serum (FBS), mouse fibroblast cells were inoculated from a cryopreserved vial. After inoculation, the cells were transferred in controlled conditions using a cell culture grade incubator (37^{o}C in a humidified atmosphere with 5% CO_2) to favor their growth on T-flask surface. The incubation continued, and the medium was changed every second day until cells confluence 80-90% of the T-flask surface.

Leachate collection from E2As-SNAP catheters: The catheter was cut into small pieces and weighed. 10 mg of the catheter piece was transferred in 10 mL of complete DMEM medium and incubated at 37C to allow leaching of possible extract from the material. After 24 h the catheter pieces were removed, and the leachates were stored in the fridge before used in the experiment.

Leachate exposure to mammalian cells: After reaching a confluence of 80-90%, fibroblast cells were enzymatically detachment from the T-flask using 2.5 mL trypsin based (0.18% trypsin and 5 mM EDTA). Using a dye exclusion method, cells were counted in a hemocytometer by first diluting them with 0.4% trypan blue solution (1:10 ratios of cells: trypan blue) and then transferring 50 µL of the mixture in the hemocytometer and observed under a microscope. After this, the cells from the original source were diluted to get 5000 cells/mL and 100 µL of cells were seeded in each of the well of a 96 well plate (n=7 for each sample type). The leachate collected from the E2As-SNAP catheters were transferred to these cells (10 µL/ well) in each of the wells except for the negative control. The well plate was then incubated for 24 h in the cell culture grade incubator.

After 24 h, 10 µL of a water-soluble tetrazolium salt, WST-8 [2-(2-methoxy-4-nitrophenyl)-3-(4-nitrophenyl)-5-(2,4-disulfophenyl)-2H-tetrazolium monosodium salt] dye based Cell Culture Kit solution (CCK-8). Live mammalian cells secrete dehydrogenases enzymes which can reduce WST-8 into formazan which is bright orange in color and can be detected by a spectrophotometric plate reader. Thus, the amount of orange color product formazan that can be detected at 450 nm is directly proportional to the number of live cells (i.e. lesser the formazan means lesser the viable cells). The background created by DMEM was normalized by using plane DMEM as a reference. Relative mammalian cell viability with respect to the negative control was measured using the following formula.

$$Realtive\ Cell\ Viability\ (\%) = \frac{\text{Absorbance of the test samples}}{\text{Absorbance of the control samples}} \times 100$$

2.2.7 Statistical Analysis

Data for all the experiments are expressed as mean ± SEM (standard error of the mean). Comparison of means using a two-tailed student's t-test assuming unequal variances was utilized to analyze a statistical difference between the samples. Values of $p < 0.05$ were considered statistically significant and graphically illustrated.

3. Results and Discussion

3.1 Hydrophobicity of E2As-SNAP material

Binding of blood plasma protein such as albumin and fibrinogen to the polymeric surface leads to platelet activation, which ultimately causes thrombus formation.[45-46] Fibrinogen is a positive acute phase protein related to blood infection, inflammatory disease and tissue damage ultimately causing patient mortality via trauma coagulopathy.[47-48] Thus a reduction in fibrinogen adhesion is not only expected to reduce thrombus formation but also minimize

infection. One way to reduce fibrinogen interaction is by altering the surface properties of a polymer in terms of its hydrophobicity/hydrophilicity. The contact angle measurement provides an easy way to determine the relative hydrophobicity and hydrophilicity of a material surface. It is the measurement of solid-liquid interfacial tension that is performed by establishing the tangent (angle) of a liquid drop with a solid surface at the base.

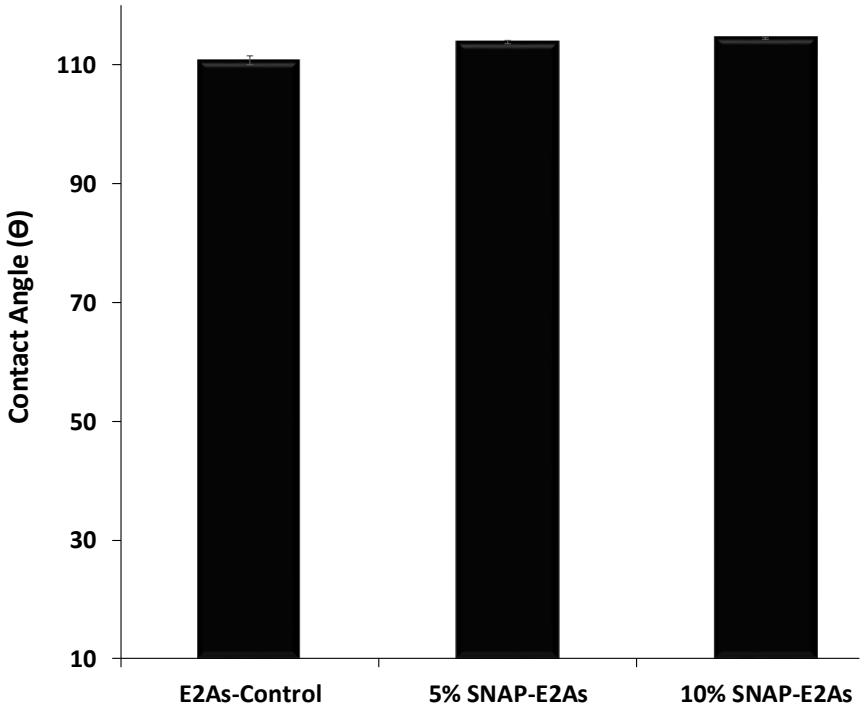

Figure 4.1. The contact angle analysis of E2As-control and E2As-SNAP. The data is reported as a mean ± standard deviation for n=3 samples and the significance with a p-value < 0.05 is stated for comparisons.

This surface property of a polymer can control the interaction of blood proteins and bacteria with the catheter. In general, a surface with a contact angle higher than 90° is considered hydrophobic.[49] A highly hydrophobic surface with low surface energy can exhibit a contact angle as high as ~ 120°.[50]

In this experiment, the change in hydrophobicity of E2As in the absence and presence of NO donor (SNAP) was tested (n=3) using a Kruss DA100 Drop Shape Analyzer. The control E2As

without any SNAP incorporation showed a contact angle of 110.78° ± 0.73°. The 5 wt% SNAP-E2As and 10 wt% SNAP-E2As catheters showed similar contact angles of 113.81° ± 0.23° and 114.53° ± 0.14°. The results confirmed the highly hydrophobic nature of the E2As polymer in combination with SNAP (Figure 4.1). This property is particularly significant in the reduction of clot formation and eventual inhibition of bacterial infection. We have earlier shown that due to its highly hydrophobic nature, E2As forms a smaller thrombus area as compared to another biomedical grade polymer.[16] This can be attributed to E2As higher affinity to albumin as compared to fibrinogen.[17] Due to the abundance of albumin protein in blood, it competes with fibrinogen protein to bind to the polymer surface.[51-53] An inverse correlation between the binding affinity of fibrinogen and albumin to the polymer has been observed in the past.[54] Fibrinogen plays a pivotal role in the coagulation cascade ultimately leading to clot formation.[17] At the same time, fibrinogen also mediates bacterial adhesion on bacterial adhesion to a biomaterial surface.[55-56] E2As higher affinity towards albumin would ultimately result in a decreased fibrinogen binding and hence reduced clotting and bacterial adhesion.

Thus, the contact angle study provides a supporting evidence that E2As catheters due to their inherent hydrophobic surface will ultimately result in reduction blot clots and bacterial interaction on the polymer surface. Ultimately any little number of bound bacteria will be killed in the presence of NO released by incorporated SNAP.

3.2 NO release with and without exposure to plasma fibrinogen

S-Nitroso-*N*-Acetyl-Penicillamine (SNAP) is an S-nitrosothiol which decomposes to release antimicrobial NO by homolytic cleavage of S-N bond under appropriate conditions.[57]

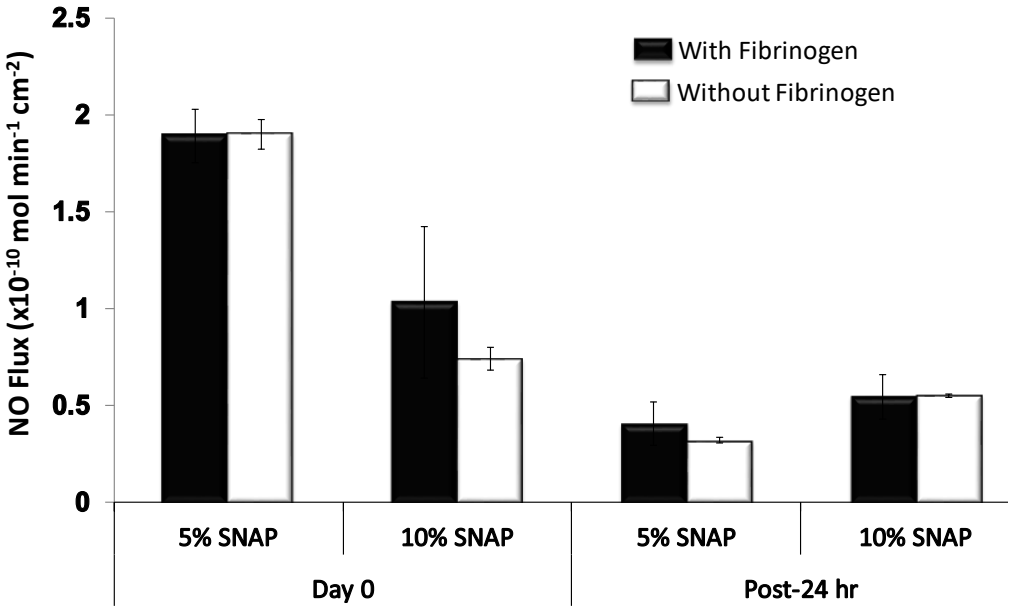

Figure 4.2. Graphical representation of nitric oxide (NO) flux analysis of E2As-control and E2As-SNAP catheters obtained from Sievers chemiluminescence NOA of E2As-control and E2As-SNAP. The data is reported as a mean ± standard error of mean for n=3 samples and the significance with a p-value < 0.05 is stated for comparisons.

The NO release profiles of the 5 wt% and 10 wt% SNAP-E2As catheters were measured both with and without previous exposure to plasma fibrinogen over a 24 h period. The results indicated no significant effect on NO release (Figure 4.2) due to prior exposure to fibrinogen and were found to be consistent with the previous findings. [58-60] The fibrinogen-coated catheters exhibited the NO in the physiological flux range of 0.5-4.0 x 10^{-10} mol min^{-1} cm^{-2}. It is important that the catheters support a NO flux in the physiological range even after exposure to plasma fibrinogen. Differences in NO flux between the 5 wt% and 10 wt% catheters can be attributed to differences in SNAP crystallization due to SNAP solubility within the E2As polymer.[1] These crystalline regions are responsible for the extended storage stability and release rates when used at higher weight percentages. While increasing the loading of SNAP is beneficial for the stability and extended release, increasing loading of the donor can begin to have significant effects on the mechanical properties of the material. [19] It is noteworthy, that although the NO flux in the case of

5 wt% SNAP-E2As catheters was higher than 10 wt% SNAP-E2As towards the beginning (represented as 0 h in the graph), it eventually turned out that 10 wt% SNAP-E2As showed higher NO flux at 24 h time point. This is attributed to the slow and sustained release of NO from the crystallized SNAP structure at higher SNAP loading in a hydrophobic polymer. No significant differences between fibrinogen-coated and non-coated catheters were observed which is in line with the existing literature.[16] The incorporation of SNAP into biomedical grade polymers such as E2As can yield remarkably stable biomaterials, with excellent storage stability and mechanical strength.[20] In the past, SNAP-E2As material has been shown to release NO for 20 days as measured by chemiluminescence NO analyzer with very low levels of leaching.[61] We have recently shown in a stability study that E2As-SNAP can retain 82% of the SNAP during a 2 months period at 37°C.[19] The simplicity and flexibility of SNAP-E2As catheters' fabrication method allow the fine tuning of polymer and NO donor concentration. Hence higher NO flux levels than those shown in the present study can be achieved if needed.

3.3 Inhibition of gram-positive and gram-negative bacterial growth on catheter surface

An increase in bacterial adhesion in the presence of blood protein mainly happens due to the non-specific interactions such as gravitational, Van der Walls, and Coulomb forces between adsorbed protein layer and bacterial cells.[10] Additionally, some catheters surfaces due to their surface properties are more susceptible to thrombus formation as compared to others which predispose them to increased bacterial adhesion.[16, 62-63] Catheters with irregular surfaces facilitate the binding of bacteria to the catheter's surface.[62, 64] Besides the surface properties of the polymer used in catheter fabrication, the adherence properties of bacteria are also crucial for the pathogenesis of bacterial related infections. For instance, as compared to other blood pathogens, *Staphylococci* has the greater binding ability to the implant surface that leads to the formation of a slimy extracellular polysaccharide.[65] This extracellular matrix protects the bacteria from the

action of antibiotics, silver nanoparticles, and other microbicidal agents. However, NO due to its small size can penetrate through the matrix and hence kill the bacteria embedded in the biofilms. In this study, we could successfully show a significant reduction in the population of *S. aureus* as discussed below. As a proof of concept to show the bacterial inhibition properties, fibrinogen-coated SNAP-E2As catheters were exposed to gram-positive *S. aureus* and gram-negative *E. coli* bacteria. The amount of bacterial inhibition was directly proportional to the amount of NO flux (see Table 4.1).

Table 4.1. Comparative analysis of NO flux and adhered viable bacteria cells (CFU/cm^2)

Sample	NO flux (10^{-10} molmin^{-1}cm^{-2})		*S. aureus* (CFU/cm^2)	*E. coli* (CFU/cm^2)
	0 hour	24 hour		
E2As- Control	--		$6.7 \pm 2.2 \times 10^7$	$1.6 \pm 0.2 \times 10^8$
5% SNAP-E2As-Fibrinogen	1.9 ± 0.1	0.40 ± 0.1	$1.3 \pm 0.3 \times 10^6$	$4.2 \pm 0.6 \times 10^6$
10% SNAP-E2As-Fibrinogen	1.03 ± 0.4	0.55 ± 0.1	$5.5 \pm 2.2 \times 10^5$	$1.4 \pm 0.3 \times 10^5$

When 5 wt% SNAP-E2As and 10 wt% SNAP-E2As catheters were compared with each other, 10 wt% SNAP-E2As killed twice the number of bacteria due to sustaining NO flux for full 24 h period. Overall, a bacterial inhibition up to 2 logs was observed for both *S. aureus* (Figure 4.3) and *E. coli* (Figure 4.4) using the NO releasing catheters. On a percentage scale, the efficiency of *S. aureus* and *E. coli* inhibition was up to 99.20 ± 0.11 % and 99.10 ± 0.20 % respectively. Such a high level of reduction in bacterial colony forming units on a polymeric surface is a significant stride in direction of development of new class of biopolymers needed for biomedical device fabrication.

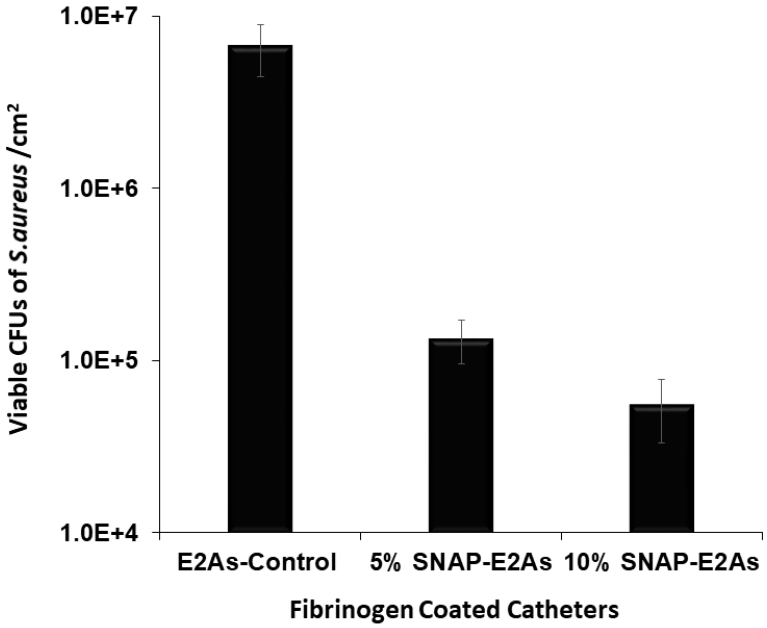

Figure 4.3. The antibacterial efficacy of NO releasing E2As catheters against a gram-positive bacterium, *S. aureus* tested. Approximately, 2-log reduction in *S. aureus* CFU/cm^2 was observed between NO releasing SNAP-E2As catheters vs control catheters with or without fibrinogen. The data is reported as a mean ± standard deviation for n=3 samples and the significance with a p-value < 0.05 is stated for comparisons.

The NO-dependent bacterial killing mechanism includes DNA cleavage, lipid peroxidation, tyrosine nitration and nitrosation of amines, and thiols [66-67]. In the recent years, we and other scientific groups have demonstrated that the antimicrobial activity of the various NO delivery systems could be used against a variety of microorganisms to prevent infection in blood contacting devices. [20, 68-69] In this regard, antibacterial properties of NO donors have been proven against pathogens such as *Staphylococcus aureus,* [25, 70-72] *Staphylococcus epidermis,* [70] *Pseudomonas aeruginosa,* [25, 27, 71] *Escherichia coli,* [70-75] *Acinetobacter baumanii,* [76-77] *Listeria monocytogenes,* and *Enterococcus faecalis.*[26] Along these lines, the results from the current study provide an important proof of concept for the killing of bacteria attached to surface-bound plasma proteins on E2As-SNAP catheters via the bactericidal action of NO. Furthermore, NO due to its

short half-life (< 5 secs), rapid and nonspecific bactericidal action is not expected to trigger any resistance in bacteria, unlike antibiotics.[27, 30-32] One of the major advantages of this strategy is that it can be combined with other antimicrobial agents such as quaternary ammonium ions, silicone oil, and nanoparticles to bring about a more enhanced antibacterial effect without negatively impacting the NO release. [23, 25, 78]

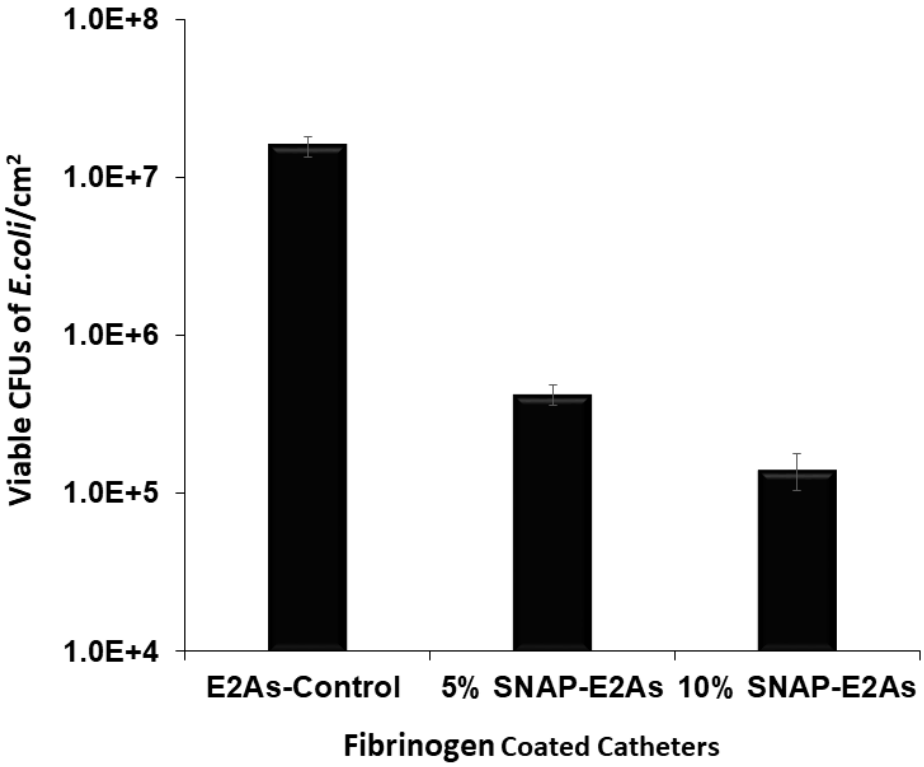

Figure 4.4. The antibacterial efficacy of NO releasing E2As catheters against a gram-negative bacterium, *E. coli* tested via a standard bacteria adhesion test. Around 2 log reductions in *E. coli* CFU/cm^2 was seen between NO releasing SNAP-E2As catheters vs control catheters with or without fibrinogen. The data is reported as a mean ± standard deviation for n=3 samples and the significance with a p-value < 0.05 is stated for comparisons.

Along these lines, the results from the current study provide an important proof of concept for the killing of bacteria attached to surface-bound plasma proteins on E2As-SNAP catheters via the bactericidal action of NO. Furthermore, NO due to its short half-life (< 5 secs), rapid and nonspecific bactericidal action is not expected to trigger any resistance in bacteria, unlike

antibiotics.[27, 30-32] One of the major advantages of this strategy is that it can be combined with other antimicrobial agents such as quaternary ammonium ions, silicone oil, and nanoparticles to bring about a more enhanced antibacterial effect without negatively impacting the NO release. [23, 25, 78]

3.4 Cytotoxicity assay

The absence of any cytotoxic response is inevitable for the success of any biomedical device application. In the current study, leachates from control E2As and SNAP-E2As catheters were collected and mouse fibroblast cells (ATCC 1658) were exposed to them for a 24 h period and the viability of the cells was compared. As Figure 4.5 shows, the cells exposed to leachates collected from SNAP-E2As catheters and control E2As catheters (n=7) demonstrated similar cell viability when compared to cells without any leachate exposure (positive control). The results from our current study are in agreement with another study where SNAP incorporation in Carbosil was shown to possess bactericidal properties with minimal platelet activation and no cytotoxicity.[41]

This is an important attribute for the safety and efficacy since many therapeutic agents pose remarkable antibacterial properties but at the same time can cause toxicity to the host cells. For instance, antibiotics application offers a popular lock solution for venous catheters but at the compromise of antibiotic resistance and cytotoxicity of antibiotics towards mammalian cells.[13-15] Nitric oxide due to its endogenous nature, rapid action, non-specific bactericidal mechanism, and short half-life is not expected to allow development of resistant bacterial strains and cytotoxic response. [27, 31-32] SNAP-E2As catheters which can inhibit bacteria up to 2 logs in the presence of blood protein without causing cytotoxicity to provide an initial proof of concept for their potential biocompatibility. The results from this study overlap with other studies which show NO releasing surfaces to be highly effective in their antibacterial potential without any cytotoxic response, hemolysis, and platelet activation [16, 19, 41, 79]

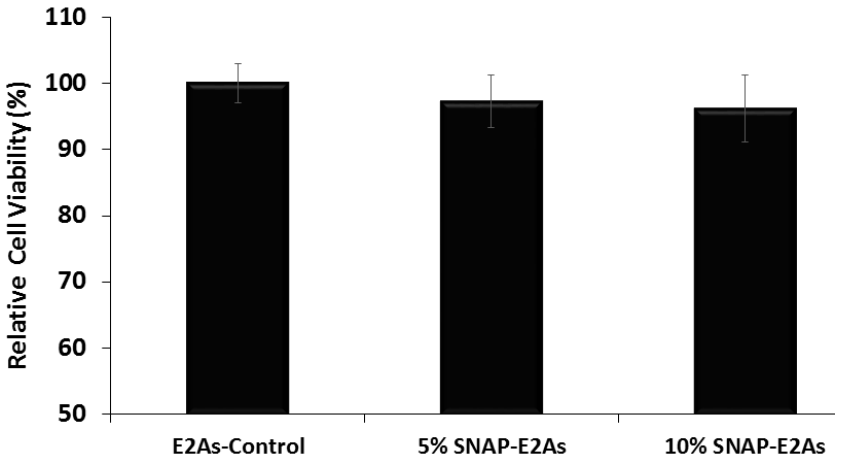

Figure 4.5. Graphical representation of results from the cytotoxicity test done using a standard WST-8 dye based CCK-8 kit with mouse fibroblast cells. The data clearly shows the non-toxic nature of leachates obtained from control and SNAP containing catheters. The results were measured as percentage cytotoxicity of leachate obtained from SNAP-E2As catheters relative to control catheters without SNAP. The data is reported as a mean ± standard deviation for n=7 samples (each type) and the significance with a p-value < 0.05 is stated for comparisons.

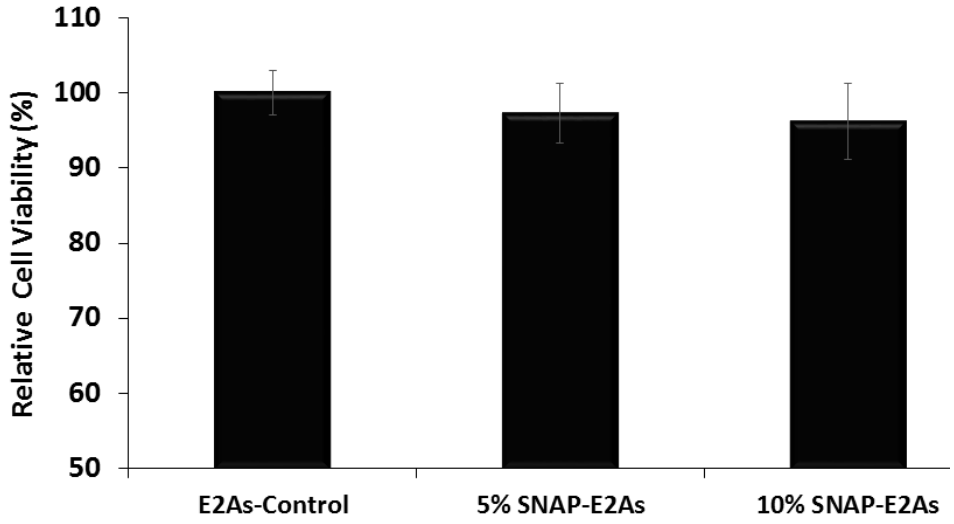

Figure 4.6. Graphical representation of non-cytotoxic nature of SNAP-E2As catheters

4. Conclusions

Blood clotting and infection are two common problems associated with vascular catheters. E2As with its inherent hydrophobic nature can bind to higher albumin and hence lower fibrinogen. Fibrinogen, blood plasma protein plays a key role in clot formation and eventual bacterial adhesion to the implant surface. Based on this concept, SNAP-E2As catheters were developed, coated with blood protein fibrinogen and their antibacterial potential was tested against gram-positive and gram-negative bacteria. The NO releasing E2As catheters owing to its hydrophobic surface were expected to show reduced bacterial adhesion because of reduction in fibrinogen binding. As expected, the NO releasing SNAP-E2As catheters resulted in > 99 % both grams positive and negative as compared to control E2As catheters (with fibrinogen coating). This result stems from the fact that, the highly hydrophobic nature of E2As helps to reduce the adhesion of fibrinogen, while the free radical NO killed bacteria via lipid peroxidation, DNA cleavage, tyrosine nitration and nitrosation of amines and thiols. The fabricated SNAP-E2As catheters exposed to fibrinogen protein exhibited a NO flux in the physiological range. The cell viability assay on mouse fibroblast cells confirmed that SNAP-E2As catheters can prevent bacterial adhesion without causing cytotoxicity towards mammalian cells thus providing supporting evidence for their biocompatibility. From a translational perspective, SNAP-E2As based biomaterials have excellent storage stability, can undergo popular sterilization methods and have excellent mechanical strength.[19]

Acknowledgement

This work is supported by National Institutes of Health, USA grant K25HL111213, R01HL134899, and Centers for Disease Control and Prevention, USA contract 200-2016-9193.

References

(1) Wo, Y.; Li, Z.; Brisbois, E. J.; Colletta, A.; Wu, J.; Major, T. C.; Xi, C.; Bartlett, R. H.; Matzger, A. J.; Meyerhoff, M. E. Origin of long-term storage stability and nitric oxide release behavior of carbosil polymer doped with s-nitroso-n-acetyl-d-penicillamine. *ACS Appl. Mater. Interfaces* **2015,** *7* (40), 22218-22227.

(2) O'grady, N. P.; Alexander, M.; Dellinger, E. P.; Gerberding, J. L.; Heard, S.; Maki, D.; Masur, H.; Mccormick, R.; Mermel, L.; Pearson, M. Draft guideline for the prevention of intravascular catheter-related infections. *Centers for Disease Control: Atlanta, GA* **2001**.

(3) Crnich, C. J.; Maki, D. G. The promise of novel technology for the prevention of intravascular device—related bloodstream infection. I. Pathogenesis and short-term devices. *Clin. Infect. Dis.* **2002,** *34* (9), 1232-1242.

(4) Maki, D. G.; Kluger, D. M.; Crnich, C. J. In *The risk of bloodstream infection in adults with different intravascular devices: A systematic review of 200 published prospective studies*, Mayo Clinic Proceedings, Elsevier: **2006**; pp 1159-1171.

(5) Raad, I.; Hanna, H.; Maki, D. Intravascular catheter-related infections: Advances in diagnosis, prevention, and management. *The Lancet infectious diseases* **2007,** *7* (10), 645-657.

(6) O'grady, N. P.; Alexander, M.; Dellinger, E. P.; Gerberding, J. L.; Heard, S. O.; Maki, D. G.; Masur, H.; Mccormick, R. D.; Mermel, L. A.; Pearson, M. L. Guidelines for the prevention of intravascular catheter–related infections. *Clinical infectious diseases* **2002,** *35* (11), 1281-1307.

(7) Mirijello, A.; Impagnatiello, M.; Zaccone, V.; Ventura, G.; Pompa, L.; Addolorato, G.; Landolfi, R. Catheter-related bloodstream infections by opportunistic pathogens in immunocompromised hosts. *European review for medical and pharmacological sciences* **2015,** *19* (13), 2440-2445.

(8) Daniels, K. R.; Frei, C. R. The united states' progress toward eliminating catheter-related bloodstream infections: Incidence, mortality, and hospital length of stay from 1996 to 2008. *Am. J. Infect. Control* **2013,** *41* (2), 118-121.

(9) Anaissie, E.; Samonis, G.; Kontoyiannis, D.; Costerton, J.; Sabharwal, U.; Bodey, G.; Raad, I. Role of catheter colonization and infrequent hematogenous seeding in catheter-related infections. *European Journal of Clinical Microbiology and Infectious Diseases* **1995,** *14* (2), 134-137.

(10) Pascual, A. Pathogenesis of catheter-related infections: Lessons for new designs. *Clin. Microbiol. Infect.* **2002,** *8* (5), 256-264.

(11) Katsikogianni, M.; Missirlis, Y. Concise review of mechanisms of bacterial adhesion to biomaterials and of techniques used in estimating bacteria-material interactions. *Eur Cell Mater* **2004,** *8* (3).

(12) Donlan, R. M.; Costerton, J. W. Biofilms: Survival mechanisms of clinically relevant microorganisms. *Clinical microbiology reviews* **2002,** *15* (2), 167-193.

(13) Chung, K. K.; Schumacher, J. F.; Sampson, E. M.; Burne, R. A.; Antonelli, P. J.; Brennan, A. B. Impact of engineered surface microtopography on biofilm formation of staphylococcus aureus. *Biointerphases* **2007,** *2* (2), 89-94.

(14) Veenstra, D. L.; Saint, S.; Saha, S.; Lumley, T.; Sullivan, S. D. Efficacy of antiseptic-impregnated central venous catheters in preventing catheter-related bloodstream infection: A meta-analysis. *Jama* **1999,** *281* (3), 261-267.

(15) O'grady, N. P.; Alexander, M.; Burns, L. A.; Dellinger, E. P.; Garland, J.; Heard, S. O.; Lipsett, P. A.; Masur, H.; Mermel, L. A.; Pearson, M. L. Guidelines for the prevention of intravascular catheter-related infections. *Clinical infectious diseases* **2011,** *52* (9), e162-e193.

(16) Handa, H.; Major, T. C.; Brisbois, E. J.; Amoako, K. A.; Meyerhoff, M. E.; Bartlett, R. H. Hemocompatibility comparison of biomedical grade polymers using rabbit thrombogenicity model

for preparing nonthrombogenic nitric oxide releasing surfaces. *J. Mater. Chem. B* **2014,** *2* (8), 1059-1067.

(17) Cozzens, D.; Luk, A.; Ojha, U.; Ruths, M.; Faust, R. Surface characterization and protein interactions of segmented polyisobutylene-based thermoplastic polyurethanes. *Langmuir* **2011,** *27* (23), 14160-14168.

(18) Simmons, A.; Padsalgikar, A. D.; Ferris, L. M.; Poole-Warren, L. A. Biostability and biological performance of a pdms-based polyurethane for controlled drug release. *Biomaterials* **2008,** *29* (20), 2987-2995.

(19) Goudie, M. J.; Brisbois, E. J.; Pant, J.; Thompson, A.; Potkay, J. A.; Handa, H. Characterization of an s-nitroso-n-acetylpenicillamine–based nitric oxide releasing polymer from a translational perspective. *International Journal of Polymeric Materials and Polymeric Biomaterials* **2016,** *65* (15), 769-778.

(20) Brisbois, E. J.; Davis, R. P.; Jones, A. M.; Major, T. C.; Bartlett, R. H.; Meyerhoff, M. E.; Handa, H. Reduction in thrombosis and bacterial adhesion with 7 day implantation of s-nitroso-n-acetylpenicillamine (snap)-doped elast-eon e2as catheters in sheep. *Journal of Materials Chemistry B* **2015,** *3* (8), 1639-1645.

(21) Brisbois, E. J.; Handa, H.; Davis, R.; Jones, A.; Bartlett, R. H.; Meyerhoff, M. E. S-nitroso-n-acetylpenicillamine (snap)-doped elast-eon catheters reduce thrombosis and bacterial adhesion.

(22) Carpenter, A. W.; Schoenfisch, M. H. Nitric oxide release: Part ii. Therapeutic applications. *Chem. Soc. Rev.* **2012,** *41* (10), 3742-3752.

(23) Pant, J.; Gao, J.; Goudie, M. J.; Hopkins, S.; Locklin, J.; Handa, H. A multi-defense strategy: Enhancing bactericidal activity of a medical grade polymer with a nitric oxide donor and surface-immobilized quaternary ammonium compound. *Acta Biomater.* **2017**.

(24) Pant, J.; Goudie, M.; Brisbois, E.; Handa, H. Nitric oxide-releasing polyurethanes. *Advances in Polyurethane Biomaterials* **2016**, 417.

(25) Pant, J.; Goudie, M. J.; Hopkins, S. P.; Brisbois, E. J.; Handa, H. Tunable nitric oxide release from s-nitroso-n-acetylpenicillamine via catalytic copper nanoparticles for biomedical applications. *ACS Appl. Mater. Interfaces*.

(26) Sundaram, J.; Pant, J.; Goudie, M. J.; Mani, S.; Handa, H. Antimicrobial and physicochemical characterization of biodegradable, nitric oxide-releasing nanocellulose-chitosan packaging membranes. *J. Agric. Food Chem.* **2016**.

(27) Hetrick, E. M.; Schoenfisch, M. H. Antibacterial nitric oxide-releasing xerogels: Cell viability and parallel plate flow cell adhesion studies. *Biomaterials* **2007,** *28* (11), 1948-1956.

(28) Bogdan, C.; Röllinghoff, M.; Diefenbach, A. The role of nitric oxide in innate immunity. *Immunol. Rev.* **2000,** *173* (1), 17-26.

(29) Thomas, D. D.; Liu, X.; Kantrow, S. P.; Lancaster, J. R. The biological lifetime of nitric oxide: Implications for the perivascular dynamics of no and o2. *Proceedings of the National Academy of Sciences* **2001,** *98* (1), 355-360.

(30) Heilman, B. J.; Halpenny, G. M.; Mascharak, P. K. Synthesis, characterization, and light-controlled antibiotic application of a composite material derived from polyurethane and silica xerogel with embedded photoactive manganese nitrosyl. *Journal of Biomedical Materials Research Part B: Applied Biomaterials* **2011,** *99* (2), 328-337.

(31) Feelisch, M. The use of nitric oxide donors in pharmacological studies. *Naunyn-Schmiedeberg's Arch. Pharmacol.* **1998,** *358* (1), 113-122.

(32) Bogdan, C. Nitric oxide and the immune response. *Nat. Immunol.* **2001,** *2* (10), 907-916.

(33) Lee, Y.-H.; Cheng, F.-Y.; Chiu, H.-W.; Tsai, J.-C.; Fang, C.-Y.; Chen, C.-W.; Wang, Y.-J. Cytotoxicity, oxidative stress, apoptosis and the autophagic effects of silver nanoparticles in mouse embryonic fibroblasts. *Biomaterials* **2014,** *35* (16), 4706-4715.

(34) Park, E. J., Yi, J., Kim, Y., Choi, K., Park, K. Silver nanoparticles induce cytotoxicity by a trojan-horse type mechanism. *Toxicology In Vitro* **2010,** *24* (3), 872-878.

(35) Baldi, C., Minoia, C., Di Nucci, A., Capodaglio, E., Manzo, L. Effects of silver in isolated rat hepatocytes. *Toxicology Letters* **1988,** *41* (3), 261-268.

(36) Asharani, P. V., Mun, G.L.K., Hande, M.P., Valiyaveettil. Cytotoxicity and genotoxicity of silver nanoparticles in human cells. *ACS Nano* **2009,** *3* (2), 279-290.

(37) Stewart, P. S.; Costerton, J. W. Antibiotic resistance of bacteria in biofilms. *The lancet* **2001,** *358* (9276), 135-138.

(38) Que, Y.-A.; Haefliger, J.-A.; Piroth, L.; François, P.; Widmer, E.; Entenza, J. M.; Sinha, B.; Herrmann, M.; Francioli, P.; Vaudaux, P. Fibrinogen and fibronectin binding cooperate for valve infection and invasion in staphylococcus aureus experimental endocarditis. *J. Exp. Med.* **2005,** *201* (10), 1627-1635.

(39) Cho, S.-H.; Strickland, I.; Boguniewicz, M.; Leung, D. Y. Fibronectin and fibrinogen contribute to the enhanced binding of staphylococcus aureus to atopic skin. *J. Allergy Clin. Immunol.* **2001,** *108* (2), 269-274.

(40) An, Y. H.; Friedman, R. J. Concise review of mechanisms of bacterial adhesion to biomaterial surfaces. *J. Biomed. Mater. Res.* **1998,** *43* (3), 338-348.

(41) Pant, J.; Goudie, M. J.; Hopkins, S. P.; Brisbois, E. J.; Handa, H. Tunable nitric oxide release from s-nitroso-n-acetylpenicillamine via catalytic copper nanoparticles for biomedical applications. *ACS Appl. Mater. Interfaces* **2017,** *9* (18), 15254-15264.

(42) Donlan, R. M. Biofilms and device-associated infections. *Emerging infectious diseases* **2001,** *7* (2), 277.

(43) Allan, N. D.; Giare-Patel, K.; Olson, M. E. An in vivo rabbit model for the evaluation of antimicrobial peripherally inserted central catheter to reduce microbial migration and colonization as compared to an uncoated picc. *BioMed Research International* **2012,** *2012*.

(44) Otto, M. Staphylococcal infections: Mechanisms of biofilm maturation and detachment as critical determinants of pathogenicity. *Annu. Rev. Med.* **2013,** *64*, 175-188.

(45) Nieswandt, B.; Moser, M.; Pleines, I.; Varga-Szabo, D.; Monkley, S.; Critchley, D.; Fässler, R. Loss of talin1 in platelets abrogates integrin activation, platelet aggregation, and thrombus formation in vitro and in vivo. *J. Exp. Med.* **2007,** *204* (13), 3113-3118.

(46) Jackson, S. P.; Nesbitt, W. S.; Kulkarni, S. Signaling events underlying thrombus formation. *J. Thromb. Haemost.* **2003,** *1* (7), 1602-1612.

(47) Kushner, I. The acute phase response: An overview. *Methods Enzymol.* **1988,** *163*, 373.

(48) Fries, D.; Martini, W. Role of fibrinogen in trauma-induced coagulopathy. *Br. J. Anaesth.* **2010,** *105* (2), 116-121.

(49) Förch, R.; Jenkins, A. T. A., *Surface design: Applications in bioscience and nanotechnology*. John Wiley & Sons: **2009**.

(50) Zisman, W. A., Relation of the equilibrium contact angle to liquid and solid constitution. ACS Publications: **1964**.

(51) Tang, L.; Thevenot, P.; Hu, W. Surface chemistry influences implant biocompatibility. *Curr. Top. Med. Chem.* **2008,** *8* (4), 270-280.

(52) Ghitescu, L.; Fixman, A.; Simionescu, M.; Simionescu, N. Specific binding sites for albumin restricted to plasmalemmal vesicles of continuous capillary endothelium: Receptor-mediated transcytosis. *The Journal of Cell Biology* **1986,** *102* (4), 1304-1311.

(53) Warkentin, P.; Wälivaara, B.; Lundström, I.; Tengvall, P. Differential surface binding of albumin, immunoglobulin g and fibrinogen. *Biomaterials* **1994,** *15* (10), 786-795.

(54) Ben-Ami, R.; Barshtein, G.; Mardi, T.; Deutch, V.; Elkayam, O.; Yedgar, S.; Berliner, S. A synergistic effect of albumin and fibrinogen on immunoglobulin-induced red blood cell aggregation. *Am. J. Physiol.: Heart Circ. Physiol* **2003,** *285* (6), H2663-H2669.

(55) Elgalai, I.; Foster, H. Comparison of adhesion of wound isolates of staphylococcus aureus to immobilized proteins. *J. Appl. Microbiol.* **2003,** *94* (3), 413-420.

(56) Taylor Jr, F. B.; Wada, H.; Kinasewitz, G. Description of compensated and uncompensated disseminated intravascular coagulation (dic) responses (non-overt and overt dic)

in baboon models of intravenous and intraperitoneal escherichia coli sepsis and in the human model of endotoxemia: Toward a better definition of dic. *Crit. Care Med.* **2000,** *28* (9), S12-S19.

(57) Ignarro, L. J.; Lippton, H.; Edwards, J. C.; Baricos, W. H.; Hyman, A. L.; Kadowitz, P. J.; Gruetter, C. A. Mechanism of vascular smooth muscle relaxation by organic nitrates, nitrites, nitroprusside and nitric oxide: Evidence for the involvement of s-nitrosothiols as active intermediates. *Journal of Pharmacology and Experimental Therapeutics* **1981,** *218* (3), 739-749.

(58) Brisbois, E. J.; Major, T. C.; Goudie, M. J.; Meyerhoff, M. E.; Bartlett, R. H.; Handa, H. Attenuation of thrombosis and bacterial infection using dual function nitric oxide releasing central venous catheters in a 9day rabbit model. *Acta Biomater.* **2016,** *44*, 304-312.

(59) Handa, H.; Brisbois, E. J.; Major, T. C.; Refahiyat, L.; Amoako, K. A.; Annich, G. M.; Bartlett, R. H.; Meyerhoff, M. E. In vitro and in vivo study of sustained nitric oxide release coating using diazeniumdiolate-doped poly (vinyl chloride) matrix with poly (lactide-co-glycolide) additive. *J. Mater. Chem. B* **2013,** *1* (29), 3578-3587.

(60) Major, T. C.; Brant, D. O.; Reynolds, M. M.; Bartlett, R. H.; Meyerhoff, M. E.; Handa, H.; Annich, G. M. The attenuation of platelet and monocyte activation in a rabbit model of extracorporeal circulation by a nitric oxide releasing polymer. *Biomaterials* **2010,** *31* (10), 2736-2745.

(61) Brisbois, E. J.; Handa, H.; Major, T. C.; Bartlett, R. H.; Meyerhoff, M. E. Long-term nitric oxide release and elevated temperature stability with s-nitroso-n-acetylpenicillamine (snap)-doped elast-eon e2as polymer. *Biomaterials* **2013,** *34* (28), 6957-6966.

(62) Nachnani, G. H.; Lessin, L. S.; Motomiya, T.; Jensen, W. N. Scanning electron microscopy of thrombogenesis on vascular catheter surfaces. *New Engl. J. Med.* **1972,** *286* (3), 139-140.

(63) Stillman, R. M.; Soliman, F.; Garcia, L.; Sawyer, P. N. Etiology of catheter-associated sepsis: Correlation with thrombogenicity. *Arch. Surg.* **1977,** *112* (12), 1497-1499.

(64) Locci, R.; Peters, G.; Pulverer, G. Microbial colonization of prosthetic devices. Iv. Scanning electron microscopy of intravenous catheters invaded by yeasts. *Zentralblatt fur Bakteriologie, Mikrobiologie und Hygiene. 1. Abt. Originale B, Hygiene* **1981,** *173* (6), 419-424.

(65) Gray, E.; Verstegen, M.; Peters, G.; Regelmann, W. Effect of extracellular slime substance from staphylococcus epidermidis on the human cellular immune response. *The Lancet* **1984,** *323* (8373), 365-367.

(66) Fang, F. C. Perspectives series: Host/pathogen interactions. Mechanisms of nitric oxide-related antimicrobial activity. *Journal of Clinical Investigation* **1997,** *99* (12), 2818-2825.

(67) Fang, F. C. Antimicrobial actions of nitric oxide. *Nitric oxide : biology and chemistry / official journal of the Nitric Oxide Society* **2012,** *27, Supplement*, S10.

(68) Jitendra Pant, M. J. G., Elizabeth.J. Brisbois, Hitesh Handa. Nitric oxide-releasing polyurethanes. *Advances in Polyurethane Biomaterials* **2016,** *1*, 417–449.

(69) Reynolds, M. M.; Frost, M. C.; Meyerhoff, M. E. Nitric oxide-releasing hydrophobic polymers: Preparation, characterization, and potential biomedical applications. *Free Radical Biol. Med.* **2004,** *37* (7), 926-936.

(70) Charville, G. W.; Hetrick, E. M.; Geer, C. B.; Schoenfisch, M. H. Reduced bacterial adhesion to fibrinogen-coated substrates via nitric oxide release. *Biomaterials* **2008,** *29* (30), 4039-4044.

(71) Engelsman, A. F.; Krom, B. P.; Busscher, H. J.; Van Dam, G. M.; Ploeg, R. J.; Van Der Mei, H. C. Antimicrobial effects of an no-releasing poly(ethylene vinylacetate) coating on soft-tissue implants in vitro and in a murine model. *Acta Biomaterialia* **2009,** *5* (6), 1905-1910.

(72) Cai, W.; Wu, J.; Xi, C.; Meyerhoff, M. E. Diazeniumdiolate-doped poly(lactic-co-glycolic acid)-based nitric oxide releasing films as antibiofilm coatings. *Biomaterials* **2012,** *33* (32), 7933-7944.

(73) Carlsson, S.; Weitzberg, E.; Wiklund, P.; Lundberg, J. O. Intravesical nitric oxide delivery for prevention of catheter-associated urinary tract infections. *Antimicrobial Agents and Chemotherapy* **2005,** *49* (6), 2352-2355.

(74) Regev-Shoshani, G.; Ko, M.; Crowe, A.; Av-Gay, Y. Comparative efficacy of commercially available and emerging antimicrobial urinary catheters against bacteriuria caused by e-coli in vitro. *Urology* **2011,** *78* (2), 334-339.

(75) Regev-Shoshani, G.; Ko, M.; Miller, C.; Av-Gay, Y. Slow release of nitric oxide from charged catheters and its effect on biofilm formation by escherichia coli. *Antimicrobial Agents and Chemotherapy* **2010,** *54* (1), 273-279.

(76) Mihu, M. R.; Sandkovsky, U.; Han, G.; Friedman, J. M.; Nosanchuk, J. D.; Martinez, L. R. The use of nitric oxide releasing nanoparticles as a treatment against acinetobacter baumannii in wound infections. *Virulence* **2010,** *1* (2), 62-67.

(77) Brisbois, E. J.; Bayliss, J.; Wu, J.; Major, T. C.; Xi, C.; Wang, S. C.; Bartlett, R. H.; Handa, H.; Meyerhoff, M. E. Optimized polymeric film-based nitric oxide delivery inhibits bacterial growth in a mouse burn wound model. *Acta Biomaterialia* **2014,** *10* (10), 4136-4142.

(78) Goudie, M. J.; Pant, J.; Handa, H. Liquid-infused nitric oxide-releasing (linorel) silicone for decreased fouling, thrombosis, and infection of medical devices. *Sci. Rep.* **2017,** *7* (1), 13623.

(79) Singha, P.; Pant, J.; Goudie, M. J.; Workman, C. D.; Handa, H. Enhanced antibacterial efficacy of nitric oxide releasing thermoplastic polyurethanes with antifouling hydrophilic topcoats. *Biomaterials Science* **2017**.

CHAPTER 5

IN VITRO STUDY OF ANTIBACTERIAL AND CELLULAR RESPONSE TOWARDS A S-NITROSO-GLUTATHIONE (GSNO) BASED BIOMATERIAL FOR POTENTIAL WOUND HEALING APPLICATION

1. Introduction

Wounding leads to exposure of subcutaneous tissue that provides a nutritious environment conducive to microbial colonization and proliferation. The presence of bacteria at the wound site downregulates the host immune response, ultimately delaying the natural wound healing process. Inappropriate progression of the healing process in chronic wounds can often make the total healing time unpredictable.[1-2] It can also result in life-threatening complications like pressure sores and diabetic foot ulcers, which can lead to amputation of the affected limb.[3] Skin infections contribute to 200 million visits to physicians costing over $350 million annually.[4] Therefore, controlling infection at the wound site is considered one of the parameters in wound healing applications. Another challenge during the wound healing process is to rejuvenate the ruptured blood vessels in the wounded tissue (angiogenesis) important for the transfer of chemokines, nutrients, and oxygen.[5] In addition, fibroblast cell proliferation and migration are required for ultimate collagen matrix formation and scarring of the tissue.[6] Antibiotic and silver nanoparticle based antimicrobial agents that are popularly used as topical ointments for wounded surface are limited by several factors. The bacterial biofilms are protected by extracellular polysaccharide matrix leading to bacterial resistance against antibiotics. This also perpetuates the inflammatory phase of wound healing.[7] Silver nanoparticles have shown to be genotoxic and

cytotoxic to host cells.[8-9] Moreover, these antimicrobial agents only target wound infection while other important host cell responses such as fibroblast proliferation and migration as well as angiogenesis are left to their natural fates. Given the complexity of the wound healing process, it is obvious that a holistic approach is needed to target different biological responses desirable for faster wound healing while simultaneously preventing antibiotic resistance and cytotoxicity to host cells.

In the last two decades, nitric oxide (NO) has emerged as a critical player in all four phases of natural wound healing namely hemostasis, inflammation, fibroblast proliferation and tissue remodeling.[10] Nitric oxide can act against a wide variety of microorganisms: gram-positive and -negative bacteria, fungus, yeast, and viruses.[11-14] The gaseous nature of NO allows penetration through the matrix in the biofilm, which gives it an extra advantage over antibiotics and silver-based antibacterial strategies. Due to its rapid action, short-half life and non-specific action it does not promote antibacterial resistance. Moreover, NO is more than an antibacterial agent due to its proven role in angiogenesis, vasodilation, cell proliferation, inflammation, collagen synthesis and tissue remodeling.[10, 15-18] Thus, mimicking the endogenous NO release by utilizing donor molecules such as *S*-Nitroso-glutathione (GSNO) and integrating it in a polymer system can offer great potential in wound healing application. *S*-Nitroso-glutathione is a well-known endogenously produced *S*-nitrosothiol in humans. Decomposition of GSNO via thermal stimuli, moisture and reduced metal ions can lead to NO release and the corresponding biological effects. Endogenous GSNO functions range from preventing embolization within the vasculature to modulating angiogenesis by promoting vascular endothelial growth factor (VEGF) production within damaged tissue.[19-20] Along with these functions, GSNO has also been shown to be involved in collagen deposition in cutaneous wound repair, further demonstrating its abilities in wound healing.[21]

Integration of GSNO in a hybrid formulation of alginate and polyvinyl alcohol would enhance inherent wound healing properties of these polymers. Sodium alginate (NaAlg) provides an ideal matrix material for wound dressing applications. [22-24] It is an inexpensive biopolymer that

has widely been used in biomedical applications due to its high hydrophilicity and biocompatibility.[25-26] The bioadhesive and biodegradable behavior of alginate films in addition to maintaining a moist environment are important characteristics of an effective wound dressing.[27-28] Unfortunately, natural polymers like alginate, despite possessing great wound healing potential, undergo rapid *in vivo* degradation by proteases due to poor mechanical strength, making it difficult to prolong the diffusion of an encapsulated therapeutic agent.[1-2] Therefore, PVA, due to its chemical and mechanical resistance, can complement alginate for wound dressing fabrication. In addition, owing to its biocompatibility with tissue and plasma proteins, PVA is a potential candidate for wound healing applications.[29] Similarly, glycerol, a trihydroxy alcohol, is a popular ingredient of dermatological preparations. Endogenous glycerol has proven roles in cutaneous elasticity, skin hydration, and epidermal barrier repair.[30] The hybrid combination helps overcome the limitation possessed by natural or synthetic polymer individually.[22, 31]

In this work, a NO releasing Alginate-PVA-GSNO wound dressing was developed by integrating a synthetic GSNO in a hybrid formulation of alginate and PVA; glycerol is used as a plasticizer. The biomaterial is processed via lyophilization resulting in a porous morphology. This study discusses the fabrication and characterization of NO releasing Alginate-PVA-GSNO biomaterials and validates its antibacterial, angiogenic and fibroblast proliferation attributes.

2. Materials and Methods

2.1 Materials

Sodium salts of alginic acid, calcium chloride, ethylenediaminetetraacetic acid (EDTA), sodium chloride, were obtained from Sigma-Aldrich (St. Louis, MO). Polyvinyl alcohol (PVA- 88% hydrolyzed, M.W. approximately 13,000-23,000) was bought from Acros Organics (New Jersey) and glycerol was bought from Fischer Chemicals (Fair Lawn, NJ). LB broth and LB Agar were obtained from Fisher Bioreagents (Fair Lawn, NJ). Dulbecco's Modification of Eagle's medium

(DMEM) and trypsin-EDTA were purchased from Corning (Manassas, VA). The Cell Counting Kit-8 (CCK-8) was obtained from Sigma-Aldrich (St Louis, MO). The antibiotic Penicillin-Streptomycin (Pen-Strep) and fetal bovine serum (FBS) were purchased from Gibco-Life Technologies (Grand Island NY 14072). L-Glutathione (reduced 98+ %) was purchased from Alfa Aesar (Ward Hill, MA). The bacterial strains *Pseudomonas aeruginosa* (ATCC 27853) and *Staphylococcus aureus* (ATCC 5538) as well as the mouse fibroblast cell line (ATCC 1658) were originally obtained from American Tissue Culture Collection (ATCC). Autoclaved phosphate buffered saline (PBS) was used for all *in vitro* experiments.

2.2 Methods

2.2.1 Synthesis of GSNO

Synthesis of S-nitroso-glutathione (GSNO) was performed by modifying a standard protocol [32]. Reduced glutathione (900 mg, 2.93 mmol) was first dissolved in 4 mL of DI water and 1.25 mL of 2M HCl. The solution was allowed to chill in ice for 10 minutes before being nitrosated with an equimolar amount of sodium nitrite. The solution was then covered and allowed to cool in an ice bath for a further 30 minutes. Chilled acetone (5 mL) was then slowly added to the solution and allowed to stir for an additional 10 minutes while still in the ice bath. The GSNO precipitate that formed was then collected by vacuum filtration and further washed with cold acetone and water. The resulting washed product was then allowed to dry under vacuum overnight before being collected and stored in the freezer.

2.2.2 Engineering NO releasing material

Fabrication of the Alginate-PVA dressings: The NO releasing wound dressings were formulated by a solvent casting method. Sodium alginate (1 g) was slowly added to a conical flask containing 20 mL of deionized water at 40°C and allowed to dissolve for 2 h. A magnetic stirrer

was used to formulate a polymeric dispersion of appropriate consistency. As recommended by existing literature, 0.2 g of PVA was dissolved in 19.6 mL of deionized water, which was simultaneously stirred using a magnetic stirrer and heated to a temperature of 90°C [33]. The temperature of the PVA solution was brought down to around 45-50˚C before adding it to the alginate solution. Both polymeric solutions were blended together for 10 minutes to obtain a uniform polymeric dispersion. To the Alginate-PVA mixture, 0.4 ml of glycerol was added. Finally, it produced a solvent mixture of 40 mL (total) with 2.5 % (w/v) sodium alginate, 0.5% (w/v) PVA and 1% (v/v) glycerol. The resulting formulation was cast into Petri dishes and was kept in the freezer for 3 h.

Crosslinking of the wound dressings: A 2% (w/v) calcium chloride ($CaCl_2$) was prepared by dissolving 0.4 g of $CaCl_2$ in 20 mL of deionized water. In parallel, 30 mg/mL GSNO solution was prepared by using water as a solvent. Finally, $CaCl_2$ and GSNO were mixed in a 1:1 ratio by adding 5 mL of 2% $CaCl_2$ and 5 mL of GSNO (30 mg/mL) using a vortex mixer to obtain a uniform solution. The final GSNO concentration was 15 mg/mL in the crosslinking solution. The frozen Alginate-PVA polymeric dispersions were soaked in the $CaCl_2$-GSNO solution and allowed to crosslink for 20 h. For the control wound dressings, the crosslinking was carried out using 2% $CaCl_2$ but without GSNO.

Lyophilization: After 20 h of crosslinking, the crosslinked films were lyophilized for 7 h at -80˚C and < 1.5 mBar pressure in a Labconco freeze dryer to create a porous matrix. Since the process happened at a temperature of -80˚C, the undesired loss of NO from GSNO via thermal stimulus could be avoided. The Alginate-PVA-GSNO biomaterial were stored in the freezer (-15°C-30°C) before being used in the experiment to avoid any heat stimulated NO release. Figure 1 shows the control (Alginate-PVA) and NO releasing (Alginate-PVA-GSNO) biomaterial.

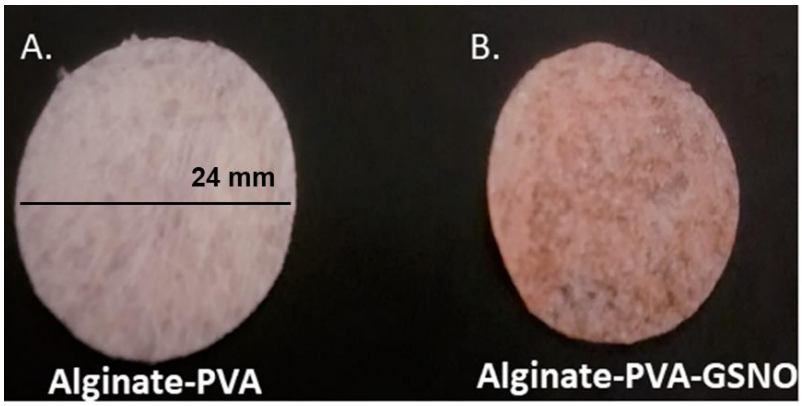

Figure 5.1. Images of Control Alginate-PVA **(A)** and NO releasing Alginate-PVA-GSNO material **(B).** The shape of the material is flexible and a round composite is shown only for representation.

2.2.3 Chemiluminescence based NO release measurement

The NO release study was performed to investigate the NO flux released from the Alginate-PVA-GSNO using a Sievers chemiluminescence Nitric Oxide Analyzer (NOA) 280i (Boulder, CO). The NOA has the capability to selectively map NO via the reaction of NO with ozone, thereby reducing intervention from other molecules.[11] As recommended by a previously published report, small circular films (diameter of a 5/16th inch) were punched out and wrapped in wipes (Kimwipes, KIMTECH) to mimic a moist wound environment prior to using them for NO flux analysis. [34] The samples were dipped in PBS (pH 7.4) containing EDTA and placed at the bottom of the sample holder. The released NO was continuously purged from the sample and swept from the headspace using nitrogen as the sweep gas into the chemiluminescence detection chamber. The films were tested for release at different time points: 0, 28, 48 and 72 h. The NO profile was measured at each time point until a stable plateau was recorded, and then stored at 37°C until the next time point and soaked again in wet Kimwipes before NO release analysis.

2.2.4 In vitro inhibition of adhered gram-positive and gram-negative bacteria

The designed NO releasing Alginate-PVA-GSNO samples were examined for their antibacterial efficacy against common bacteria responsible for skin infections: gram-positive

Staphylococcus aureus (*S. aureus*) and gram-negative *Pseudomonas aeruginosa* (*P. aeruginosa*). A modified version of the standard bacterial adhesion test was used to quantify the inhibition of colony forming units per surface area of the dressing (CFU/cm^2) [35-36].

Preparation of bacterial suspension: A single isolated colony of bacteria was picked from the pre-cultured LB-agar plate and inoculated into 10 mL of Luria Broth (LB) medium in a 50 mL Eppendorf tube and allowed to incubate at 37 °C for 14 h at a radial shaking speed of 120 rpm. After 14 h, the optical density of the bacteria was measured at 600 nm (OD_{600}) using UV-vis spectrophotometer (Thermo Scientific Genesys 10S UV-Vis). This step assures that the bacteria is in actively dividing log phase (and not in the death phase) prior to the use in the experiment to keep the experimental condition unbiased. After this step, bacterial cells were separated from the LB medium by centrifuging the bacterial culture at 2500 rpm for 8 min, the supernatant was discarded and fresh sterile phosphate buffer saline (PBS, pH 7.4) was added. The same procedure was repeated to wash off any remaining traces of LB. This step was repeated twice, and the bacterial cells were ultimately suspended in PBS (without any residual traces of LB medium) to be used in the experiment further. The removal of traces of nutrient medium (LB) and suspension of bacterial strains in the PBS assures that the bacteria would not grow back after being killed by the antibacterial agent and thus allowed a fair comparison between the control (without GSNO) and Alginate-PVA-GSNO wound dressings.

Bacterial inhibition and its quantification: Prior to exposing the wound dressing to the bacterial suspension, the OD_{600} was measured again and diluted with PBS to a bacterial cell count in the range of 10^8-10^{10} CFU/mL, which is representative for infected chronic wounds. Triplicate (n=3) samples (diameter = 2.4 cm) of both the Alginate-PVA-GSNO wound dressing and Alginate-PVA (control) were exposed for 24 h to 5 mL of bacterial suspension in a 50-mL tube incubated at 37 °C and 120 rpm. After bacterial exposure, the wound dressings were removed from the bacterial suspension and any unbound or loosely-bound bacteria were washed off by rinsing the dressings with 2 mL PBS using a pipette. The dressings with the adhered bacteria were then

transferred to 2 mL of fresh PBS and homogenized for 30 secs using a vortex mixer in order to detach the bound bacteria into the PBS solution. The resulting bacterial suspension was serially diluted (10^{-1} to 10^{-5}) using PBS, plated in pre-made LB agar Petri dishes (LB agar concentration 40 g/L) and post-incubated for 20 h at 37 °C. After 24 h, CFUs appeared on the LB agar plate. The CFUs were counted while adjusting the dilution factor for the amount of bacterial suspension. The number of CFUs per weight (CFUs/mg) of the wound dressings were obtained for both Alginate-PVA-GSNO wound dressings and control dressings. Percent bacterial inhibition was calculated relative to the control using the following formula.

$$\%\ Bacterial\ inhibition = \frac{\left(\frac{CFU}{mg}\ in\ control\ samples - \frac{CFU}{mg} in\ test\ samples\right) X100}{\frac{CFU}{mg}\ in\ control\ samples}$$

2.2.5 Zone of inhibition (ZOI) study using the agar diffusion method

The ability of the Alginate-PVA-GSNO material to inhibit bacterial growth beyond the direct point of contact was tested via standard agar diffusion method.[35] As a proof of concept, *S. aureus* was used. The strain culture was spread uniformly and aseptically on premade LB agar petridishes. Circular wound dressing disks (diameter: 2.7 cm) of control Alginate-PVA and Alginate-PVA-GSNO were placed and gently pressed on top of the bacterial culture. The petridishes were then placed in an incubator at 37 °C for 20 h to allow the formation of a zone of inhibition (ZOI).

2.2.6 Cell culture

Mouse fibroblast cells and human umbilical vein endothelial cells (HUVEC) were maintained in a tissue culture grade T-flask. More specifically, fibroblast cells were maintained in Dulbecco Modification of Eagle's Medium (DMEM with 4.5g/L glutamine, 10% fetal bovine serum and 1% pen-strep antibiotics (10,000 units/mL)) and HUVEC cells were maintained in F-12 K medium with ATCC growth supplements kit. Both types of cell were incubated in humidified

incubator with 5% CO_2 at 37°C. The medium was replaced every alternate day until cells were 80% confluent. Thereafter, the cells were detached from the T-flask surface by enzymatically degrading their extracellular matrix layer by treating them with 0.18% trypsin and 5 mM EDTA for 5 min.

2.2.7 Human endothelial cell proliferation

Angiogenesis facilitated by endothelial cell proliferation plays a vital role in the delivery of nutrients, oxygen and important blood factors at the wound site. HUVEC cells are widely regarded as the *in vitro* model cells for angiogenesis.[37] We investigated if GSNO containing wound dressings can enhance endothelial cell proliferation thus suggesting its contribution to angiogenesis. 10,000 HUVEC cells/mL were seeded in each of the wells of a 96 well plate and allowed to be attached to the plate surface by incubating in 5% CO_2, 37 °C for 24 h. Meanwhile, a sample of wound dressing weighing 10 mg was added to 10 mL F-12K medium for 24 h to collect the materials released out of the dressing. The F-12 K medium in the 96 well plate was replaced by leachate solution exposing the cells for next 24 h. Thereafter, 10 µl CCK-8 dye solution was added and allowed to react with NADH released by viable cells for 4 h leading to the formation of orange color formazan absorbed at 450 nm. A relative increase in cell number was measured when comparing the formazan absorbance of cells exposed to the NO releasing (test) and non-NO releasing samples (control) using the following formula.

$$\%\ Cell\ Viability = \frac{\text{Absorbance of the test samples}}{\text{Absorbance of the control samples}} \times 100$$

2.2.8 Fibroblast cell proliferation and migration

The effect of materials released from the wound dressing were (similarly) tested against fibroblast cell proliferation in DMEM medium. The study was carried out for 24 h in 5% CO_2, 37

°C. Percent cell viability was measured relative to the NO releasing (test) and non-NO releasing samples (control) as previously described.

The cell migration assay allowed an *in vitro* evaluation of the wound healing potential of the Alginate-PVA-GSNO material. A cell migration kit that consists of a disk containing culture inserts (2 well in µ-Dish 35 mm high (ibidi GmbH)) was used for the assay. The cell culture inserts were filled with a culture containing 5000 cells/ml and incubated in 5% CO_2, 37 °C for 24 h for cells to attach and grow in the dish. After 24 h, the medium and cell culture inserts were removed, leaving a linear cell-free zone separating the cells growing on either side. Two mL of leachates was added to the disk. As the cell migrated to the cell-free zone, optical images were taken at different time intervals from 0 to 36 h to trace the progress of cell migration.

2.2.9 Water permeability, moisture content, and swelling index

Water permeability: The water permeability of the wound dressings was determined using a standard protocol [11]. The wound dressings with a diameter of 2 cm were wrapped around the opening of a 10 mL glass vial after filling them with 5 g of dehydrated silica. The weight of the vials (n=3 each) with wound dressings were reported and then placed in a humid environment established with saturated sodium salt (75% relative humidity, 22 ± 2 °C). The weight of the vials was measured every 24 h over seven days. A linear curve was plotted between gained weight (dw) and time (dØt) in order to calculate the water vapor permeability K (kg m m^{-2} day^{-1} Pa^{-1}) of the wound dressing, given. $K = \frac{dw/d\emptyset t}{Ap*P}$

dw = weight gain due to moisture retention (kg), dØt= time point (day), dw/dØt = slope between weight gain and time point (day), Ap is the surface area of the dressing (m^2), P is the saturation vapor pressure of water at 22°C.

Moisture content: The moisture content (MC%) was determined by using a recommended protocol.[38] After measuring, the thickness and the surface area, the samples' weights were

recorded. Thereafter these samples were dried in a vacuum oven for 24 h at 105 °C and dry weight was recorded. The MC% was calculated by comparing the weights of dressings before and after drying using the following formula.

$$MC\% = \frac{Weight\ before\ drying - Weight\ after\ drying}{Weight\ before\ drying} * 100$$

Swelling index (SI): To measure the swelling ratio (SR) of the wound dressings, a recommended protocol was slightly modified [31]. Samples of dimension 2 x 2 cm^2 size (n=3) were weighed and dried in a vacuum oven at 105 °C for an hour. The weight of both control Alginate-PVA and NO releasing Alginate-PVA-GSNO were taken again after drying. Thereafter, the samples were swelled in 0.1 M phosphate buffer saline (PBS, pH 7.4) at room temperature. After soaking for an hour, the weight of the dressing was measured again. The SI was calculated has follows:

$$SI\ (\%) = \frac{Weight\ after\ soaking - Weight\ after\ drying}{Weight\ after\ drying} * 100$$

2.3.0 Morphology of the dressing surface and porosity analysis

Scanning electron microscopy: Scanning electron microscopy (SEM) is a useful tool to understand the surface characteristics of a polymer. In the present study, microstructure and surface morphology of the wound dressing (before and after NO donor incorporation) were examined using SEM (FEI Inspect F FEG-SEM). A total of three samples of each of the control (without GSNO) and Alginate-PVA-GSNO were sputter coated with gold-palladium (10 nm) using a Sputter Coater (Leica EM ACE200) after mounting them on a metal stub. An accelerating voltage of 5 kV was used to capture SEM images of the sample at 100 X magnification.

Porosity measurement: Pore size was determined using Image J software from images taken with light microscopy (Thermo Fisher scientific EVOS™ XL Cell Imaging System). At least 30 pores were used to determine average measurements of the pore diameter of each sample.

3.0 Results and Discussion

3.1 NO release kinetics

S-nitrosothiols (RSNO's) such as GSNOs are capable of passively releasing NO from heat, moisture, and catalytically in the presence of certain metal ions.[39] It is generally assumed that RSNOs decompose by homolytic cleavage of the S-N bond. This process generates a thiyl radical ($RS^{\cdot}$) and nitric oxide ($NO^{\cdot}$) gas.

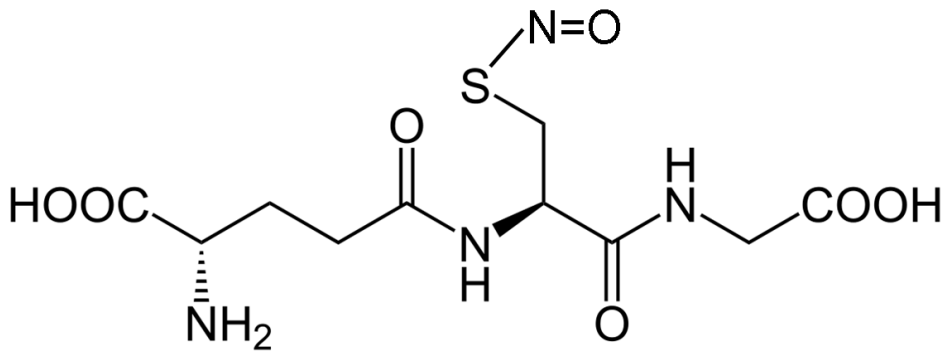

RSNO ⟶ **$RS^{\cdot}$ + $NO^{\cdot}$**

The product of RSNO homolytic cleavage, i.e NO, is one of the key players in wound repair. NO is more than just an antibacterial agent. The holistic effect of NO during wound repair may be attributed to its pivotal role in angiogenesis, fibroblast proliferation, collagen deposition, and tissue remodeling.[10, 15-18, 40] Thus, providing exogenous NO release from the Alginate-PVA-GSNO wound dressing will be crucial in achieving faster wound healing.

In this study, NO release from Alginate-PVA-GSNO material was tested in real time via a chemiluminescence nitric oxide analyzer (NOA) over the testing periods: 0h, 24h, 48h, and 72 h

at 37°C. A real-time NO release profile is shown in Figure 5.2A and the graphical representation of NO release profile over a 72-h period is presented in Figure 5.2B. An initial NO release of 5.01 ± 0.49 × 10^{-11} mol mg^{-1} min^{-1} was achieved in the first few minutes that gradually reduced to 0.54 ± 0.08 × 10^{-11} mol mg^{-1} min^{-1} over a 72-h period. The decrease in the NO flux over time could be attributed to homolytic degradation of GSNO in the presence of moisture. However, even at a level much lower than 0.54 ± 0.08 × 10^{-11} mol mg^{-1} min^{-1}, NO has been shown to possess the ability to be effective against a wide variety of bacterial pathogens.[11] Thus Alginate-PVA-GSNO material can be helpful in preventing bacterial infection in the first 72 h following abrasion during which a wound is most susceptible to infection and biofilm formation. The ability of these wound dressings to sustain NO release over a 3-day period would also eliminate the need for redressing thus not only reducing the pain caused by frequent redressing but also cutting down the associated wound-care cost. It is expected that the NO flux achieved in this study will also positively affect the important steps in wound healing process such as infection, fibroblast proliferation, cell migration and angiogenesis. To validate these assumptions, microbial and cell culture studies were carried out which are discussed in detail later.

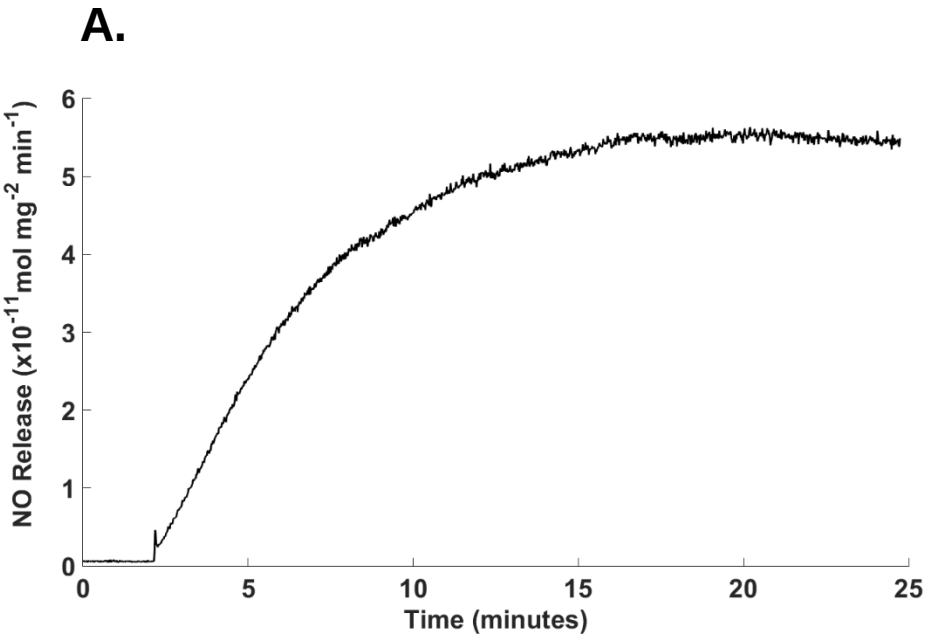

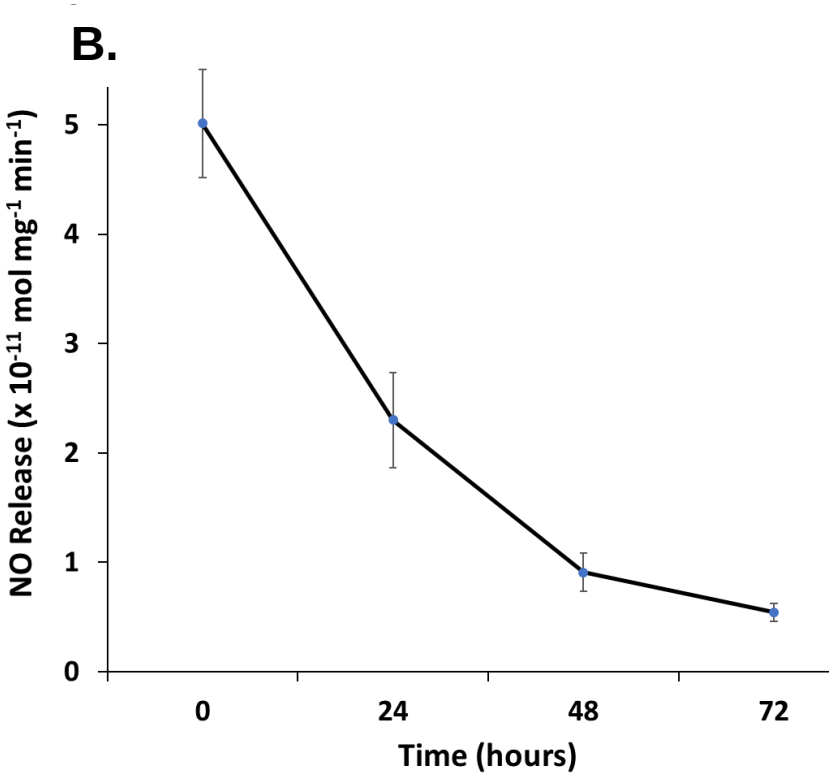

Figure 5.2 (A-B). Real-time NO-release profile from the Alginate-PVA-GSNO material as observed via chemiluminescence based Nitric Oxide Analyzer (NOA) **(A)**. The NO release from Alginate-PVA-GSNO wound dressings. Statistical data is expressed as mean ± standard error of the mean of n=3 samples. Values of $p < 0.05$ were considered statistically significant **(B)**

3.4 Antibacterial efficacy

Nitric oxide eradicates bacteria in a non-specific way which can be explained through different theories as stated below. The mechanism behind the bactericidal effect of NO seems to involve oxygen and/or its free radicals ultimately leading to the formation of nitrogen radicals.[41] Nitric oxide due to its gaseous nature can cross the cell membrane that leads to the activation of sulfur-iron complexes inhibiting respirator chain enzymes.[42] The cellular damage caused by GSNO may result from oxidative and nitrosative stress mainly facilitated by oxidation of thiol or nitrosation of thiol groups.[43] Another accepted mechanism is the NO-mediated inhibition of enzyme activity in bacterial cells. Lipid peroxidation, nitrosation of amines and thiols in the extracellular matrix, tyrosine nitration in the cell wall and DNA damage also explain the antibacterial mechanisms of NO.[44]

Commercially available advanced wound dressings often contain antibiotics (Septocoll® by Biomet Merck; Collatamp® by Innocoll) or other antibacterial agents such as silver (e.g., Acticoat® by Smith & Nephew, Actisorb® by J&J and Aquacel® by ConvaTec), chlorohexidine (Biopatch® by J&J), or iodine (Iodosorb® by Smith & Nephew). However, there are growing concerns about the emergence of antibiotic-resistant bacterial strains. Worldwide many strains of *S. aureus* are resistant against most antibiotics available for treatment.[45] Due to resistance against β-lactam family of antibiotics, methicillin-resistant *S. aureus* (MRSA) are a huge concern for wound treatment. [46] Topical macromolecules and antibiotics cannot penetrate through biofilms and thereby require a 1000-fold higher dose when compared to freely floating planktonic bacteria.[47] This only worsens the existing issue of antibiotic resistance in addition to causing cytotoxicity. Antibiotics can also delay healing if applied indiscriminately to damaged tissue areas, which defies the actual purpose of their application.[8, 48-49] The inefficiency of currently available therapeutic agents not only adds to the suffering of the patient but also causes huge healthcare expenses. The gaseous nature of NO allows penetration through the matrix in the biofilm, which gives it an extra advantage over antibiotics and silver-based antibacterial strategies. Moreover, unlike antibiotics, NO application would not lead to the emergence of resistant bacterial strains owing to its rapid action, short half-life (< 5 sec) and endogenous nature.[50-52] From an application point of view, local administration of even smaller doses of NO donor at the wounded site would allow efficient delivery in addition to reducing the emergence of antibiotic resistance.

In this study, the NO releasing Alginate-PVA-GSNO wound dressings were tested for ability to inhibit *S. aureus* and *P. aeruginosa*. The looming threat of incurable *S. aureus* is a serious concern for wound infections. *S. aureus* contributes to more than 70% of the skin infections at the surgical site while *P. aeruginosa* is among the other major pathogens.[53] S. *aureus* and *P.aeruginosa* are also known to cause biofilm formation in which the bacteria are protected against the inhibitory effect of antibiotics via an extracellular matrix. Bacteria entry in human blood

through biofilm can result in septicemia and inflammation. Since these bacteria are frequently found in hospital settings, they can lead to nosocomial infections in the hospital environment.[54] Surgical site infections are associated with increased mortality and hospital care costs amounting to ~$1.6 billion in the United States alone. The results from our study showed that the NO releasing wound dressings (with GSNO) showed 99.89 ± 0.4% bacterial inhibition of gram-positive *S. aureus* and 99.93 ± 0.7% inhibition of gram-negative *P. aeruginosa* as compared to the control Alginate-PVA dressing without the NO donor. In the log scale this amounts to around a three-log reduction (see Figure 5.3). This is in line with other studies done on the antibacterial effect of NO releasing polymers for biomedical applications against a wide variety of bacteria including *S. aureus*, *P. aeruginosa*, *A. baumanni*, and *E. coli* .[11, 35-36] The rapid action of NO releasing Alginate-PVA-GSNO biomaterial would also limit the side-effects of overexposure in the surrounding tissue such as platelet inactivation.[55]

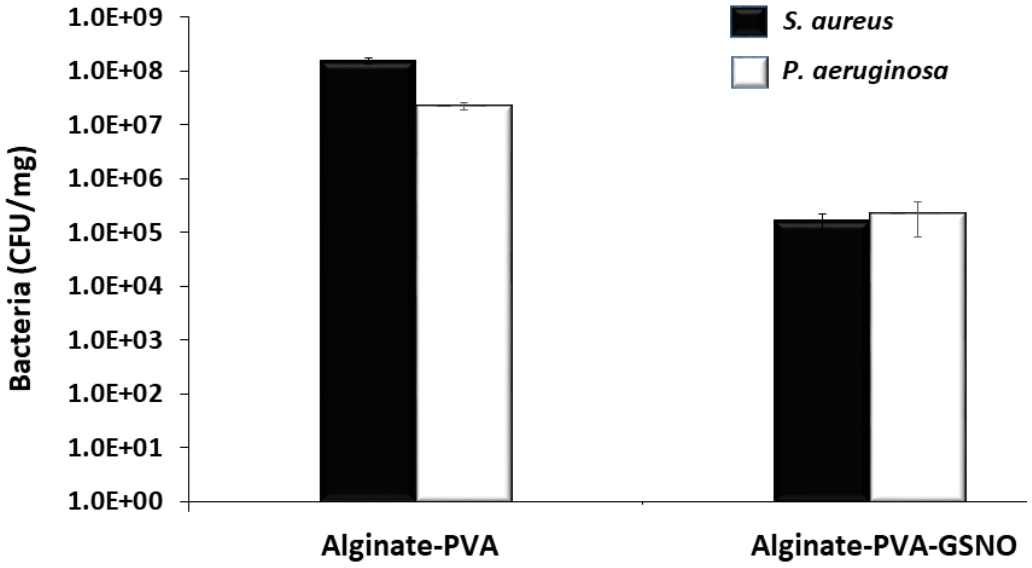

Figure 5.3. Antibacterial efficacy of nitric oxide releasing wound dressings.

The agar diffusion method showed the ability of NO releasing wound dressings to eradicate *S. aureus* beyond the direct point of contact when placed in an incubator at 37 °C for 24 h. As expected, the results showed no zone of inhibition (ZOI) around control Alginate-PVA

wound dressings while a 2.6 cm ZOI was formed with alginate-PVA-GSNO dressing (see Figure 5.4). In the past, another *in vitro* studies where SNAP was used as a NO donor showed effective biofilm eradication against *P. aeruginosa* and *S. aureus* resulting in a zone of inhibition.[35] In the past, another *in vitro* studies where SNAP was used as a NO donor showed effective biofilm eradication against *P. aeruginosa* and *S. aureus* resulting in a zone of inhibition.[35]

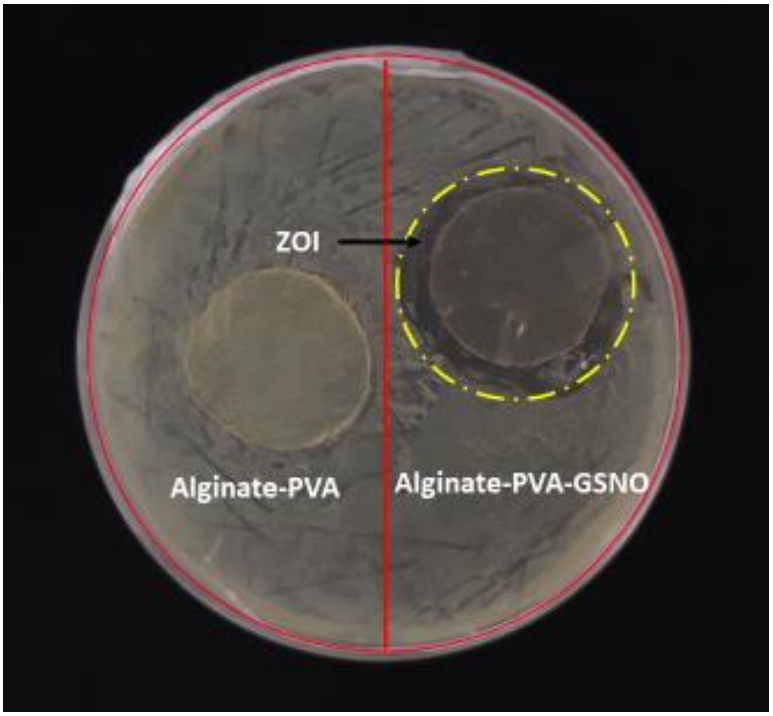

Figure 5.4. Zone of inhibition (ZOI) in *S. aureus* bacterial lawn exposed to Alginate-PVA-GSNO material. The control Alginate-PVA showed no ZOI showing the bacteria inhibition via nitric oxide diffusion to be a preventing strategy to avoid biofilm formation.

The results from both the bacterial test are indicative of the how NO based strategies can both prevent the growth of bacteria (via a zone of inhibition) as well as cure an infection via eradicating the attached viable bacteria. Effective killing of *S. aureus* and *P. aeruginosa* bacteria is a significant stride towards proving the highly effective and practical use of the designed wound dressings. Even the systemic administration of antibiotics can lead to accumulating toxic levels

of antibiotics. The NO releasing nature of the material also avoid the use of systemic administration of antibiotics during wound treatment that can led to their accumulation in key organs such as kidneys while only a very small percent is delivered to chronic wound. Our study provided important proof of concept to show that NO based strategies can be used as a stand-alone strategy for preventing and curing the infection or in combination with the traditional antibacterial agents to reduce their dose-related side-effects.

3.5 In vitro proliferation of endothelial cells supporting angiogenesis

Angiogenesis, the process through which new blood vessels form from the pre-existing blood vessels demands considerable behavioral activity of endothelial cells including cell proliferation. [56] Neovasculogenesis occurs at the wound site by the process of angiogenesis and is critical for wound repair due to its important role in the delivery of oxygen, nutrients, and other mediators at the wound site. NO is a well know vasodilator involved in the increased contraction of the smooth muscle cells that support angiogenesis.[57] Major angiogenic factors such as vascular endothelial growth factor (VEGF) and transforming growth factor (TGF-β) that are involved in stimulation, promotion, and stabilization of angiogenesis are shown to be regulated in wound healing animal models via NO donors. [34, 58]

HUVEC cells are widely regarded as *in vitro* modelling cells for angiogenesis. [37] Thus, to demonstrate that the NO releasing wound dressing can support angiogenesis HUVEC cells were used as representative endothelial cell in this study. The study was done using a cell viability assay that utilizes a highly water-soluble tetrazolium salt. In the live cells, WST-8 [2(2-methoxy-4-nitrophenyl)-3-(4-nitrophenyl)-5-(2,4-disulfophenyl)-2H-tetrazolium monosodium salt] is reduced by dehydrogenases to give formazan (an orange color product), which can be detected

at 450 nm. Hence more absorbance at 450 nm is an indicator of increased cell proliferation. After obtaining the absorbance, relative cell viability was calculated by assuming the absorbance corresponding to the HUVEC relative cell viability demonstrated by the positive control (well plate, without the dressing material) to be 100%. Cells exposed to leachates collected from Alginate-PVA-GSNO resulted in in a three-fold increase in HUVEC cell viability within the first 24 h. When the results from Alginate-PVA were compared with positive control (the well plate), there was no significant difference in viability. The enhanced proliferation can be attributed to the NO release resulting from cleavage of S-N bond when GSNO encountered the moisture at 37°C. The endogenous release of NO has been previously shown to positively affect angiogenesis [20]. This study supports angiogenesis via an exogenous supply of NO from GSNO within the first 24 h of application.

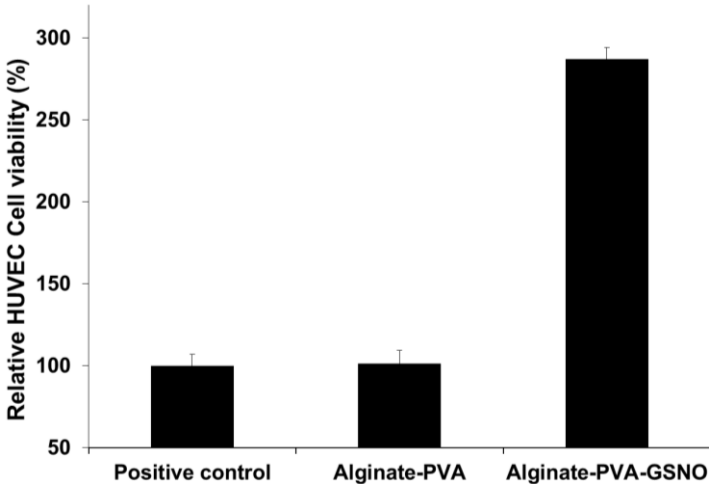

Figure 5.5. The GSNO containing material resulted in three times more cell viability when compared to the positive control whereas the HUVEC cell viability between Alginate-PVA vs positive control was similar.

Similar results can be expected when the material would be applied to a wound containing exudates at physiological temperature. This can accelerate wound healing as endothelial cells form the blood vessels responsible for supplying immune cells, cytokines, and nutrients to the site

of the wound. Figure 5 shows the graphical representation of comparative endothelial proliferation.

3.5 Fibroblast cell proliferation and migration

The onset of the proliferative phase overlaps with the inflammatory phase and is marked by fibroblasts entering the wound site. As soon as the injury occurs, the healthy dermal fibroblasts in the vicinity of the wound undergo proliferation and migrate into the provisional matrix of the wound clot to lay the foundation of a collagen-rich matrix.[59] The increased collagen synthesis by fibroblast at the wounded tissue is achieved via endogenous NO production.[60] Based on these recommendations, we considered it interesting to study the effect of exogenous NO (from Alginate-PVA-GSNO) on fibroblast proliferation and migration *in vitro*.

The proliferation assay was done on mouse fibroblast cells using 24-hour leachates from Alginate-PVA-GSNO material using WST-8 dye-based cell viability assay. Formazan formation and absorbance at 450 nm was measured as an indicator of increased proliferation. As shown in

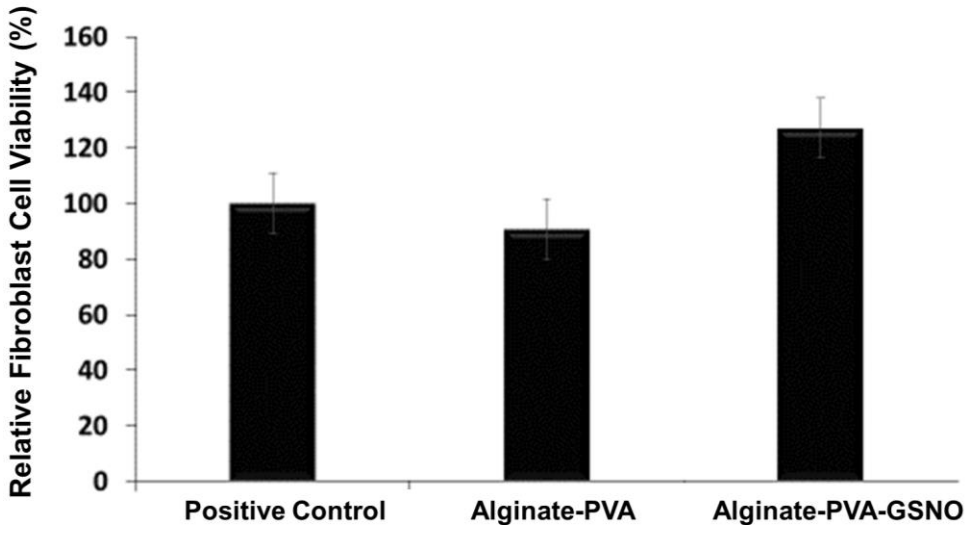

Figure 5.6. The NO releasing Alginate-PVA-GSNO resulted in a 40% increase in fibroblast cell prliferation when compared to the cells grown without leachated (positive control). Statistical data is expressed as mean ± standard error of the mean of n=3 samples. Values of $p < 0.05$ were considered statistically significant.

Figure 5.6, the Alginate-PVA-GSNO increased the proliferation of fibroblast cells by >30% as compared to positive control (without any wound dressing leachate) as well as Alginate-PVA, thus contributing to proliferation and infection control at the same time *in vitro*.

Since Alginate-PVA and control showed similar results and GSNO is the only differentiating factor, it is clear that the increased fibroblast proliferation was a result of NO release in the culture medium. This is in line with the recent study done by *Han et al., 2012* in which NO-releasing nanoparticles accelerated the fibroblast proliferation leading eventually to collagen deposition thus resulting in faster wound healing in mice.[61] These results also indicated that the Alginate-PVA-GSNO wound dressings possess no relative cytotoxicity towards the cells when compared to the control possibly due to crosslinking of the base polymer with calcium chloride which prevented any leaching. Although, even if the material leached out it cytotoxic response is not expected at the used dose due to biocompatible nature of both alginate and PVA. Regarding the cytocompatibility of the reported NO flux, published reports including ours have shown other NO releasing materials to possess biocompatibility and hemocompatibility *in vitro.*[36, 62]

In addition to fibroblast proliferation, the cell migration assay carried with the biomaterial with and without GSNO also yielded interesting results. The real-time progress of cell migration was qualitatively traced using an ibidi kit observed with optical microscopy. The ibidi kit provides a useful alternative for the scratch assay that can otherwise result in a non-uniform cell-free zone. The images were taken at 0, 6, 18, 24 and 48 h (see Figure 5.7). The results showed that the cells exposed to the extract from Alginate-PVA-GSNO wound dressing resulted in much faster migration as compared to positive control (without any dressing) or Alginate-PVA control. This led to complete closure of the *in vitro* wound within the first 48 h. However, the control sample only led to incomplete migration within first 48 h resulting in ajar wound healing. Since the only difference between the latter is GSNO, it is evident that NO release via homolytic cleavage of GSNO in moist conditions and physiological temperature resulted in the fibroblast migration eventually closing the wound *in vitro*.

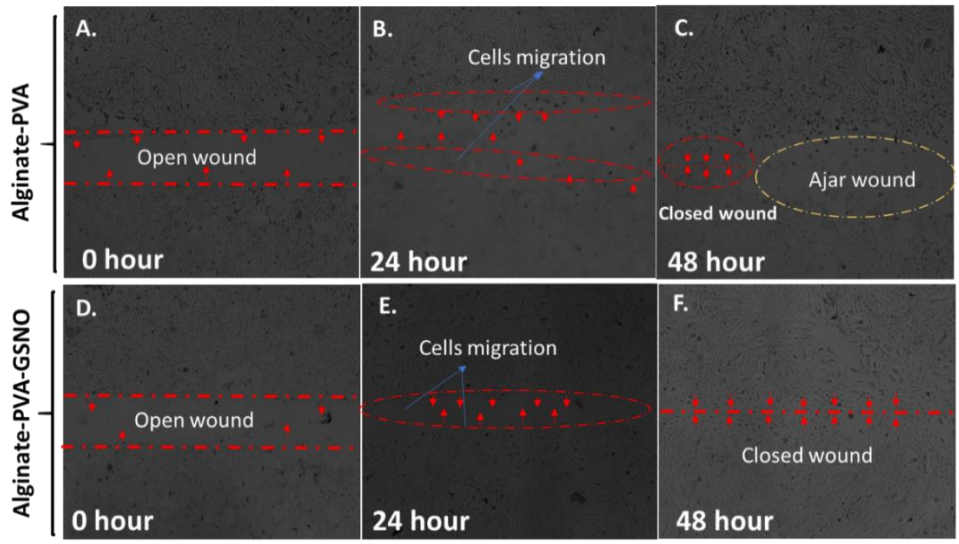

Figure 5.7 (A-F). The temporal and spatial response of an *in vitro* wound model towards the extract collected from control Alginate-PVA and Alginate-PVA-GSNO within 48 hours period. As clear from the images the fibroblast migration **(B and E)** was much faster in cells exposed to GSNO resulting in complete closure **(F)** of *in vitro* wound whereas the control wound was left ajar **(C)**.

From an application point of view, these positive *in vitro* results of fibroblast proliferation and migration can result in enhanced wound healing as they play a significant role in collagen deposition and tissue remodeling. However, to establish the effectiveness of the Alginate-PVA-GSNO wound dressing for commercialization, further *in vivo* testing on animal models is recommended as well as planned for future investigations by our group.

3.6 Surface morphology and pore size analysis

Surface electron microscopy (SEM) was used to measure the morphology of the Alginate-PVA-GSNO wound dressings relative to the controls. As shown in Figure 5.8, the surface of the dressing material was not altered in the presence of GSNO, confirming that GSNO has no negative effect on the porous surface morphology. The porous structure in the wound dressing offers a great advantage in terms of water vapor transmission as well as gaseous exchange from the wound bed.

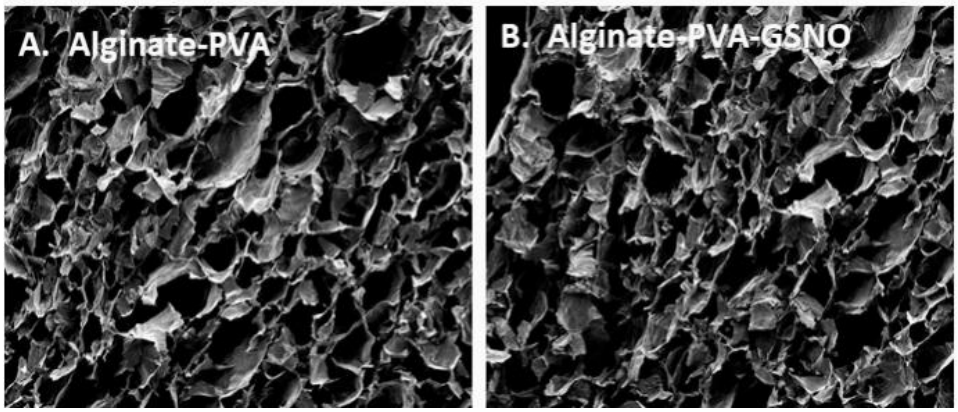

Figure 5.8 (A-B). Surface Electron Microscopy (SEM) images of samples taken at 300X magnitude Alginate-PVA **(A)** and Alginate-PVA-GSNO **(B)**.

Both the Alginate-PVA-GSNO film and the control (Alginate-PVA) exhibited macro-porous characteristics. The pore sizes for both films ranged from 400-1600 μm. The average pore size of the GSNO dressing was approximately 860 μm and the average pore size of the control dressing was approximately 900 μm. The non-homogenous, larger pore sizes are comparable to commercial wound dressings such as Cellosorb Adhesive (Urgo Medical Co).[63] When applied on a wounded surface, it can be expected that the porous structure would result in preventing building up of anaerobic condition on the injured wound while simultaneously cleaning the wound via exudate absorption. The subsequent NO release would eradicate bacteria proliferation and biofilm formation.

3.7 Thickness, water vapor permeability, moisture content, and swelling index

The physical properties like thickness, moisture content (MC%), water permeability and swelling index are important parameters that govern the healing potential of a wound dressing.

The thickness of the film was measured with a Digimatic Micrometer (Mitutoyo, Japan) and was found to be 0.29 ± 0.001 mm for control and 0.30 ± 0.006 mm for the films with GSNO. Thereafter, water permeability, MC%, and SR% were calculated and results are presented in Table 5.1.

Table 5.1. Physical characterization of the Wound dressing in terms of thickness, Vapor Permeability, Moisture, Swelling Ratio.

Characterization	Control (Alginate-PVA)	Alginate-PVA-GSNO
Thickness (mm)	0.29 ± 0.001	0.30 ± 0.006
Water Permeability ($kgmm^{-2}day^{-1}Pa^{-1}$)	3.85 X 10^{-2}	3.4 X 10^{-2}
Moisture Content (MC%)	23.9 ± 3.7	33.06 ± 2.1
Swelling Index (%)	48.94 ±3.56	64.55 ± 2.26

The water permeability of the Alginate-PVA-GSNO was found to be lower than that of the control films (without GSNO). In the past, we have shown that incorporating NO donors into natural polymers tends to decrease their water permeability due to closer networking between them [64]. The MC% from the total weight of the wound dressings was calculated based on the differences in weight before and after drying the wound dressing for 24 h at 105 °C. The MC% for the Alginate-PVA-GSNO dressings (33.06 ± 2.1) was found to be higher as compared to the control films (23.9 ± 3.7). This is in line with the water permeability (K value) results, suggesting that a decrease in water permeability due to the presence of GSNO helped them retain more moisture and hence a higher MC%. The swelling index studies were done for 24 h using PBS (pH 7.0) and the difference in weight of the wound dressings was compared before and after soaking in PBS. The SI of the Alginate-PVA-GSNO was higher (64.55 ± 2.26 %) than control films (48.94 ±3.56 %), further strengthening the conclusion that the presence of GSNO resulted in better retention of the moisture in the NO releasing films compared to the control. A similar trend resulting in an increase in swelling index after adding the drug (antibiotics) in the Alginate-PVA wound dressing has also been observed in another report.[31]

Combining all these physical attributes with morphology and porosity of wound dressing yields interesting conclusions. The water vapor permeability was shown to decrease because of

the increase in water retention by the NO releasing wound dressing. This theoretically should increase the NO release from the wound dressings over time as moisture leads to homolytic cleavage of GSNO. This would also have positive consequences when such wound dressings are applied to a wound site where wound exudates would be absorbed in the Alginate-PVA-GSNO dressing and result in the prolonged supply of NO from the wound dressings. Eventually, an increase in NO flux will benefit the wound healing through its bactericidal effect.[10, 34, 65] From a clinical perspective, this is of great advantage in the presence of infection in the wound exudates which can cause serious clinical challenges including hyperinflammation and delay the healing process.[66-68] In addition, an increase in NO flux will also positively impact all four phases of wound healing right from homeostasis until the final phase of tissue remodeling.[10, 68-70] A controlled water vapor transmission rate has been shown to help in the proliferation and regular function of fibroblast cells.[71] Table 1 shows the observed values (average mean of n=3) for different characterization parameters.

4. Conclusion

In the current study, a bio-inspired Alginate-PVA-GSNO biomaterial was developed and characterized to show its potential as a wound dressing material *in vitro.* The hybrid material that consists of a natural polymer (alginate) and synthetic polymer (PVA) helps overcome limitations possessed by natural or synthetic polymers individually. It also provides an alternative to the use of a separate antibacterial agent in wound dressings by combining the wound healing benefits of alginate, PVA, and GSNO in a single dressing material. The Alginate-PVA-GSNO material allowed a controlled release of NO which reduced more than 97% infection caused by *S. aureus* and *P. aeruginosa*. The gaseous nature of NO allowed diffusion through the agar thus preventing bacterial growth and leading to a zone of inhibition. The bacterial adhesion assay showed its ability to eradicate up to 99.5% of viable bacteria attached to it, thus qualifying it as both prevention and cure against bacterial infection. This form of local NO administration directly at the

wound site would also avoid the toxic build-up of antibiotics in kidneys as seen very often with systemic administration. The results from this study also provided important proof of concepts suggesting that Alginate-PVA-GSNO wound dressing can regulate angiogenesis, fibroblast proliferation and migration all of which are essential for faster wound healing. Physical characteristics such as moisture content, water vapor transmission, pore size, swelling ratio, surface morphology and NO release kinetics showed that the Alginate-PVA-GSNO material possesses the desired characteristics needed for enhancing the natural wound healing process. The porous matrix allows for absorption of wound exudates, water vapor transmission, and gaseous exchange. Overall, the current study provided supportive *in vitro* evidence to show that Alginate-PVA-GSNO provides a favourable environment for accelerated wound healing *in vitro*. Further animal testing is under process to validate these findings *in vivo*.

Acknowledgment

This study was supported by the funds received from the National Institute of Health, USA grant, NIH K25HL111213 and DOD grant, K-025-20

References

(1) Midwood, K. S.; Williams, L. V.; Schwarzbauer, J. E. Tissue repair and the dynamics of the extracellular matrix. *The international journal of biochemistry & cell biology* **2004,** *36* (6), 1031-1037.

(2) Desmoulière, A.; Chaponnier, C.; Gabbiani, G. Tissue repair, contraction, and the myofibroblast. *Wound Repair Regen.* **2005,** *13* (1), 7-12.

(3) Sen, C. K.; Gordillo, G. M.; Roy, S.; Kirsner, R.; Lambert, L.; Hunt, T. K.; Gottrup, F.; Gurtner, G. C.; Longaker, M. T. Human skin wounds: A major and snowballing threat to public health and the economy. *Wound Repair and Regeneration* **2009,** *17* (6), 763-771.

(4) Pangilinan, R.; Tice, A.; Tillotson, G. Topical antibiotic treatment for uncomplicated skin and skin structure infections: Review of the literature. *Expert Rev. Anti Infect. Ther.* **2009,** *7* (8), 957-965.

(5) Demidova-Rice, T. N.; Durham, J. T.; Herman, I. M. Wound healing angiogenesis: Innovations and challenges in acute and chronic wound healing. *Adv. Wound Care* **2012,** *1* (1), 17-22.

(6) Bainbridge, P. Wound healing and the role of fibroblasts. *J. Wound Care* **2013,** *22* (8).

(7) Attinger, C.; Wolcott, R. Clinically addressing biofilm in chronic wounds. *Adv. Wound Care* **2012,** *1* (3), 127-132.

(8) Lee, Y.-H.; Cheng, F.-Y.; Chiu, H.-W.; Tsai, J.-C.; Fang, C.-Y.; Chen, C.-W.; Wang, Y.-J. Cytotoxicity, oxidative stress, apoptosis and the autophagic effects of silver nanoparticles in mouse embryonic fibroblasts. *Biomaterials* **2014,** *35* (16), 4706-4715.

(9) Asharani, P.; Low Kah Mun, G.; Hande, M. P.; Valiyaveettil, S. Cytotoxicity and genotoxicity of silver nanoparticles in human cells. *ACS nano* **2008,** *3* (2), 279-290.

(10) Pant, J.; Goudie, M.; Brisbois, E.; Handa, H. Nitric oxide-releasing polyurethanes. *Advances in Polyurethane Biomaterials* **2016**, 417.

(11) Sundaram, J.; Pant, J.; Goudie, M. J.; Mani, S.; Handa, H. Antimicrobial and physicochemical characterization of biodegradable, nitric oxide-releasing nanocellulose-chitosan packaging membranes. *J. Agric. Food Chem.* **2016**.

(12) De Groote, M. A.; Fang, F. C. No inhibitions: Antimicrobial properties of nitric oxide. *Clinical Infectious Diseases* **1995,** *21* (Supplement 2), S162-S165.

(13) Jones, M. L.; Ganopolsky, J. G.; Labbé, A.; Wahl, C.; Prakash, S. Antimicrobial properties of nitric oxide and its application in antimicrobial formulations and medical devices. *Appl. Microbiol. Biotechnol.* **2010,** *88* (2), 401-407.

(14) Schairer, D. O.; Martinez, L. R.; Blecher, K.; Chouake, J. S.; Nacharaju, P.; Gialanella, P.; Friedman, J. M.; Nosanchuk, J. D.; Friedman, A. J. Nitric oxide nanoparticles: Pre-clinical utility as a therapeutic for intramuscular abscesses. *Virulence* **2012,** *3* (1), 62-67.

(15) Ziche, M.; Morbidelli, L. Nitric oxide and angiogenesis. *J. Neurooncol.* **2000,** *50* (1), 139-148.

(16) Villalobo, A. Nitric oxide and cell proliferation. *FEBS Journal* **2006,** *273* (11), 2329-2344.

(17) Fang, F. C., *Nitric oxide and infection*. Springer: **1999**.

(18) Schäffer, M. R.; Tantry, U.; Gross, S. S.; Wasserkrug, H. L.; Barbul, A. Nitric oxide regulates wound healing. *Journal of Surgical Research* **1996,** *63* (1), 237-240.

(19) Kaposzta, Z.; Baskerville, P. A.; Madge, D.; Fraser, S.; Martin, J. F.; Markus, H. S. L-arginine and s-nitrosoglutathione reduce embolization in humans. *Circulation* **2001,** *103* (19), 2371-2375.

(20) Lima, B.; Lam, G. K.; Xie, L.; Diesen, D. L.; Villamizar, N.; Nienaber, J.; Messina, E.; Bowles, D.; Kontos, C. D.; Hare, J. M. Endogenous s-nitrosothiols protect against myocardial injury. *Proceedings of the National Academy of Sciences* **2009,** *106* (15), 6297-6302.

(21) Achuth, H. N.; Moochhala, S. M.; Mahendran, R.; Tan, W. T. L. Nitrosoglutathione triggers collagen deposition in cutaneous wound repair. *Wound repair and regeneration* **2005,** *13* (4), 383-389.

(22) Kim, J. O.; Park, J. K.; Kim, J. H.; Jin, S. G.; Yong, C. S.; Li, D. X.; Choi, J. Y.; Woo, J. S.; Yoo, B. K.; Lyoo, W. S. Development of polyvinyl alcohol–sodium alginate gel-matrix-based wound dressing system containing nitrofurazone. *International journal of pharmaceutics* **2008,** *359* (1), 79-86.

(23) Dantas, M.; Cavalcante, D.; Araújo, F.; Barretto, S.; Aciole, G.; Pinheiro, A.; Ribeiro, M.; Lima-Verde, I.; Melo, C.; Cardoso, J. Improvement of dermal burn healing by combining sodium alginate/chitosan-based films and low level laser therapy. *Journal of Photochemistry and Photobiology B: Biology* **2011,** *105* (1), 51-59.

(24) Liakos, I.; Rizzello, L.; Scurr, D. J.; Pompa, P. P.; Bayer, I. S.; Athanassiou, A. All-natural composite wound dressing films of essential oils encapsulated in sodium alginate with antimicrobial properties. *International journal of pharmaceutics* **2014,** *463* (2), 137-145.

(25) Zmora, S.; Glicklis, R.; Cohen, S. Tailoring the pore architecture in 3-d alginate scaffolds by controlling the freezing regime during fabrication. *Biomaterials* **2002,** *23* (20), 4087-4094.

(26) Nandini, V. V.; Venkatesh, K. V.; Nair, K. C. Alginate impressions: A practical perspective. *Journal of Conservative Dentistry* **2008,** *11* (1), 37.

(27) Gilchrist, T.; Martin, A. Wound treatment with sorbsan—an alginate fibre dressing. *Biomaterials* **1983,** *4* (4), 317-320.

(28) Lee, K. Y.; Mooney, D. J. Alginate: Properties and biomedical applications. *Progress in polymer science* **2012,** *37* (1), 106-126.

(29) Jannesari, M.; Varshosaz, J.; Morshed, M.; Zamani, M. Composite poly (vinyl alcohol)/poly (vinyl acetate) electrospun nanofibrous mats as a novel wound dressing matrix for controlled release of drugs. *Int J Nanomedicine* **2011,** *6*, 993-1003.

(30) Fluhr, J.; Darlenski, R.; Surber, C. Glycerol and the skin: Holistic approach to its origin and functions. *Br. J. Dermatol.* **2008,** *159* (1), 23-34.

(31) Kamoun, E. A.; Kenawy, E.-R. S.; Tamer, T. M.; El-Meligy, M. A.; Eldin, M. S. M. Poly (vinyl alcohol)-alginate physically crosslinked hydrogel membranes for wound dressing applications: Characterization and bio-evaluation. *Arabian Journal of Chemistry* **2015,** *8* (1), 38-47.

(32) Hart, T. W. Some observations concerning the s-nitroso and s-phenylsulphonyl derivatives of l-cysteine and glutathione. *Tetrahedron Lett.* **1985,** *26* (16), 2013-2016.

(33) Patel, S.; Shah, D.; Tiwari, S. Bioadhesive films containing fluconazole for mucocutaneous candidiasis. *Indian J. Pharm. Sci.* **2015,** *77* (1), 55.

(34) Brisbois, E. J.; Bayliss, J.; Wu, J.; Major, T. C.; Xi, C.; Wang, S. C.; Bartlett, R. H.; Handa, H.; Meyerhoff, M. E. Optimized polymeric film-based nitric oxide delivery inhibits bacterial growth in a mouse burn wound model. *Acta Biomater.* **2014,** *10* (10), 4136-4142.

(35) Pant, J.; Gao, J.; Goudie, M. J.; Hopkins, S.; Locklin, J.; Handa, H. A multi-defense strategy: Enhancing bactericidal activity of a medical grade polymer with a nitric oxide donor and surface-immobilized quaternary ammonium compound. *Acta Biomater.* **2017**.

(36) Pant, J.; Goudie, M. J.; Hopkins, S. P.; Brisbois, E. J.; Handa, H. Tunable nitric oxide release from s-nitroso-n-acetylpenicillamine via catalytic copper nanoparticles for biomedical applications. *ACS Appl. Mater. Interfaces* **2017,** *9* (18), 15254-15264.

(37) Bishop, E. T.; Bell, G. T.; Bloor, S.; Broom, I.; Hendry, N. F.; Wheatley, D. N. An in vitro model of angiogenesis: Basic features. *Angiogenesis* **1999,** *3* (4), 335-344.

(38) Azad, A. K.; Sermsintham, N.; Chandrkrachang, S.; Stevens, W. F. Chitosan membrane as a wound-healing dressing: Characterization and clinical application. *Journal of Biomedical Materials Research Part B: Applied Biomaterials* **2004,** *69* (2), 216-222.

(39) Singh, R. J.; Hogg, N.; Joseph, J.; Kalyanaraman, B. Mechanism of nitric oxide release from s-nitrosothiols. *J. Biol. Chem.* **1996,** *271* (31), 18596-18603.

(40) Luo, J.-D.; Chen, A. F. Nitric oxide: A newly discovered function on wound healing. *Acta Pharmacol. Sin.* **2005,** *26* (3), 259.

(41) Partsch, H. Investigations on the pathogenesis of venous leg ulcers. *Acta Chir. Scand. Suppl.* **1988,** *544*, 25-29.

(42) Dykhuizen, R.; Frazer, R.; Duncan, C.; Smith, C.; Golden, M.; Benjamin, N.; Leifert, C. Antimicrobial effect of acidified nitrite on gut pathogens: Importance of dietary nitrate in host defense. *Antimicrob. Agents Chemother.* **1996,** *40* (6), 1422-1425.

(43) Vallance, P.; Charles, I. Nitric oxide as an antimicrobial agent: Does no always mean no? *Gut* **1998,** *42* (3), 313-314.

(44) Fang, F. C. Perspectives series: Host/pathogen interactions. Mechanisms of nitric oxide-related antimicrobial activity. *J. Clin. Invest.* **1997,** *99* (12), 2818.

(45) Levy, S. B. The challenge of antibiotic resistance. *Sci. Am.* **1998,** *278* (3), 46-53.

(46) Raygada, J. L.; Levine, D. P. Managing ca-mrsa infections: Current and emerging options. *Infect. Med.* **2009,** *26* (2), 49-58.

(47) Jefferson, K. K.; Goldmann, D. A.; Pier, G. B. Use of confocal microscopy to analyze the rate of vancomycin penetration through staphylococcus aureus biofilms. *Antimicrob. Agents Chemother.* **2005,** *49* (6), 2467-2473.

(48) Asharani, P. V., Mun, G.L.K., Hande, M.P., Valiyaveettil. Cytotoxicity and genotoxicity of silver nanoparticles in human cells. *ACS Nano* **2009,** *3* (2), 279-290.

(49) Stewart, P. S.; Costerton, J. W. Antibiotic resistance of bacteria in biofilms. *The lancet* **2001,** *358* (9276), 135-138.

(50) Feelisch, M. The use of nitric oxide donors in pharmacological studies. *Naunyn-Schmiedeberg's Arch. Pharmacol.* **1998,** *358* (1), 113-122.

(51) Hetrick, E. M.; Schoenfisch, M. H. Antibacterial nitric oxide-releasing xerogels: Cell viability and parallel plate flow cell adhesion studies. *Biomaterials* **2007,** *28* (11), 1948-1956.

(52) Bogdan, C. Nitric oxide and the immune response. *Nat. Immunol.* **2001,** *2* (10), 907-916.

(53) Kazimoto, T.; Abdulla, S.; Bategereza, L.; Juma, O.; Mhimbira, F.; Weisser, M.; Utzinger, J.; Von Müller, L.; Becker, S. L. Causative agents and antimicrobial resistance patterns of human skin and soft tissue infections in bagamoyo, tanzania. *Acta Trop.* **2018**.

(54) Hocevar, S. N.; Edwards, J. R.; Horan, T. C.; Morrell, G. C.; Iwamoto, M.; Lessa, F. C. Device-associated infections among neonatal intensive care unit patients: Incidence and associated pathogens reported to the national healthcare safety network, 2006–2008. *Infect. Control Hosp. Epidemiol.* **2012,** *33* (12), 1200-1206.

(55) Heilman, B. J.; Halpenny, G. M.; Mascharak, P. K. Synthesis, characterization, and light-controlled antibiotic application of a composite material derived from polyurethane and silica

xerogel with embedded photoactive manganese nitrosyl. *Journal of Biomedical Materials Research Part B: Applied Biomaterials* **2011,** *99* (2), 328-337.

(56) Yoshida, A.; Anand-Apte, B.; Zetter, B. R. Differential endothelial migration and proliferation to basic fibroblast growth factor and vascular endothelial growth factor. *Growth Factors* **1996,** *13* (1-2), 57-64.

(57) Prior, B. M.; Yang, H.; Terjung, R. L. What makes vessels grow with exercise training? *J. Appl. Physiol.* **2004,** *97* (3), 1119-1128.

(58) Semenza, G. L. Vasculogenesis, angiogenesis, and arteriogenesis: Mechanisms of blood vessel formation and remodeling. *J. Cell. Biochem.* **2007,** *102* (4), 840-847.

(59) Eckes, B.; Aumailley, M.; Krieg, T., Collagens and the reestablishment of dermal integrity. In *The molecular and cellular biology of wound repair*, Springer: **1988**, pp 493-512.

(60) Schäffer, M.; Efron, P. A.; Thornton, F. J.; Klingel, K.; Gross, S. S.; Barbul, A. Nitric oxide, an autocrine regulator of wound fibroblast synthetic function. *The Journal of Immunology* **1997,** *158* (5), 2375-2381.

(61) Han, G.; Nguyen, L. N.; Macherla, C.; Chi, Y.; Friedman, J. M.; Nosanchuk, J. D.; Martinez, L. R. Nitric oxide–releasing nanoparticles accelerate wound healing by promoting fibroblast migration and collagen deposition. *The American journal of pathology* **2012,** *180* (4), 1465-1473.

(62) Goudie, M. J.; Brisbois, E. J.; Pant, J.; Thompson, A.; Potkay, J. A.; Handa, H. Characterization of an s-nitroso-n-acetylpenicillamine–based nitric oxide releasing polymer from a translational perspective. *Int. J. Polym. Mater. Polym. Biomater.* **2016,** *65* (15), 769-778.

(63) Lee, S. M.; Park, I. K.; Kim, Y. S.; Kim, H. J.; Moon, H.; Mueller, S.; Jeong, Y. I. Physical, morphological, and wound healing properties of a polyurethane foam-film dressing. *Biomater Res* **2016,** *20*, 15.

(64) Sundaram, J.; Pant, J.; Goudie, M. J.; Mani, S.; Handa, H. Antimicrobial and physicochemical characterization of biodegradable, nitric oxide-releasing nanocellulose–chitosan packaging membranes. *J. Agric. Food Chem.* **2016,** *64* (25), 5260-5266.

(65) Pant, J.; Goudie, M. J.; Hopkins, S. P.; Brisbois, E. J.; Handa, H. Tunable nitric oxide release from s-nitroso-n-acetylpenicillamine via catalytic copper nanoparticles for biomedical applications. *ACS Appl. Mater. Interfaces*.

(66) White, R.; Cutting, K. F. Modern exudate management: A review of wound treatments. *World Wide Wounds* **2006,** *1*.

(67) Sweeney, I. R.; Miraftab, M.; Collyer, G. A critical review of modern and emerging absorbent dressings used to treat exuding wounds. *International wound journal* **2012,** *9* (6), 601-612.

(68) Lykke, A.; Cummings, R. Inflammation in healing: I. Time-course and mediation of exudation in wound healing in the rat. *Br. J. Exp. Pathol.* **1969,** *50* (3), 309.

(69) Witte, M. B.; Barbul, A. Role of nitric oxide in wound repair. *The American Journal of Surgery* **2002,** *183* (4), 406-412.

(70) Schwentker, A.; Vodovotz, Y.; Weller, R.; Billiar, T. R. Nitric oxide and wound repair: Role of cytokines? *Nitric Oxide* **2002,** *7* (1), 1-10.

(71) Xu, R.; Xia, H.; He, W.; Li, Z.; Zhao, J.; Liu, B.; Wang, Y.; Lei, Q.; Kong, Y.; Bai, Y. Controlled water vapor transmission rate promotes wound-healing via wound re-epithelialization and contraction enhancement. *Sci. Rep.* **2016,** *6*.

CHAPTER 6

ANTIBACTERIAL 3D BONE SCAFFOLDS FOR TISSUE ENGINEERING APPLICATION

Pant, Jitendra. Accepted by Journal of Biomaterial Research: Part B
Reprinted here with permission of the publisher

Abstract

Open bone fractures are not only difficult to heal but are also at a high risk of infections. Annual cases of fractures which result from osteoporosis amount to ~ 9 million. Endogenously released nitric oxide (NO) has been shown to play a role in osteogenic differentiation in addition to eradicating infection against a wide variety of pathogens. In the current work, antimicrobial NO releasing 3D bone scaffolds were fabricated using *S*-nitroso-*N*-acetyl-penicillamine (SNAP) as the NO donor. During fabrication, nHA was added to each of the scaffolds in the concentration range of 10 wt% to 50 wt% in nHA-starch-alginate and nHA-starch-chitosan scaffolds. The mechanical strength of the scaffolds increased proportionally to the concentration of nHA and 50 wt% nHA-starch-alginate possessed the highest load bearing capacity of 203.95 ± 0.3 N. The NO flux of the scaffolds was found to be $0.50 \pm 0.06 \times 10^{-10}$ mol min^{-1} mg^{-1} initially which reduced to $0.23 \pm 0.02 \times 10^{-10}$ over a 24 h period under physiological conditions. As a result, a 99.76 ± 0.33 % reduction in a gram-positive bacterium, *Staphylococcus aureus* and a 99.80 ± 0.62 % reduction in the adhered viable colonies of gram-negative bacterium, *Pseudomonas aeruginosa* were observed, which is a significant stride in the field of antibacterial natural polymers. The surface morphology and pore size were observed to be appropriate for the potential bone cell growth. The material showed no toxic response to mouse fibroblast cells.

1. Introduction

A bone injury or a bone defect is a result of lost bone integrity either due to an external physical force or due to a decrease in peak bone mass (osteoporosis). More than 75 million people are affected by osteoporosis in USA, Japan, and Europe every year.[1] Annual cases of fractures which result from osteoporosis amount to 8.9 million, i.e. one osteoporotic fracture every

3 sec. About 9 million osteoporotic fractures were reported globally in the year 2000, 51% of which were from the USA and Europe.[2] Musculoskeletal injuries, in fact, is the most common medical reason behind the failure of soldiers to be deployed in the war-field.[3] It is also the cause of 73% of total disability cases in the US army contributing to an annual compensation of $5.5 billion to affected soldiers.[4] Some bone defects may arise from tumor trauma, or bone-related diseases and affect millions of lives worldwide.[5] Open fractures are not only difficult to heal but are also at high risk of infections. Infection caused by microbial pathogens diverts the inflammatory response away from healing and hence delays the recovery. Deep infections of bone often occur in the joints and at the ends of long bones.[6] Prevention of bone infections past surgeries require courses of systemic antibiotics and surgeries prior to bone grafting.[7] Unfortunately, even in the light of optimal health management, the chances of infection in open fracture is approximately 30% (of all the cases).[8-9]

A biodegradable 3D scaffold made from natural polymers serve as a temporary skeleton to accommodate new tissue growth in bone tissue engineering.[10] They are particularly amenable to implantation and can be easily manufactured into desired shapes.[11-12] In the current study, nitric oxide (NO) releasing antibacterial 3D bone scaffolds were fabricated using chitosan-starch, or alginate-starch as the base polymer and the mechanical strength was provided using the hydroxyapatite. A comparison was made between nHA-alginate-starch vs nHA-chitosan-starch with varying nHA concentrations for its compressive strength to filter what composition is best in terms of maximum load-bearing capacity. After finding the best composition, NO donor i.e SNAP was incorporated to it. Endogenous NO synthesized by NO synthase (eNOS) promotes bone development and healing. In addition, researchers has shown that NO helps in osteogenic differentiation of bone marrow mesenchymal cells (BMSC) in 3D silk scaffolds.[13] However, its antibacterial potential as an alternative to antibiotics application during bone defects has not been studied yet. The NO released within the sinus cavities and macrophages functions as a natural antimicrobial agent to combat pathogen invasion in humans.[14] Nitric oxide is a free radical gas

with a short half-life that plays an important role in various biological processes. Moreover, the use of NO is unlikely to stimulate the production of resistant strains due to non-specific action, short half-life and rapid reduction of microbial load life.[15-17]

Owing to its biological activity and inherent bactericidal effect, chitosan has garnered great interest in bone scaffold applications.[18] Alginate is another natural polymer which is frequently used for bone grafting due to its biocompatible, biodegradable, and hydrophilic nature.[19-21] Furthermore, the integration of starch in natural polymers can adequate mechanical properties and controlled degradation of bone scaffolds.[22] Such biopolymers, when reinforced with a bioactive bone component e.g. ceramic fillers such as hydroxyapatite, pose great bone tissue regeneration capabilities. Many studies have reported that addition of a calcium phosphate such as hydroxyapatite (HA) can enhance the biological properties of bone scaffolds due to its compositional similarity to natural bone.[22] The bone implants containing higher concentrations of HA have been shown to have a better affinity towards bone *in vivo* over those with the smaller amounts of it.[23] In the past few years, HA has been extensively used in the bone cement formulations for repairing of the femur and craniofacial defects. The addition of nano-hydroxyapatite (nHA) has been shown to increase the scaffold surface area due to the decrease in the pore size.[22] Such an increase in the scaffold's surface area favored by nHA has been shown to positively affect bone cells growth.[18]

While nHA, starch, alginate, and chitosan are well-known materials used for bone tissue engineering, there has been no study done in the past to show the application of NO release in combination with these materials for developing 3D bone scaffolds. The primary objective of this work is to explore the possibility of integrating a nitric oxide donor, SNAP in 3D bone scaffolds to prevent bacterial infection without causing any cytotoxicity to the mammalian cells. In the current study, various concentrations of nHA (10 wt% - 50 wt%) were added to starch and blended with either alginate or chitosan to formulate a solution for 3D bone scaffolds. The study first tested nhA-starch combination with alginate or chitosan for its compressive strength filter what

composition is best in terms of maximum load bearing capacity. Thereafter, the 3D scaffold formulation showing maximum compressive strength were incorporated with the SNAP and characterized further for the NO release kinetics and effect of SNAP incorporation on the morphology of the scaffolds. Finally, the ability of the bone scaffolds to prevent infection was tested against common infectious agents such as gram-positive *Staphylococcus aureus* and gram-negative *Pseudomonas aeruginosa*.

2. Materials and Methods

2.1 Materials

Alginic acid sodium salt, chitosan, and reagent grade hydroxyapatite (calcium phosphate tribasic, MW: 502.31 g/mol) were obtained from Sigma-Aldrich, Co. (St. Louis, MO). Cornstarch was purchased from ACH Food Companies, Inc. (Memphis, TN). Sodium hydroxide and hydrochloric acid were obtained from Fisher Scientific (Fair Lawn, NJ). Glutaraldehyde and calcium chloride (anhydrous, granular ≤7.0mm, ≥ 93%) were purchased respectively from Fischer Scientific (Fair Lawn, NJ) and Sigma-Aldrich, Co. (St. Louis, MO). The bacterial strains *Pseudomonas aeruginosa* (ATCC 27853) and *Staphylococcus aureus* (ATCC 5538) used in this were originally obtained from American Type Culture Collection (ATCC).

2.2 Methods

2.2.1 Synthesis of nano-hydroxyapatite (nHA)

Nano-hydroxyapatite (nHA) particles can penetrate through the surface of the bone and can aid in the remineralization of a decayed bone. Therefore, a standard protocol was used to synthesize nHA particles from hydroxyapatite (HA).[22] Hydroxyapatite solution (3.4 wt%) was

dissolved completely in 150 mL of 0.1 N HCl using a magnetic stirrer. 1N NaOH was dropwise added to the beaker containing 3.4% (w/v) HA solution. The mixture was allowed to agitate continuously using a magnetic stirrer. As the reaction progressed, nanocrystals of HA started to precipitate in the beaker. The pH was readjusted to 6.8-7.2 using concentrated HCl. The resulting solution was stirred for 20 h to allow aging of nHA crystals. Then, the crystals were collected by centrifuging the solution for 20 min at 3000 rcf (Eppendorf Centrifuge 5702). The supernatant was discarded and the nHA pellet was stored at 4-8°C until used in the preparation of scaffolds.

2.2.2 Fabrication of nHA-starch-alginate and nHA-starch-chitosan composites

Five different types of nHA-starch-alginate composites and nHA-starch-chitosan composites were prepared using different wt% of nHA: 10 wt%, 20 wt%, 30 wt%, 40 wt%, and 50 wt%. Firstly, 2% (w/v) solution of alginic acid (n=5) was prepared by adding 1 g of alginic acid in 50 mL of deionized water (diH_2O) and stirred at 40-45°C for 3 h. Separately, 2% (w/v) solution of cornstarch (n=5) was heated up to at 60-65°C while constantly stirring it for 4 h using a magnetic stirrer. As the starch solution became dense and thick, different wt% of nHA (10 wt%-50 wt%) were added to individual starch solutions and stirred for another 10 min at room temperature. The starch-nHA blend was added to alginate solution to get a formulation of nHA-starch-alginate with varying concentration of nHA in the range of 10 wt%- 50 wt%. Similarly, the nHA-starch-chitosan blend was obtained using the same reaction condition except for dissolving 2% (w/v) solution of chitosan in 1 M acetic acid solution instead of diH_2O. The resulting formulations with varying levels of nHA-starch-alginate (10-50 wt% of nHA) and nHA-chitosan (10-50 wt % of nHA) were cast in molds and were frozen at -15°C to -35°C in the freezer for 24 hours to get solid scaffold composites.

2.2.3 Cross-linking of the biopolymer composites

A collection of 10 wt%, 20 wt%, 30 wt%, 40 wt%, and 50 wt% of nHA-starch-alginate and nHA-starch-chitosan formulations were cross-linked. The nHA-starch-alginate bone scaffolds were cross-linked with 2% $CaCl_2$ solution. 2% $CaCl_2$ solution was prepared by dissolving 4 grams of $CaCl_2$ in 200 mL of distilled water. The nHA-starch-alginate bone scaffolds were cross-linked

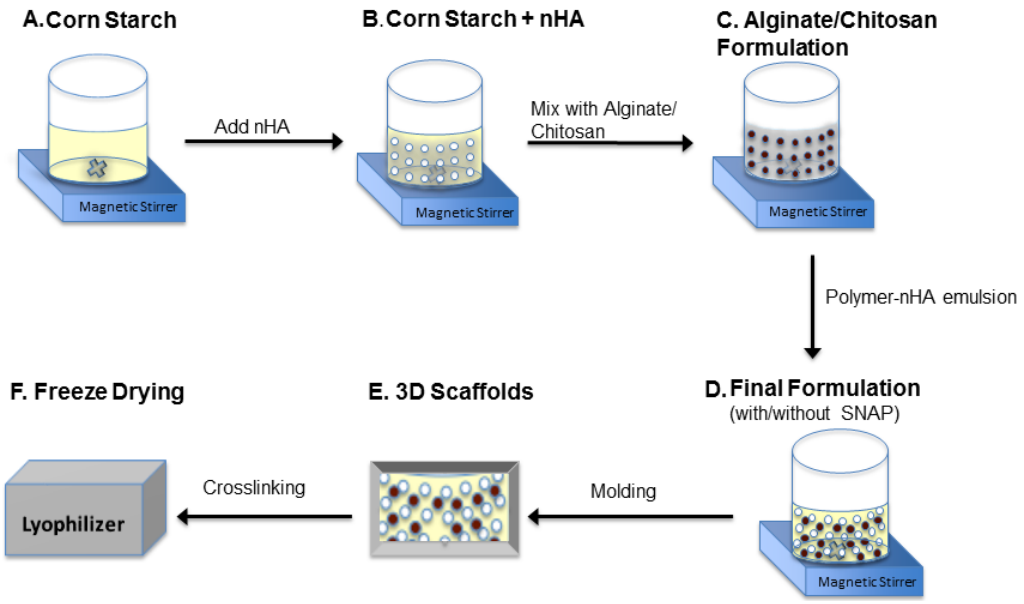

Figure 6.1. The fabrication process of 3D bone scaffolds: nHA-starch-alginate and nHA-starch-chitosan scaffolds. At step D, the NO donor, SNAP, was added to the 3D scaffolds to provide antimicrobial characteristics while the control 3D scaffolds were fabricated without SNAP. Ultimately the emulsion was frozen below -15°C for at least 24 h. Afterward, scaffolds were crosslinked and frozen again below -15°C overnight. Finally, 3D scaffolds were freeze-dried in a lyophilizer.

in 5% glutaraldehyde. The 5% glutaraldehyde was prepared by dissolving 10 ml of glutaraldehyde in distilled water volume made up to 200 ml. Once the crosslinking solution became homogenized, scaffolds were immersed in the solution to crosslink for 2-3 h. Figure 6.1 represents the stepwise fabrication process of 3D bone scaffolds. Based on the mechanical strength results the NO donor, *S*-nitroso-*N*-acetyl-penicillamine (SNAP) was added in the formulation of the scaffolds showing maximum compression strength (sections 2.2.5 and 2.2.6).

2.2.4 Creation of porous morphology using freeze-drying methods

In order to serve as a vehicle to deliver the drug, promote cell interactions and retain cells at a specific site and prevent infections for faster bone healing, a porous biodegradable composite is needed as a scaffold.[10] In addition, the drug release profile and the cell growth are strongly influenced by the pore size. Hence, it is crucial to execute appropriate processing and drying method to get the desired pore size. A greater surface area provides a platform for cell adhesion and in return allows cell proliferation, which sequentially assists bone tissue formation. In addition, it facilitates exchanges of nutrients and gasses for faster cells growth and hence enhanced healing.

An innovative yet simple technique of lyophilization was used to freeze dry the cross-linked 3D scaffolds. To create microscopic pores in the scaffolds, freeze-drying was carried out using a LABCONCO FreeZone 4.5 Plus freeze dryer. After crosslinking the 3D scaffolds with their respective chemical cross-linkers the scaffolds were frozen again in the freezer (-15°C to -30°C) overnight. Afterward, they were placed in a sealed beaker attached to a freeze drier and dried for 22 ± 2h at 0.5 mBar vacuum and -84°C. The images of completely processed freeze-dried bone scaffolds are shown in Figure 6.2.

Figure 6.2. Representative images of the final 3D bone scaffolds after complete cross-linking and lyophilization: A. nHA-starch-Chitosan and B. nHA-starch-alginate. Right before, lyophilization the chitosan scaffold and alginate scaffolds were crosslinked with 5% glutaraldehyde and 2% $CaCl_2$ solution in water.

2.2.5 Mechanical testing

Completely dried scaffolds (n=3 samples with l = 3 cm, w = 2 cm, h = 2 cm) were used to measure mechanical strength in terms of compressive force using an Instron model 5545. the plateau in the load vs strain curve was observed at compression ratios between 0.15 and 0.2 signifying a transition from the elastic to plastic deformation regime. No preload was used. A force perpendicular to the direction of the scaffold was applied and the cross-head speed was set to 1 mms^{-1}. Force and distance were recorded and analyzed to obtain compressive strength.

A comparison was made between nHA-alginate-starch and nHA-chitosan-starch with varying nHA concentrations for its compressive strength to filter what composition is best in terms of maximum load-bearing capacity. The bone scaffolds composition with best mechanical strength was then screened to finally add 10 wt% SNAP during the fabrication process.

2.2.6 SNAP synthesis and incorporation in bone scaffolds

SNAP synthesis: *S*-nitroso-*N*-acetylpenicillamine (SNAP) was synthesized using recommendations from a previously reported method.[24-25] An equimolar amount of *N*-acetylpenicillamine (NAP) and sodium nitrite was added to a solution with 1:1 ratio of water and methanol containing 2M H_2SO_4 and 2M HCl. The resulting solution was stirred for 30 minutes. The precipitation of SNAP crystals was achieved by continuously aerating the reaction mixture for 4 h while the reaction vessel was cooled in an ice bath. The SNAP crystals were collected by filtering the solvent using a 70 mm Whatman® filter paper and allowed to air dry overnight while the SNAP crystals were protected from light. The crystals' purity was found to be greater than 95% using the Sievers Chemiluminescence Nitric Oxide Analyzer.

SNAP incorporation in the bone scaffolds: The SNAP was incorporated in the bone scaffolds with the maximum compressive strength to provide it with NO releasing property. Briefly, 10 wt% SNAP was added to nHA-starch blend (prepared as shown in section *2.2.2*) and dissolved

using a magnetic stirrer at room temperature. The resulting solution was added to completely dissolved 2 % (w/v) alginate solution. The nHA-starch-alginate formulation containing NO donor, SNAP was cast in a mold and placed in the freezer at -15°C to -35°C for 12-16 h overnight. The frozen material was cross-linked using 2% $CaCl_2$ for 2-3 h and the cross-linked scaffolds were frozen again overnight. Finally, the scaffolds were freeze-dried; using LABCONCO FreeZone 4.5 Plus freeze dryer at ≤ 0.5 mBar vacuum and -84°C.

2.2.7 Morphological analysis

The surface morphology and microstructure of the scaffolds were examined using scanning electron microscopy (SEM) (FEI Inspect F FEG-SEM) in triplicates for each of the 3D bone scaffolds of nHA-starch-alginate and of nHA-starch-chitosan containing 10-50 wt% nHA. Freeze dried scaffolds were mounted on a metal stub with double-sided carbon tape and sputter coated with 10 nm gold-palladium using a Leica EM ACE200 sputter coater. Images were taken at an accelerating voltage of 20 kV at 100 X magnification.

In addition, cross-sectional images of the 50 wt% nHA-starch-alginate scaffold with SNAP were taken using EVOS XL microscope at a resolution of 10X.

2.2.8 NO flux measurement of SNAP incorporated nHA-starch-alginate scaffolds

Nitric oxide released by the 50 wt% nHA-starch-alginate composites were measured using a Sievers Chemiluminescence Nitric Oxide Analyzer (NOA) model 280i (Boulder, CO). The NOA can selectively measure NO through the reaction of NO with oxygen plasma, giving it the ability to reduce interference from molecules such as nitrates and nitrites. Portions of the dried SNAP-nHA-starch-alginate scaffolds were placed in the NOA cell with 3 mL of PBS with EDTA in triplicates (n=3). Nitrogen was aerated into the PBS to facilitate the release of NO from solution at a rate of ~200 ml/min as recommended by NOA manufacturer. Following the initial measurement, the scaffolds were maintained at 37^{O}C in a water-jacketed incubator (Thermo

Fisher Scientific, Waltham, MA USA) in PBS. Following 24 hours, the scaffold was removed from the PBS solution and placed in the NOA cell with fresh PBS with EDTA. Release rates from the scaffolds are normalized on a per mass basis. The NO release rate per weight of the bone scaffolds was reported as NO flux (x 10^{-10} mol min^{-1} mg^{-1}).

2.2.9 Bacterial adhesion test

A standard bacterial adhesion test was used to assess the antibacterial properties of NO releasing scaffolds.[26-27] A single isolated colony of *P. aeruginosa* and *S. aureus* strain was picked from an LB agar Petri dish, introduced to 10 mL of liquid LB medium and incubated for 14 h at 37°C. The optical density of the culture was measured at 600 nm (O. D_{600}) using UV-vis spectrophotometer (Thermo Scientific Genesys 10S UV-Vis). The traces of LB medium were removed by centrifuging the bacterial culture for 7.5 min at 2500 rpm, the supernatant was then discarded and sterile phosphate buffer saline (PBS, pH 7.4) of the equivalent amount was added and centrifuged again for 7.5 min at 2500 rpm twice. The $O.D_{600}$ of the culture in PBS was measured again using PBS as the blank and diluting the bacterial culture in PBS to get the concentration in the range of 10^6-10^8 colony forming units per ml (CFU/ml). Segments of bone scaffolds, with and without SNAP, were weighed and exposed to a 50 mL tube containing 10 mL bacterial culture of *S. aureus* suspension and *P. aeruginosa* (n=3). These scaffolds were incubated for 24 h at 2500 rpm in 37°C environment. After the 24 h bacteria study, each of these bone scaffolds was placed in a new 50 L sterile tube containing 10 mL of fresh PBS, followed by 60 seconds of mixing in the vortex to remove loosely bound bacteria. Subsequently, the resulting bacterial suspension was serially diluted (10^{-1} to 10^{-5}) and plated in petri dishes with LB agar medium and incubated at 37°C for 24 h. After incubation, colony forming units per weight of the bone scaffolds (CFU/mg) were counted and compared to control and SNAP bone scaffolds to detect their efficacy to inhibit bacterial adhesion on the surface of bone scaffolds. Percentage bacterial inhibition was calculated using the formula below

$$\% \text{ Bacterial inhibition} = \frac{\text{CFU /mg in control samples - CFU/mg in test sample}}{\text{CFU /mg in control samples}} X100$$

2.2.10 Cytotoxicity test

The NO oxide releasing scaffolds were tested for the absence of cytotoxic response towards mammalian cells by modifying a recommended cell cytotoxicity assay.[27] The leachates from the samples (n=7) were collected by putting 10 mg of sample per 10 mL of Dulbecco Modified Eagle's Medium (DMEM) for 24 hours at 37°C.

For cell culture, a cryopreserved vial containing 3T3 mouse fibroblast cells (ATCC-1658) was thawed and cells were cultured in a 75 cm^2 T-flask with complete DMEM medium. The cells were incubated in humidified conditions of 37°C with 5% CO_2. DMEM was replaced intermittently every second day and cells were observed daily for the absence of contamination. After reaching a confluence of 80% (adherent culture) cells were detached from the surface by enzymatic trypsinization (trypsin with 0.18% trypsin and 5 mM EDTA). Finally, the cells were counted using a hemocytometer with 0.4% trypan blue (dye exclusion method). Thereafter, in a 96 well plate (cell culture grade), 100 µL of 5000 cells/ml were seeded in each of the wells (7 wells for each sample type) and incubated for 24 hours. As per the manufacturer's recommendation, to each of the wells, 10 µL of the leachate from control (starch-alginate) and NO releasing biopolymer (SNAP-alginate) was added. Cells put in an incubator (5% CO_2, 37°C) were allowed to respond to the leachate for 24 hours. Thereafter, 10 µL of the WST-8 solution (Sigma-Aldrich) was added and cells were incubated further for 24 hours. WST-8 is converted to a formazan (an orange-colored product measured at an absorbance of 450 nm) in the presence of dehydrogenase enzyme secreted by live cells only. The relative viability (%) of the mouse fibroblast cells as a response to the leachate was measured using the formula below.

$$\%\ Cell\ Viability = \frac{Absorbance\ of\ the\ test\ samples}{Absorbance\ of\ the\ control\ samples} \times 100$$

2.2.11 Statistical analysis

Statistical data is expressed as a mean ± standard error of the mean. Comparison of means using student's t-test: two samples assuming unequal variance were used to analyze if there was a statistical difference between the data for SNAP-incorporated vs control bone scaffolds. Values of $p < 0.05$ were considered statistically significant and were reported for all the experimental results unless otherwise mentioned.

3. Results and Discussions

Biomaterials that can imitate the natural template for bone cells growth in terms of structure and composition can act as a potential candidate for bone tissue engineering applications. In the current study, we developed 3D bone scaffolds by combining nHA (nano-hydroxyapatite) with natural polymers: alginate and chitosan and incorporated a NO donor in the scaffolds The NO donor (SNAP) was incorporated into the bone scaffolds to prevent bacterial infection that can potentially occur at the site of implantation. In the past, the bactericidal effect of NO has been shown against a wide variety of pathogens: virus, bacteria, and fungus.[28-32] Besides its highly effective antibacterial nature, NO has crucial roles to play in bone growth, angiogenesis, tissue healing, and remodeling, which ensures faster recovery.[33] After determining the 3D scaffolds with maximum compressive strength between nHA-chitosan-starch and nHA-alginate-starch, SNAP was incorporated in the scaffolds with best load-bearing capacity. Therefore, the NO release kinetics, SEM, antibacterial potential and cytotoxicity is tested and presented with only the scaffolds with maximum compressive strength.

3.1 Mechanical testing of the bone scaffolds

Compressive strength refers to the local stress maximum after the linear elastic region of the curve[34] which is one of the important functions of a bone scaffold to provide sufficient mechanical support temporarily to withstand in *vivo* loading and stresses.[35] The compressive strength of the scaffold should be retained until the tissue engineered transplant is fully remodeled by the host tissue and can assume its structural role. The maximum load bearing capacity of bone scaffolds should be high to provide proper load transfer at the site of implantation. A recent study showed that bone healing capacity increases in direct proportion to the amount of mechanical force applied.[36]

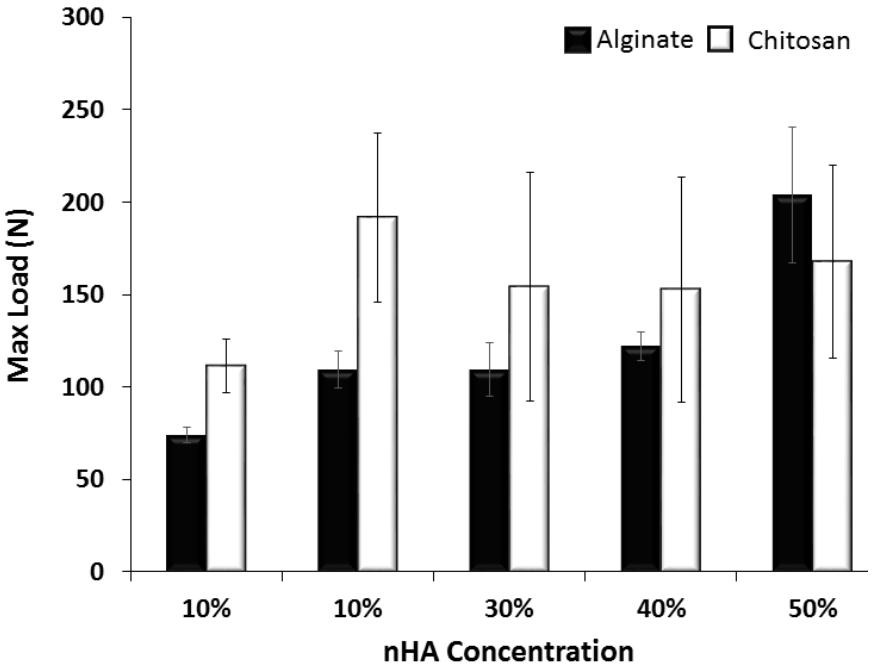

Figure 6.3. Completely freeze-dried scaffolds were used to measure mechanical strength in terms of compressive force (N) using an Instron model 5545. The nHA was added at a concentration range of 10 wt% to 50 wt% in both alginates (nHA-starch-alginate) and chitosan (nHA-starch-chitosan) scaffolds. Overall, 50 wt% nHA-starch-alginate scaffold showed the highest strength among all bone scaffolds. Statistical data are expressed as a mean ± standard error of the mean of n=3 samples. Values of $p < 0.05$ were considered statistically significant.

During fabrication, nHA was added to each of starch-alginate and starch-chitosan solutions in the concentration range of 10 wt% to 50 wt%. The cross-linking of the nHA-starch-alginate mix was achieved via two different mechanisms. Firstly, during the covalent cross-linking of alginate with calcium ions present in the calcium chloride (cross-linker)[22] and secondly, during the freeze-drying process. Removal of water promotes interchain cross-links in polysaccharides as in the case of proteins.[37] In general, there is more collapse of pore structures in freeze-dried samples because of processing at low temperature that results in less dense interchain cross-linking. However, due to the addition of nHA, the 3D scaffolds could not collapse and hence resulted in an improved compressive strength.

For the 3D scaffolds made with nHA-alginate-starch, the maximum load-bearing capacity increased proportionally with the amount of nHA added to them as expected (Figure 6.3). In a previous study, a proportional increase in scaffolds strength with respect to nHA concentration has been shown.[38] The alginate-based scaffolds with 10 wt% nHA showed the least load bearing capacity at 74.0 ± 4.3 N as compared to 50 wt% nHA-starch-alginate scaffolds, which could tolerate a load of 203.9 ± 36.6 N before getting deformed. The 20 wt%, 30 wt%, and 40 wt% nHA-starch-alginate scaffolds corresponded to maximum load bearing capacities of 109.3 ± 10.0 N, 109.5 ± 14.3 N, and 122.2 ± 7.6 N respectively. However, with the nHA-starch-chitosan, the compressive strength didn't vary proportionally with nHA. Instead, with 20 wt % nHA, exhibited highest load-bearing capacity which then slightly decreases and then remained constant for 30-50%. The nHA-starch-chitosan-based scaffolds (with 10 wt% to 50 wt% nHA) showed maximum load-bearing capacity in the range of 111.5 ± 14.4 to 167.6 ± 52.2 N. Since both alginate and chitosan-based scaffolds were freeze-dried, the reason for the change in the mechanical strength might be due to covalent cross-linking which is material-dependent. In addition, many other factors such as the concentration of components, type of cross-linking agents, cross-linking time, composition of the solvent mixture, and cross-linking temperatures might affect the final mechanical strength. Overall, 50 wt% nHA-starch-alginate scaffolds showed the highest strength

(203.9 ± 36.6 N) among all bone scaffolds and hence was chosen to incorporate 10 wt% SNAP and further characterization. In the past, it has been shown that the ultimate load to failure of and above 69.56 ± 4.74 N resulted in faster bone healing and thus 50 wt% nHA-starch-alginate scaffolds with highest compressive strength is expected to perform the best among all other scaffolds.[36] Furthermore, using the 50 wt% nHA can be advantageous with respect to other bone healing attributes, such as efficient bonding with the host's bone tissue and osteoconductive behavior, important for bone cells growth.[39]

3.2 Nitric oxide flux analysis of 3D bone scaffolds

Nitric oxide released from the 50 wt% nHA-starch-alginate scaffolds was measured using Sievers Chemiluminescence Nitric Oxide Analyzer (model 280i) under simulated physiological conditions (37°C, 3 mL PBS, pH 7.4). A representative release profile from the scaffolds is shown in Figure 6.4. An initial burst of NO was seen prior to maintaining a steady release rate after ~30 minutes. Initial NO release rates from the scaffolds were $0.5 \pm 0.06 \times 10^{-10}$ mol min^{-1} mg^{-1} (Figure 6.5). After 24 h in PBS at 37°C, the alginate scaffold continued to release NO at a rate of $0.23 \pm 0.02 \times 10^{-10}$ mol min^{-1} mg^{-1}.

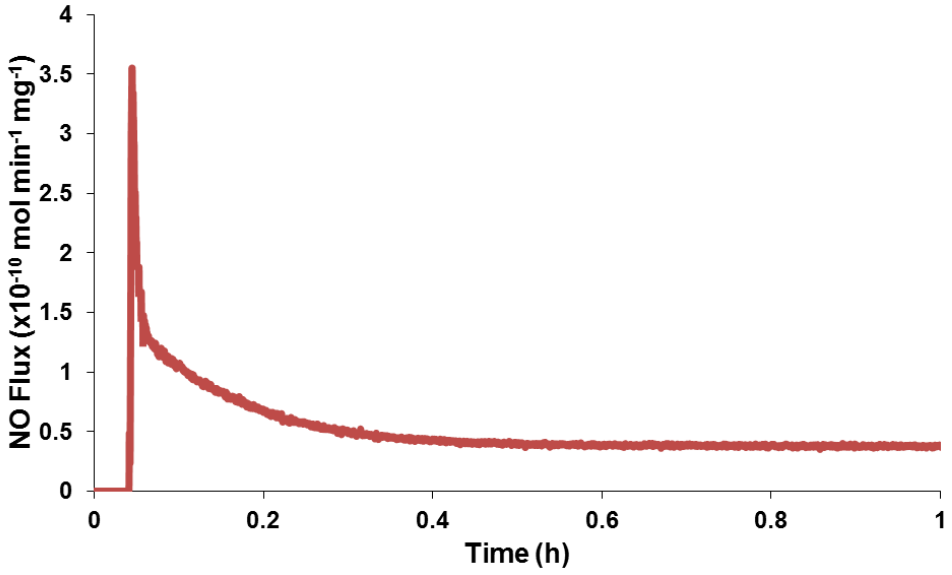

Figure 6.4. Real-time NO release profile of SNAP incorporating 50 wt% nHA-starch-alginate scaffold.

The theoretical lifetime of the NO release by the scaffold is extrapolated to be ~9 days when averaging the NO release rate over the first 24 h. The risk of infection is highest at the time of implantation and the pathogens can proliferate at the site of implantation. The bacteria are able to colonize a biofilm over the implant that is resistant to the therapeutic agents. Therefore, bone scaffolds that can control bacterial infection during the first week of implantation hold great therapeutic promise. The NO release over the first week may allow for adequate preliminary healing of the area and prevent immediate infection. The key point here is that preventing infection is most important in the first one week after implantation and thereafter, the 3D scaffolds can continue to support bone growth even in the absence of SNAP. However, if prolonged NO release is needed beyond one-week, possible steps to improve the lifetime of the NO release may include increasing the overall NO donor concentration, as well as altering the composition of the scaffold material or crosslinking NO donor with the base polymer.

In the past, controlled NO release from polymeric materials has been demonstrated by incorporating the NO donors into materials with low water uptake, whereas materials with high water uptake exhibit a large burst of NO release, where the NO supply is quickly depleted.[40-41] For instance, SNAP has been shown to release NO for >18 days at physiological levels when incorporated into hydrophobic synthetic polymers at a concentration of 10 wt%.[24, 40] These materials have been used in medical device coating applications, such as urinary and vascular catheters, and lend themselves to relatively low surface areas of release compared to those of porous scaffolds, where the surface area per unit weight (per mg) can be orders of magnitude higher. The more the surface area per mg is increased, the more the water uptake and hydrophilicity of the material will impact the NO release kinetics. While increasing the concentration of SNAP within the polymer matrix will aid in the stability and long-term release capabilities of the polymeric matrix through localized crystal formation of the NO donor, there are also negative impacts on the physical properties of the material.[24, 42] In essence, the flexible fabrication model of the 3D bone scaffolds presented in the current study can be modified

depending on the extent of the injuries by altering the type of polymers, NO donors, and their respective concentrations.

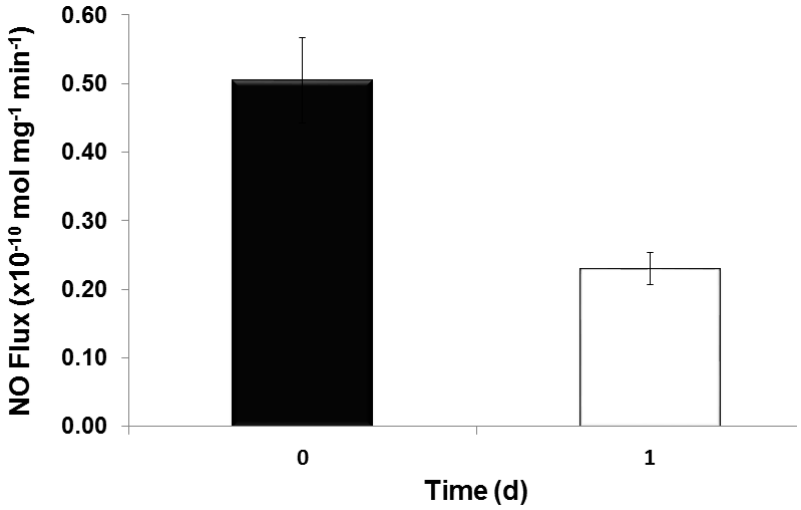

Figure 6.5. The comparative NO flux from SNAP incorporated 50 wt% nHA-starch-alginate bone scaffolds in the beginning day 0 (0 h) and day 1 (24 h). The theoretical lifetime of the scaffolds is extrapolated to be 8.6 days by averaging the release rate over the first 24 hours. The flux corresponds to the lower end of physiological NO flux range i.e 0.5-4.0 10^{-10} - 0.23 ± 0.02 × 10^{-10} mol $min^{-1}mg^{-1}$. Statistical data are expressed as mean ± standard error of the mean of n=3 samples. Values of $p < 0.05$ were considered statistically significant

3.3 Surface morphology of 3D bone scaffolds

The morphology of a bone scaffold is another important property considered for replacement of bone to allow growth of bone cells. In addition, the strength of the 3D scaffolds can be adjusted to match site-specific requirements by manipulating overall porosity. In order to serve as a vehicle to deliver the drug, promote cell interactions and retain cells at a specific site and prevent infections for faster bone healing, a porous biodegradable composite is needed as a scaffold.[10] In addition, the drug release profile and the cell growth are strongly influenced by the pore size. A greater surface area provides a platform for cell adhesion and in return allows cell proliferation, which sequentially assists bone tissue formation. In addition, it facilitates exchanges of nutrients and gasses for faster cells growth and hence enhanced healing.

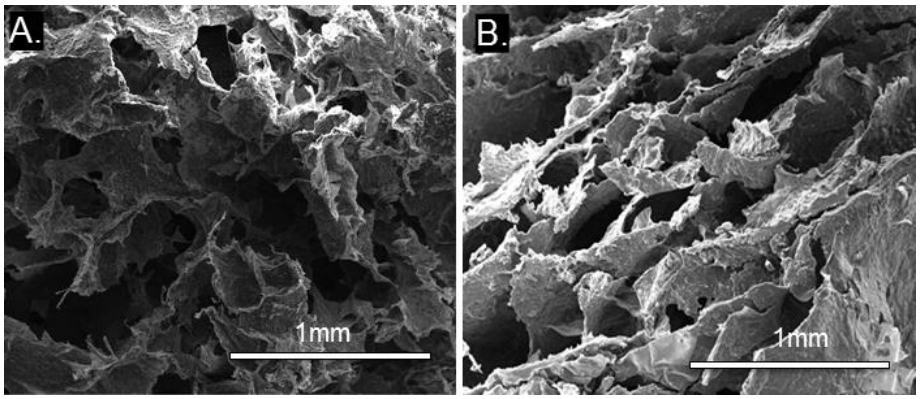

Figure 6.6. Surface Electron Microscopy (SEM) images of A. Control 3D bone scaffold and B. 3D bone scaffold with SNAP. There were no observed regions of SNAP crystallization on the surface of the scaffolds. The highly-interconnected pores are one of the desired characteristics of bone scaffolds needed for cells seeding, gaseous exchange, nutritional transfer, and mass flow.

Morphologies of the 50 wt% control nHA-alginate-scaffolds, as well as those containing SNAP, were examined under SEM. The addition of SNAP to the scaffold appeared to result in a decrease in the layering of the scaffold, possibly due to decreased cross-linking time. There were no observed regions of SNAP crystallization on the surface of the scaffolds. This combined with the steady NO release indicates that the SNAP is homogeneously mixed throughout the scaffold. The morphological analysis recorded by SEM is shown in Figure 6.6(A-B). Previous reports have shown that the scaffolds with high porosity and interconnection provide the desired amount of

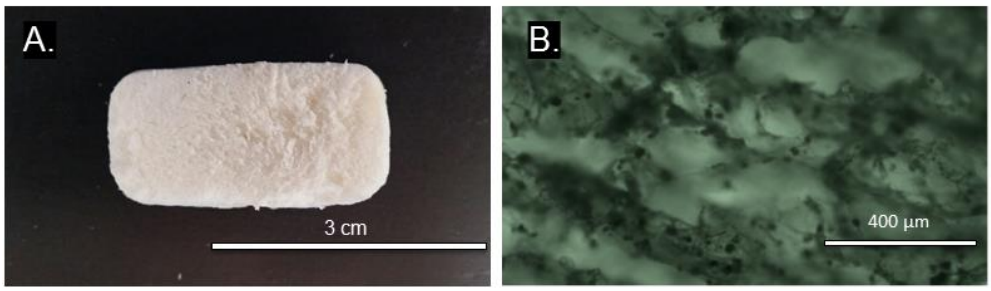

Figure 6. 7. Cross-sectional view of freeze-dried 50 wt% nHA-starch-alginate scaffolds shows a uniform matrix of the biopolymer materials. The image on the left (A) is taken with a 10-megapixel camera. The image on the right is taken using an optical microscope (EVOS XL) at a resolution of 10X. The image B shows a pattern of the uniform layer and void spaces in the scaffold. These images combined with Figure 6.5b and Figure 6.2 gives a holistic view of the physical morphology of the bone scaffolds both internally and externally.

space for cell seeding, growth and metabolites exchange.[43-44] The SEM analysis in the present study showed that the NO releasing bone scaffolds have a highly interconnected porous structure.

The structural collapse in freeze-dried biomaterial is common; however, SEM analysis for the 50 wt% nHA-alginate-starch-based 3D scaffolds showed the uniform organization of pores within the scaffolds possibly due to prior screening that was done in selecting the optimized formulation in terms of maximum load for scaffold fabrication. Therefore, there was no pore structure collapse in 50 wt% nHA-starch-alginate scaffolds which synchronizes with the observations made in the mechanical strength testing. Another reason might be the addition of cornstarch. The cornstarch used in this study was thermally stabilized through starch gelatinization procedure, which gives strong interchain linkage when homogeneously mixed with alginate and chitosan gels. Additionally, nHA was added to improve the mechanical strength of the scaffolds. By increasing the mechanical strength, pore structure collapse during freeze-drying was eliminated as observed during SEM analysis. This is in line with the observation made from the cross-sectional images of freeze-dried scaffolds that shows a continuous and uniform matrix of the biopolymer materials (Figure 6.7 (A-B)). In addition to these observations, no surface shrinkage was observed in the 3D scaffolds (Figure 6.2). The pore size based on SEM analysis were reported to be less than 1mm. Different bone types have different requirement of pore sizes due to differences in their location, size, strength, and function. In general, tissue engineering scaffolds with a pore size in the range of 20-1500 μm are commonly used.[10, 45-46] Pore size greater than 300 μm is recommended for promoting angiogenesis at the site of osteogenesis.[47] In addition, the highly interconnected pores in the NO releasing 3D bone scaffolds are expected to facilitate exchanges of nutrients and gasses for faster cells growth and hence enhanced healing which is in line with the earlier published work.[43-44] In the past also, studies have shown that starch-based bone scaffolds with nHA can support the growth of osteoblast cells in a 2 weeks study.[48]

3.4 Bacterial inhibition on 3D bone scaffolds

Per the American Academy of Orthopedic Surgeons (AAOS), patients with bone replacement often require another surgery to cure the bacterial infection, despite the use of

antibiotics and preventative treatments. 33% of the bone implantations results in infection even in the presence of optimal healthcare. Antibiotics are used at the site of implantation to control pathogenic population, but the never-ending issue of antibiotic resistance raises an alarming concern and questions its application as a long-term solution. If the infection prevails, it becomes necessary to remove the bone implant. Autografts are limited by the donor site morbidity while allografts can cause an undesired immune response in the host. These challenges have spurred the need for the development of polymeric 3D bone scaffolds with antibacterial properties. The 3D scaffolds are expected to only provide a matrix for bone cells to restore damaged bone function, but the problem of infection remains that slows down healing and prolong hospital stays thus increasing the overall cost of treatment. Gram-positive *Staphylococcus aureus* (*S. aureus)* remains the principal causal agent while the gram-negative *Pseudomonas aeruginosa* (*P. aeruginosa)* also contributes significantly towards bone infection that follows post-implantation.[49]

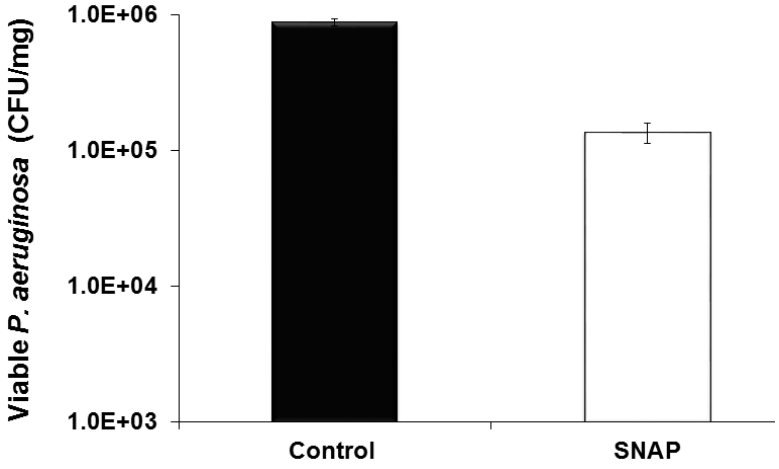

Figure 6.8. The NO releasing 3D bone scaffolds (SNAP) resulted in 96.7% decrease in *S. aureus* CFU/mg as compared to the control scaffolds (without SNAP). Statistical data are expressed as mean ± standard error of the mean of n=3 samples. Values of $p < 0.05$ were considered statistically significant.

Therefore, the study was carried out using common bacteria present in infected tissues *S. aureus* and *P. aeruginosa*. The NO flux released by the 50 wt% alginate-starch-SNAP bone

scaffolds ranged from 0.50 ± 0.06 × 10^{-10} to 0.23 ± 0.02 × 10^{-10} mol min^{-1} mg^{-1} over a 24 h period. This resulted in a 99.76 ± 0.33 % reduction in a gram-positive bacterium, *S. aureus* and a 99.80 ± 0.62 % reduction in the adhered viable colonies of gram-negative bacterium, *P. aeruginosa* as compared to alginate controls without SNAP ($p < 0.05$) in a 24 h study (Figure 6.8 and 6.9).

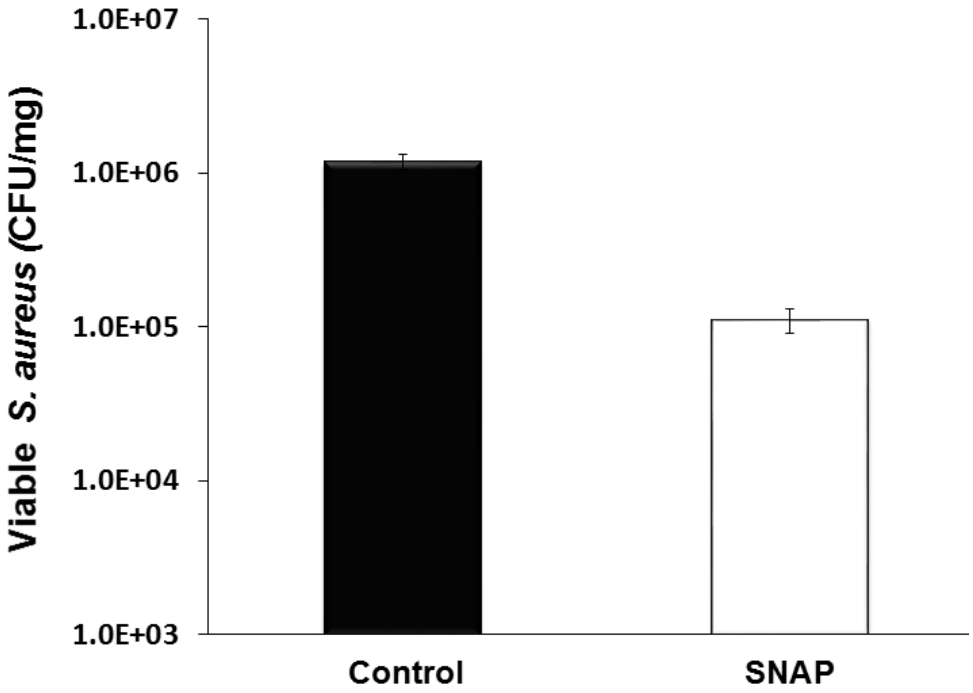

Figure 6.9. The NO release resulted in an observed 87.0% decrease in gram-negative *P. aeruginosa* on alginate-SNAP scaffold surface as compared to alginate controls in a 24 h study. Statistical data are expressed as a mean ± standard error of the mean of n=3 samples. Values of $p < 0.05$ were considered statistically significant.

This result is in line with the past reports including ours which have reported the antibacterial success of NO donors against pathogens such as *S. aureus, S. epidermis*, *P. aeruginosa, S. epidermis*, *P. aeruginosa, E. coli, A. baumanii.*[26, 50-51,32,27, 52] The antimicrobial activity of NO involves deactivation of enzymes, deamination of DNA, and oxidation of lipids in the cellular membrane.[53-54]

During bone surgeries, a joint spacer is often used to maintain space between the joint and the alignment. Space is filled with antibiotics that flow into the joint and surrounding tissue to eradicate the infection. The growing concern with the emerging antibiotics resistance bacterial

strains and the associated mortality rises an alarming question about their use in the future. According to a recent report in 2017 by the Center for Diseases Control and Prevention (CDC) approximately 2 million people get infected with antibiotic-resistant bacteria resulting in around 23,000 deaths per year in the United States alone. Nitric oxide-based approach not only inhibits>99% bacteria but can also provide an important alternative for the antibiotic based antibacterial treatment during bone surgeries. Nitric oxide acts via multiple mechanisms to kill the bacterial cells: membrane disruption, DNA breakage, and protein denaturation which ensures the high efficacy of killing.[54] In nature, the sustained release of endogenous NO endows macrophages with toxic activity against pathogens.[55] Moreover, the use of NO is unlikely to stimulate the production of resistant strains due to non-specific action, short half-life, and rapid reduction of microbial load life.[15-17] Another advantage of SNAP donor based strategies is its compatibility with other antimicrobial agents such as quaternary ammonium ions,[26] copper nanoparticles, [27] and silicone oil [56] and its easy blending in a variety of natural and synthetic polymers.[24, 32]

3.5 Absence of cytotoxic response towards mammalian cells

While inhibiting the bacterial infection at the site of biomedical device application is important, it's equally important that the material does not cause any toxic response toward the mammalian cells. Very often, the leachates from the materials that can cause side effect to the nearby tissue and in some cases may have negative systemic implications too. Therefore, in the current study, leachates from the bone scaffolds were collected after soaking them in DMEM medium at 37°C for 24 hours and then tested on mouse fibroblast cells for any potential cytotoxicity. Our results confirmed that while the material inhibited, up to 99.8% bacteria, it did not show any toxic effect on the mammalian cells (Figure 6.10).

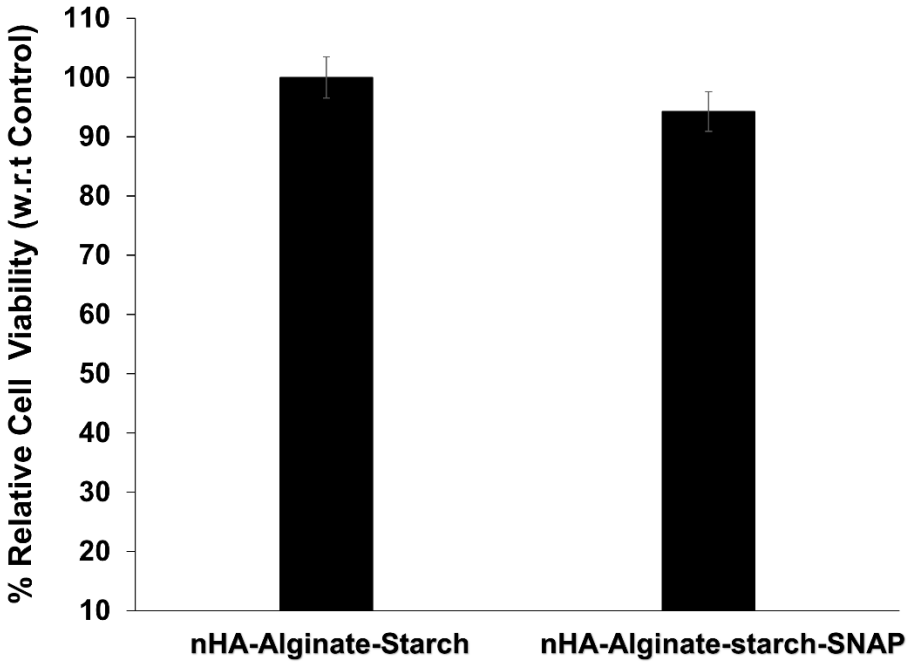

Figure 6.10. Non-cytotoxic nature of the 3D bone scaffold as analyzed via WST-8 assay

A plausible explanation for its non-cytotoxic nature can be as follows. SNAP breaks down to NAP and NO after cleavage of thiol bond. While NO is endogenous in nature it is expected to be harmless to mammalian cells in the physiological range, NAP is an FDA approved molecule used in the treatment of heavy-metal poisoning. Similarly, alginate and starch are derived from natural resources and are approved as edible food materials by FDA. Thus, any small amount of leaching from the composites was not expected to be toxic towards mammalian cells. In the past also, non-cytotoxic nature of NO releasing materials has been illustrated at different concentrations with a wide variety of materials such as Carbosil, Elasteon, silicone oil, and diatomaceous silica particle.[24, 27, 57,58] In addition to preventing bacterial infection, these NO releasing bone scaffolds are also expected to increase the overall healing process at the site of bone injury. Endogenous NO released by nitric oxide synthases in mammals has been shown to regulate osteoblasts activity and physiology of the bone.[59-60] Small amounts of NO released by osteoblast might act as a natural autocrine stimulator to trigger the cytokine production and

osteoblast cell growth.[61] Nitric oxide also plays an important role in angiogenesis which would be crucial for the supply of blood at the site of bone injury.[62] The NO release plays a critical role in tissue remodeling which would be crucial during the final phase of recovery in any musculoskeletal injury.[63] Studies have shown the application of NO releasing materials in tissue healing processes angiogenesis, inflammation, and proliferation.[33] The hemocompatibility, biocompatibility, and healing attributes of NO releasing polymers have also been positively proven in the recent years.[5, 7, 24] However, more testing on *in vivo* animal's models is warranted for transitioning into clinical stages for such NO releasing biopolymeric composites

4. Conclusion

In the present study, nHA-alginate-starch and nHA-chitosan-starch scaffolds were fabricated with varying level of nHA (10 wt%-50 wt%) and tested for their load-bearing capacity. 50 wt% nHA-alginate-starch 3D scaffolds showed maximum load bearing capacity among all the scaffolds and hence were integrated with 10 wt% SNAP to further develop NO releasing antibacterial bone scaffolds. NO flux released by these 3D bone scaffolds resulted in significant eradication (>99%) of both gram-positive and gram-negative bacterial strains in addition to the excellent compressive strength. The material was shown to be non-toxic to mouse fibroblast cells. Other studies have also suggested that due to its rapid action, short half-life, and nonspecific bactericidal action, NO is unlikely to cause any resistance in the bacterial strains which is a major concern with antibiotic use. Beyond the current platform, these NO releasing 3D scaffolds can be used to achieve osteoblast growth, angiogenesis, regulation of gene expression and tissue at the site of bone injury and infections. Further *in vitro* and *in vivo* studies are recommended to validate the multidimensional effect of NO releasing nHA-starch-alginate bone scaffolds. Such NO releasing 3D bone scaffolds are not only capable of providing a 3D potential matrix to restore damaged bone function but can also reduce infections resulting in faster healing and shorter hospital stays, ultimately bringing down the cost of treatment.

Acknowledgments

Funding for this work was supported by National Institutes of Health, USA grant K25HL111213.

References

(1) Lindsay, R.; Christiansen, C.; Einhorn, T.; Hart, D.; Ljunghall, S.; Mautalen, C.; Meunier, P.; Morii, H.; Mundy, G.; Rapado, A. Who are candidates for prevention and treatment for osteoporosis? *Osteoporosis International* **1997,** *7* (1), 1-6.

(2) Johnell, O.; Kanis, J. An estimate of the worldwide prevalence and disability associated with osteoporotic fractures. *Osteoporosis international* **2006,** *17* (12), 1726-1733.

(3) Teyhen, D. S.; Shaffer, S. W.; Butler, R. J.; Goffar, S. L.; Kiesel, K. B.; Rhon, D. I.; Williamson, J. N.; Plisky, P. J. What risk factors are associated with musculoskeletal injury in us army rangers? A prospective prognostic study. *Clinical Orthopaedics and Related Research*® **2015,** *473* (9), 2948-2958.

(4) Allison, S.; Knapik, J.; Jones, B., Prevention and control of musculoskeletal injuries associated with physical training. Department of the army, 2011. **2015**.

(5) Murugan, R.; Ramakrishna, S. Bioresorbable composite bone paste using polysaccharide based nano hydroxyapatite. *Biomaterials* **2004,** *25* (17), 3829-3835.

(6) Mcgrath, P. Giant-cell tumour of bone an analysis of fifty-two cases. *Journal of Bone & Joint Surgery, British Volume* **1972,** *54* (2), 216-229.

(7) Mclaren, J.; White, L.; Cox, H.; Ashraf, W.; Rahman, C.; Blunn, G.; Goodship, A.; Quirk, R.; Shakesheff, K.; Bayston, R. A biodegradable antibiotic-impregnated scaffold to prevent osteomyelitis in a contaminated in vivo bone defect model. *Eur Cell Mater* **2014,** *27*, 332-49.

(8) Giannoudis, P.; Papakostidis, C.; Roberts, C. A review of the management of open fractures of the tibia and femur. *Journal of Bone & Joint Surgery, British Volume* **2006,** *88* (3), 281-289.

(9) Zalavras, C. G.; Marcus, R. E.; Levin, L. S.; Patzakis, M. J. Management of open fractures and subsequent complications. *Instructional course lectures* **2007,** *57*, 51-63.

(10) Murphy, C. M.; Haugh, M. G.; O'brien, F. J. The effect of mean pore size on cell attachment, proliferation and migration in collagen–glycosaminoglycan scaffolds for bone tissue engineering. *Biomaterials* **2010,** *31* (3), 461-466.

(11) Frost, M. C.; Reynolds, M. M.; Meyerhoff, M. E. Polymers incorporating nitric oxide releasing/generating substances for improved biocompatibility of blood-contacting medical devices. *Biomaterials* **2005,** *26* (14), 1685-1693.

(12) Niklason, L. E. Engineering of bone grafts. *Nature biotechnology* **2000,** *18* (9), 929-930.

(13) Damoulis, P. D.; Drakos, D. E.; Gagari, E.; Kaplan, D. L. Osteogenic differentiation of human mesenchymal bone marrow cells in silk scaffolds is regulated by nitric oxide. *Ann. N. Y. Acad. Sci.* **2007,** *1117* (1), 367-376.

(14) Rouby, J. J. The nose, nitric oxide, and paranasal sinuses: The outpost of pulmonary antiinfectious defenses? *American Journal of Respiratory and Critical Care Medicine* **2003,** *168* (3), 265-266.

(15) Feelisch, M. The use of nitric oxide donors in pharmacological studies. *Naunyn-Schmiedeberg's Arch. Pharmacol.* **1998,** *358* (1), 113-122.

(16) Hetrick, E. M.; Schoenfisch, M. H. Antibacterial nitric oxide-releasing xerogels: Cell viability and parallel plate flow cell adhesion studies. *Biomaterials* **2007,** *28* (11), 1948-1956.

(17) Bogdan, C. Nitric oxide and the immune response. *Nat. Immunol.* **2001,** *2* (10), 907-916.

(18) Ge, S.; Zhao, N.; Wang, L.; Yu, M.; Liu, H.; Song, A.; Huang, J.; Wang, G.; Yang, P. Bone repair by periodontal ligament stem cellseeded nanohydroxyapatite-chitosan scaffold. *Int J Nanomedicine* **2012,** *7* (5), 405-414.

(19) Gutowska, A.; Jeong, B.; Jasionowski, M. Injectable gels for tissue engineering. *The Anatomical Record* **2001,** *263* (4), 342-349.

(20) Wang, L.; Shelton, R.; Cooper, P.; Lawson, M.; Triffitt, J.; Barralet, J. Evaluation of sodium alginate for bone marrow cell tissue engineering. *Biomaterials* **2003,** *24* (20), 3475-3481.

(21) Erol, M.; Mouriño, V.; Newby, P.; Chatzistavrou, X.; Roether, J.; Hupa, L.; Boccaccini, A. R. Copper-releasing, boron-containing bioactive glass-based scaffolds coated with alginate for bone tissue engineering. *Acta Biomater.* **2012,** *8* (2), 792-801.

(22) Sundaram, J.; Durance, T. D.; Wang, R. Porous scaffold of gelatin–starch with nanohydroxyapatite composite processed via novel microwave vacuum drying. *Acta biomaterialia* **2008,** *4* (4), 932-942.

(23) Kurashina, K.; Kurita, H.; Wu, Q.; Ohtsuka, A.; Kobayashi, H. Ectopic osteogenesis with biphasic ceramics of hydroxyapatite and tricalcium phosphate in rabbits. *Biomaterials* **2002,** *23* (2), 407-412.

(24) Goudie, M. J.; Brisbois, E. J.; Pant, J.; Thompson, A.; Potkay, J. A.; Handa, H. Characterization of an s-nitroso-n-acetylpenicillamine–based nitric oxide releasing polymer from a translational perspective. *Int. J. Polym. Mater. Polym. Biomater.* **2016,** *65* (15), 769-778.

(25) Chipinda, I.; Simoyi, R. H. Formation and stability of a nitric oxide donor: S-nitroso-n-acetylpenicillamine. *The Journal of Physical Chemistry B* **2006,** *110* (10), 5052-5061.

(26) Pant, J.; Gao, J.; Goudie, M. J.; Hopkins, S.; Locklin, J.; Handa, H. A multi-defense strategy: Enhancing bactericidal activity of a medical grade polymer with a nitric oxide donor and surface-immobilized quaternary ammonium compound. *Acta Biomater.* **2017**.

(27) Pant, J.; Goudie, M. J.; Hopkins, S. P.; Brisbois, E. J.; Handa, H. Tunable nitric oxide release from s-nitroso-n-acetylpenicillamine via catalytic copper nanoparticles for biomedical applications. *ACS Appl. Mater. Interfaces*.

(28) De Groote, M. A.; Fang, F. C. No inhibitions: Antimicrobial properties of nitric oxide. *Clin. Infect. Dis.* **1995,** *21* (Supplement 2), S162-S165.

(29) Jones, M. L.; Ganopolsky, J. G.; Labbé, A.; Wahl, C.; Prakash, S. Antimicrobial properties of nitric oxide and its application in antimicrobial formulations and medical devices. *Appl. Microbiol. Biotechnol.* **2010,** *88* (2), 401-407.

(30) Schairer, D. O.; Martinez, L. R.; Blecher, K.; Chouake, J. S.; Nacharaju, P.; Gialanella, P.; Friedman, J. M.; Nosanchuk, J. D.; Friedman, A. J. Nitric oxide nanoparticles: Pre-clinical utility as a therapeutic for intramuscular abscesses. *Virulence* **2012,** *3* (1), 62-67.

(31) Hetrick, E. M.; Schoenfisch, M. H. Reducing implant-related infections: Active release strategies. *Chem. Soc. Rev.* **2006,** *35* (9), 780-789.

(32) Sundaram, J.; Pant, J.; Goudie, M. J.; Mani, S.; Handa, H. Antimicrobial and physicochemical characterization of biodegradable, nitric oxide-releasing nanocellulose–chitosan packaging membranes. *J. Agric. Food Chem.* **2016,** *64* (25), 5260-5266.

(33) Pant, J.; Goudie, M.; Brisbois, E.; Handa, H. Nitric oxide-releasing polyurethanes. *Advances in Polyurethane Biomaterials* **2016**, 417.

(34) Woodard, J. R.; Hilldore, A. J.; Lan, S. K.; Park, C.; Morgan, A. W.; Eurell, J. a. C.; Clark, S. G.; Wheeler, M. B.; Jamison, R. D.; Johnson, A. J. W. The mechanical properties and osteoconductivity of hydroxyapatite bone scaffolds with multi-scale porosity. *Biomaterials* **2007,** *28* (1), 45-54.

(35) Hutmacher, D. W. Scaffolds in tissue engineering bone and cartilage. *Biomaterials* **2000,** *21* (24), 2529-2543.

(36) Zhang, J.; He, F.; Zhang, W.; Zhang, M.; Yang, H.; Luo, Z.-P. Mechanical force enhanced bony formation in defect implanted with calcium sulphate cement. *Bone research* **2015,** *3*, 14048.

(37) Yannas, I.; Tobolsky, A. Cross-linking of gelatine by dehydration. **1967**.

(38) Thein-Han, W.; Misra, R. Biomimetic chitosan–nanohydroxyapatite composite scaffolds for bone tissue engineering. *Acta Biomater.* **2009,** *5* (4), 1182-1197.

(39) Tret'yakov, Y. D.; Brylev, O. New generation of inorganic functional materials. *Ross. Khim. Zh* **2000,** *7* (4), 10-16.

(40) Brisbois, E. J.; Handa, H.; Major, T. C.; Bartlett, R. H.; Meyerhoff, M. E. Long-term nitric oxide release and elevated temperature stability with s-nitroso-n-acetylpenicillamine (snap)-doped elast-eon e2as polymer. *Biomaterials* **2013,** *34* (28), 6957-6966.

(41) Singha, P.; Pant, J.; Goudie, M. J.; Workman, C. D.; Handa, H. Enhanced antibacterial efficacy of nitric oxide releasing thermoplastic polyurethanes with antifouling hydrophilic topcoats. *Biomaterials Science* **2017**.

(42) Wo, Y.; Li, Z.; Brisbois, E. J.; Colletta, A.; Wu, J.; Major, T. C.; Xi, C.; Bartlett, R. H.; Matzger, A. J.; Meyerhoff, M. E. Origin of long-term storage stability and nitric oxide release behavior of carbosil polymer doped with s-nitroso-n-acetyl-d-penicillamine. *ACS applied materials & interfaces* **2015**.

(43) Cai, Q.; Yang, J.; Bei, J.; Wang, S. A novel porous cells scaffold made of polylactide–dextran blend by combining phase-separation and particle-leaching techniques. *Biomaterials* **2002,** *23* (23), 4483-4492.

(44) Nam, Y. S.; Park, T. G. Porous biodegradable polymeric scaffolds prepared by thermally induced phase separation. *J. Biomed. Mater. Res.* **1999,** *47* (1), 8-17.

(45) Lee, S. J.; Lee, I. W.; Lee, Y. M.; Lee, H. B.; Khang, G. Macroporous biodegradable natural/synthetic hybrid scaffolds as small intestine submucosa impregnated poly (d, l-lactide-co-glycolide) for tissue-engineered bone. *J. Biomater. Sci. Polym. Ed.* **2004,** *15* (8), 1003-1017.

(46) Petrie Aronin, C. E.; Sadik, K. W.; Lay, A. L.; Rion, D. B.; Tholpady, S. S.; Ogle, R. C.; Botchwey, E. A. Comparative effects of scaffold pore size, pore volume, and total void volume on cranial bone healing patterns using microsphere-based scaffolds. *Journal of Biomedical Materials Research Part A* **2009,** *89* (3), 632-641.

(47) Karageorgiou, V.; Kaplan, D. Porosity of 3d biomaterial scaffolds and osteogenesis. *Biomaterials* **2005,** *26* (27), 5474-5491.

(48) Salgado, A.; Figueiredo, J.; Coutinho, O.; Reis, R. Biological response to pre-mineralized starch based scaffolds for bone tissue engineering. *J. Mater. Sci. Mater. Med.* **2005,** *16* (3), 267-275.

(49) Chahoud, J.; Kanafani, Z.; Kanj, S. S. Surgical site infections following spine surgery: Eliminating the controversies in the diagnosis. *Frontiers in medicine* **2014,** *1*, 7.

(50) Pant, J.; Goudie, M. J.; Chaji, S. M.; Johnson, B. W.; Handa, H. Nitric oxide releasing vascular catheters for eradicating bacterial infection. *Journal of Biomedical Materials Research Part B: Applied Biomaterials*, n/a-n/a.

(51) Pant, J.; Goudie, M.; Brisbois, E.; Handa, H., Nitric oxide-releasing polyurethanes. In *Advances in polyurethane biomaterials*, Elsevier: **2016**, pp 417-449.

(52) Brisbois, E. J.; Bayliss, J.; Wu, J.; Major, T. C.; Xi, C.; Wang, S. C.; Bartlett, R. H.; Handa, H.; Meyerhoff, M. E. Optimized polymeric film-based nitric oxide delivery inhibits bacterial growth in a mouse burn wound model. *Acta Biomaterialia* **2014,** *10* (10), 4136-4142.

(53) Fang, F. C. Antimicrobial reactive oxygen and nitrogen species: Concepts and controversies. *Nature Reviews Microbiology* **2004,** *2* (10), 820-832.

(54) Fang, F. C. Perspectives series: Host/pathogen interactions. Mechanisms of nitric oxide-related antimicrobial activity. *Journal of Clinical Investigation* **1997,** *99* (12), 2818-2825.

(55) Macmicking, J.; Xie, Q.-W.; Nathan, C. Nitric oxide and macrophage function. *Annu. Rev. Immunol.* **1997,** *15* (1), 323-350.

(56) Goudie, M. J.; Pant, J.; Handa, H. Liquid-infused nitric oxide-releasing (linorel) silicone for decreased fouling, thrombosis, and infection of medical devices. *Sci. Rep.* **2017,** *7* (1), 13623.

(57) Pant, J.; Goudie, M. J.; Chaji, S. M.; Johnson, B. W.; Handa, H. Nitric oxide releasing vascular catheters for eradicating bacterial infection. *Journal of Biomedical Materials Research Part B: Applied Biomaterials*.

(58) Grommersch, B.; Pant, J.; Hopkins, S. P.; Goudie, M. J.; Handa, H. Bio-templated synthesis and characterization of mesoporous nitric oxide-releasing diatomaceous earth silica particles. *ACS Appl. Mater. Interfaces* **2017**.

(59) Fox, S.; Chow, J. Nitric oxide synthase expression in bone cells. *Bone* **1998,** *23* (1), 1-6.

(60) Bakker, A. D.; Soejima, K.; Klein-Nulend, J.; Burger, E. H. The production of nitric oxide and prostaglandin e 2 by primary bone cells is shear stress dependent. *J. Biomech.* **2001,** *34* (5), 671-677.

(61) Riancho, J. A.; Salas, E.; Zarrabeitia, M. T.; Olmos, J. M.; Amado, J. A.; Fernández-Luna, J. L.; González-Macías, J. Expression and functional role of nitric oxide synthase in osteoblast-like cells. *J. Bone Miner. Res.* **1995,** *10* (3), 439-446.

(62) Lee, P. C.; Salyapongse, A. N.; Bragdon, G. A.; Shears, L. L.; Watkins, S. C.; Edington, H. D.; Billiar, T. R. Impaired wound healing and angiogenesis in enos-deficient mice. *Am. J. Physiol.: Heart Circ. Physiol* **1999,** *277* (4), H1600-H1608.

(63) Chae, H. J.; Park, R. K.; Chung, H. T.; Kang, J. S.; Kim, M. S.; Choi, D. Y.; Bang, B. G.; Kim, H. R. Nitric oxide is a regulator of bone remodelling. *J. Pharm. Pharmacol.* **1997,** *49* (9), 897-902.

CHAPTER 7

CONCLUSIONS AND FUTURE DIRECTIONS

Nitric oxide is a cellular signaling molecule released by the NOS enzyme system: eNOS, nNOS, and iNOS. Due to its crucial role in several biological processes such as antibacterial effect, wound healing, thrombosis, and cell proliferation, it has garnered great interest to the scientists in the medical research. In the last two decades, a wide variety of NO donor molecules have been developed and studied out of which SNAP and GSNO were mostly used during my doctoral research.

This dissertation report has detailed characterization of physiochemical and biological properties of these NO releasing materials from a translational perspective. Various applications such as vascular catheters, 3D bone scaffolds, wound healing and combinatorial drug for synergistic antibacterial effect were studied in detail. The results obtained during my doctoral thesis has demonstrated the highly antibacterial, hemocompatibility, and biocompatible nature of the NO releasing platforms that were developed. Besides proving its effectiveness in the biomedical and tissue engineering applications, my work has also demonstrated how NO donors can be used in combination with the existing therapeutic agents such as quaternary ammonium ions.

The work has successfully shown greater than 99.5% bacterial reduction with most common pathogens found in HAIs such as *Staphylococcus aureus, Pseudomonas aeruginosa*, *Acinetobacter baumannii*, *Listeria monocytogenes, Enterococcus faecalis,* and *Escherichia coli* while simultaneously showing its cytocompatibility towards mammalian cells.

The work has also proved the cell proliferation capability of NO releasing platforms particularly with biocompatible polymers such as alginate, and polyvinyl alcohol. In this regard, up to 3-fold increases in the endothelial cell viability, and a significant increase in fibroblast cells viability has been observed. These results are important in proving the potential of NO releasing platforms in tissue engineering applications.

The Cu-NPs assisted NO releasing materials are exceptionally promising to fabricate a new generation of medical devices with controlled NO release, reduced platelet adhesion and superior degree of microbial inhibition with potential biocompatibility. This material can be particularly useful as the invasive device topcoats or developing antibacterial and antithrombic devices such as ECC, stents, catheters, or sutures. The fundamentals of this study can be tested further with other NO donors or in combination with other metal ions.

The combination of SNAP with a quaternary ammonium ion can enhance the antibacterial effect of either of the antibacterial agent and can be used to fabricate antibacterial surfaces for medical devices. These characteristics are ideal for controlling biomedical device related infections, especially in preventing bacteria from developing antibiotic resistance due to the different killing mechanisms exhibited by SNAP and BPAM. Such highly effective antimicrobial attributes offer a new paradigm in the fabrication of antimicrobial surfaces for various medical device applications and implants.

From a translational perspective, SNAP-E2As based biomaterials have excellent storage stability, can undergo popular sterilization methods and have excellent mechanical strength. In future, the results from the present study can be used as a proof of concept to fabricate other blood contacting medical devices that utilize similar NO chemistry.

The current study on the Alginate-PVA-GSNO based wound dressings provided supportive *in vitro* evidence to show that Alginate-PVA-GSNO provides a favorable environment for accelerated wound healing *in vitro*. This material can also be helpful in making artificial skin

template that can be particularly useful for burn injuries. Further animal testing is under process to validate these findings *in vivo*.

Beyond the current platform, the NO releasing 3D scaffolds can be used to achieve osteoblast growth, angiogenesis, regulation of gene expression and tissue at the site of bone injury and infections. Further *in vitro* and *in vivo* studies are recommended to validate the multidimensional effect of NO releasing nHA-starch-alginate bone scaffolds. Such NO releasing 3D bone scaffolds are not only capable of providing a 3D potential matrix to restore damaged bone function but can also reduce infections resulting in faster healing and shorter hospital stays, ultimately bringing down the cost of treatment.

Each of the materials developed during my doctoral research has high commercialization potentials however it warrants more extensive testing *in vivo*. In the future, these materials can be tested in respective animal models for wound healing, vascular catheters, bone tissue engineering, and device coatings applications before graduating to the clinical trials.